2020-01-24

Modelling long term ice sheet changes to understand the stability of the Greenland Ice Sheet in a warmer world

Rahimian, Zahra

UNIVERSITY OF CALGARY

Modelling long term ice sheet changes to understand the stability of the Greenland Ice Sheet in a warmer world

by

Zahra Rahimian

A THESIS

SUBMITTED TO THE FACULTY OF GRADUATE STUDIES

IN PARTIAL FULFILMENT OF THE REQUIREMENTS FOR THE

DEGREE OF MASTER OF SCIENCE

GRADUATE PROGRAM IN GEOGRAPHY

CALGARY, ALBERTA

JANUARY, 2020

Abstract

The Greenland Ice Sheet is under stress with the rising temperature. Ice sheet sensitivity to temperature changes and its contribution to global sea level rise can be estimated using ice sheet/climate models. This study combines an ice dynamics model and an isotope tracer model to carry out long-term coupled ice-sheet/climate simulations to investigate the vulnerability of the Greenland ice sheet to higher temperatures during the Eemian warming. I also examine how Eemian melting may have altered isotopic ratios and temperature reconstructions. The simulations are benchmarked against NEEM and Summit ice core observations to provide validation of model performance. I find that there is ice in central Greenland for climates up to 12ºC higher than present. Greenland's contribution due to Eemian sea level most likely ranges between 2.8 to 4.3 m, associated with temperature anomalies from 5 to 9ºC. Melt-induced isotopic modifications can cause overestimation of 0.1-2ºC warming in proxy records.

Keywords: Greenland ice sheet, isotopes, ice sheet/climate model, melting modifications, Eemian

Preface

This thesis consists of a series of altered (to ensure consistency with the thesis format) and unaltered figures from publications in academic journals and websites within chapters 1 and 2. The license and copyright agreements allow sharing and adapting material for non-commercial purposes as long as credit is attributed to the author. The source has been referenced within the figure caption and is listed in the References section. This thesis is original, unpublished, independent work by the author Z. Rahimian.

Acknowledgements

This thesis would not have been possible without the assistance and support of many friends, colleagues, and family members.

First, I would like to thank my supervisor Dr. Shawn Marshall for his mentorship and guidance. Thank you for opening my eyes to this chapter of my life and believing in me all the way. I would also like to thank my supervisory committee; Dr. Brent Else and Dr. Ann-Lise Norman for their support and guidance.

Many thanks to my friends and colleagues at the University of Calgary, who have made this journey even more enjoyable. I especially would like to thank my office-mates Kristina Miller and Hoi Ming Lam for their friendship and input into my project.

This research has been financially supported by grants from NSERC and the U.S. National Center for Atmospheric Research (NCAR), awarded to Dr. Shawn Marshall and the Department of Geography at the University of Calgary. Modelling work would not have been possible without WestGrid and Compute Canada.

I would also like to thank my parents who raise me to be free and choose my own passion and dreams in life. Last but not least, thank you to my incredible husband Armin Heirati for encouraging me every step of the way, for his rock solid patience and support, and his endless love and friendship.

"You were born with wings, why prefer to crawl through life."

Rumi

Table of Contents

Abstract ii

Preface iii
Acknowledgements iv
Table of Contents v
List of Tables vii
List of Figures and Illustrations viii
List of Symbols, Abbreviations and Nomenclature xi

Chapter 1 Introduction and Objectives 1

Chapter 2 Literature Review 12
2.1. Ice sheets 13
2.1.1. Greenland Ice Sheet. 15
2.2. Stable water isotopes 16
2.3. Post-depositional isotopic modifications 21
2.3.1. Effects of vapour diffusion. 22
2.3.2. Effects of wind scouring. 23
2.3.3. Snow isotopic content change by melts. 23
2.4. The last interglacial period (Eemian) 25
2.5. Ice cores 26
2.6. Coupled ice-sheet/climate models 29
2.6.1. The U of C ice sheet model. 30

Chapter 3 Methods 32
3.1. Paleoclimate data 33
3.1.1. Temperature Scenarios. 34
3.1.2. NEEM ice core. 36
3.2. Defining present and LIG target intervals 36
3.3. The ice sheet model 37
3.4. Climate forcing 38
3.4.1. Present day climate forcing. 38
3.4.2. Model initialization. 39
3.5. The tracer model 40
3.6. Reconstructing the ice cores 40
3.7. Temperature modifications and data analysis 41

Chapter 4 Results and analysis 42
4.1. Greenland Ice Sheet over the last 200 kyr 42
4.2. Model Reconstructions in the Eemian Period 45
4.3. Melting modifications 52
4.4. Summit 56
4.5. Tracing 57
4.6. Ice core reconstructions 59

Chapter 5 Discussion 66
5.1. Summary of the Ice Sheet Reconstructions 66
5.2. Effects of meltwater on the NEEM isotope-temperature reconstructions 68
5.3. Tracer Modelling 69
5.4. Comparison with observations 72
5.5. Implications for the stability of GrIS 76

Chapter 6 Conclusions 78
6.1. Recommendations for future work 79

References 81

List of Tables

Table 4.1. Observed and modelled present-day ice area, volume, and sea level equivalent for the T2, T6, and T10 temperature scenarios. 43

Table 4.2. Observed and modelled present-day elevation (h_s), ice sheet thickness (H) and air temperature (T_a) for T2 (minimum T forcing), T6 (mean T forcing), and T10 (maximum T forcing) temperature scenarios at the Summit and NEEM sites. 45

Table 4.3. Modelled minimum ice volume and area (10^6 km^3), sea level equivalent of this volume, maximum temperature change (ΔT), maximum NEEM source surface temperature, maximum Summit elevation (h_s), and the time they occur (ka) for all temperature scenarios during the Eemian. 51

Table 4.4. Elevation (h_s) at NEEM, NEEM source, and Summit at 126 ka, as well as PDD for NEEM source for all temperature scenarios. 52

Table 4.5. Modelled Eemian maximum temperature anomalies, minimum ice sheet volume and their time of occurrence after modifications for all the scenarios. Where dT and dV are the changes from before modifications. 54

Table 4.6. Modelled elevation (h_s) of NEEM source and Summit, as well as PDD of NEEM source for the T2, T6, and T10 scenarios after modifications compared with the initial simulations for 126 ka. 55

Table 4.7. Modelled Eemian minimum surface elevation (h_s) and time of occurrence after melting modifications for T2, T6, and T10 scenarios, where Δh is the change from the initial simulation. 57

Table 5.1. Observations versus model results (T2-T10 and Summit forcing) of ice thickness change (ΔH) from 128-122 ka and elevation (h_s) for every 2000 years from 128 ka to 122 ka at the NEEM source location. Crosses indicate failed scenarios of the model to produce the observed data. 74

Table 5.2. Present-day observations versus model results (T2-T10 and Summit forcing) of temperature (T_a), elevation (h_s), and ice thickness (H) at the NEEM site, total ice sheet volume and area, plus elevation (h_s) and time (ka) of highest temparaute of the NEEM source ice site. 75

Table 5.3. Summit observation versus model results (T2-T10) of temperature changes over the Eemian, and present temperature. Crosses indicate failed scenarios of the model to produce the observed data. 76

List of Figures and Illustrations

Figure 1.1. Ice sheet mass loss over (a) Antarctica (b) Greenland shown in centimeters of water per year (cm of water yr^{-1}) from 2003 to 2012 (IPCC, 2013). 1

Figure 1.2. Temperature from the Eemian (left) through the last glacial cycle to present. The red colour indicates ice from a warm period, the blue from a cold period, and the rest of the colours from periods in between (adapted from University of Copenhagen, 2013). 3

Figure 1.3. Temperature (^{o}C) difference during the Eemian period relative to mean of past millennium (adapted from Nature, 2013). 5

Figure 1.4. Surface elevation (m) difference during the Eemian period relative to past millennium (adapted from Nature, 2013). 6

Figure 1.5. Annual LIG surface air temperature (^{o}C) simulation minus preindustrial anomalies in a global climate model (adapted from McKay et al., 2011). 7

Figure 1.6. Multi-millennial equilibrated sea level (m) per °C of warming (x-axis) above preindustrial (PI) levels (y-axis). Resulted from physical models (black lines/grey shading) and proxy-data estimates from past warm periods (black boxes). PI = pre-industrial, LIG = last interglacial period, M11 = Marine Isotope Stage 11, Plio = Mid-Pliocene. M11 is marine isotope stage 11, another interglacial period ca. 400 kyr BP. Plio is another warm interval ca. 3.3 to 3.0 Ma [Ma equals million years ago] with about 400 ppmv CO_2 and global mean surface temperature of 1.9°C to 3.6°C higher than pre-industrial values. Shading represents the uncertainty range. Red lines indicate fitted relationships (adapted from Church et al., 2013, fig. 13.14). 9

Figure 2.1. Global mean sea level change accompanied by coloured lines (of annual values) indicating different data sets. Shadings represent uncertainty (adapted from IPCC, 2013). 13

Figure 2.2. An image of the different glacier zones on Greenland ice sheet (Nolin and Payne, 2007, fig. 1). 14

Figure 2.3. Satellite image (SeaWiFS) taken of the Greenland Ice Sheet on July 15, 2000 (Alley et al., 2010, fig. 1). 16

Figure 2.4. The isotopic fractionation process at each phase change with hypothetical ^{18}O values (adapted from Bruckner, 2019). 17

Figure 2.5. Stable water isotopic value depletion during fractionation processes by comparing summer and winter seasons with the distinguishable summer and winter layers within the ice (adapted from Centre for Ice and Climate, 2019). 20

Figure 2.6. $\delta^{18}O$ profiles of five Greenland deep ice-cores that extend from the present to some period before the beginning of the last glacial stage. Warm Greenland Interstadials

(GI) and cold Greenland Stadials (GS) are numbered to the right and left of some profiles, respectively (Johnsen et al., 2001, fig. 2). 26

Figure 2.7. The location of five deep drilling sites in Greenland (adapted from Abbott and Davies, 2012). 27

Figure 2.8. Greenland temperature (^{o}C) deviations compared to present time calculated from the GRIP ice core (adapted from Dansgaard, 2005). 28

Figure 3.1. Schematic diagram illustrating the big picture behind the ice sheet modelling, and reconstruction of ice cores. 33

Figure 3.2. Temperature forcing anomalies (T2-T10) over the past 200 kyr. 35

Figure 3.3. Summit temperature forcing anomalies over the past 200 kyr. 35

Figure 4.1. Ice volume change over the past 200 kyr using T2-T10 temperature forcing..... 43

Figure 4.2. Temperature forcing anomalies during the Eemian (130-115 ka) for scenarios T2 to T10. 47

Figure 4.3. Ice volume change over the Eemian (130-115 ka) for scenarios T2-T10. 48

Figure 4.4. Ice surface topography showing elevation over Greenland. The legend shown in (c) applies to all ice sheet scenarios. The ice sheet is shown at 125 ka for scenarios (a) T2 and (b) T4 and 125.5 ka for (c) T6, (d) T8, and (e) T10. 49

Figure 4.5. Evolution of the ice sheet surface elevation over Eemian (130-115 ka) for T2, T6, and T10 scenarios at (a) Summit, (b) NEEM source, and (c) NEEM..... 50

Figure 4.6. Temperature forcing anomalies (a) before and (b) after modifications for meltwater enrichment over the Eemian (115-130 ka)..... 53

Figure 4.7. Ice volume change (a) before and (b) after the modifications for meltwater enrichment over the Eemian (130-115 ka) using T2-T10 scenarios. 54

Figure 4.8. Surface elevation before (T2, T6, and T10) and after (T2', T6', and T10') melting modifications at NEEM source ice core site over the Eemian (130-115 ka) using T2, T6, and T10 scenarios..... 56

Figure 4.9. Surface elevation before (T2, T6, and T10) and after (T2', T6', and T10') melting modifications at the Summit site over the Eemian (130-115 ka) using T2, T6, and T10 scenarios. 57

Figure 4.10. Surface elevation map of the position of the NEEM ice core site with the tracing of the snow deposition over time on GrIS is shown for (a) T2, (b) T5, (c) T7, and (d) T10. 58

Figure 4.11. NEEM and Summit ice core provenance trajectories for (a) T2, (b) T6, and (c) T10 scenarios. 59

Figure 4.12. Deposition depth and time for NEEM ice core site for T2, T6, and T10 scenarios (to compare with observations). 61

Figure 4.13. Surface paleo-temperature for NEEM ice core site for (a) T2, (b) T6, and (c) T10 scenarios. 61

Figure 4.14. Surface paleo-elevation for NEEM ice core site for (a) T2, (b) T6, and (c) T10 scenarios. 62

Figure 4.15. Modelled ice age for west-to-east (a1-a3) and south-to-north (b1-b3) profiles through the NEEM site for T2, T6 and T10. a1-a3: ice age vs longitude from 70º to 20ºW at a latitude of 77.45ºN. b1-b3: ice age vs. latitude from 68º to 83ºN at a longitude of 51.06ºW. 63

Figure 4.16. Deposition depth and time for the Summit site for T2, T6, and T10 scenarios (to compare with observations). 64

Figure 4.17. Paleo-surface temperature for the Summit site for (a) T2, (b) T6, and (c) T10 scenarios. 65

Figure 4.18. Modelled Summit ice core of $\delta^{18}O$ (‰) versus depth (m). 65

List of Symbols, Abbreviations and Nomenclature

Symbol	Definition
δ	Delta notation used to express the sample's enrichment or depletion relative to Vienna Standard Mean Ocean Water (V-SMOW)
‰	Per mil (symbol) and unit indicates parts per thousands
^{18}O	Oxygen-18 isotope with 10 neutrons and 8 protons
^{16}O	Oxygen-16 isotope with 8 neutrons and 8 protons
^{2}H or D	Deuterium, a hydrogen isotope with 1 neutron and 1 proton
^{1}H	Hydrogen isotope with 0 neutron and 1 proton
R_{sample}	The isotopic ratio in a sample water
R_{SMOW}	The isotopic ratio of V-SMOW
PDD	Positive degree-day defined as the summation of all temperatures above $0^{o}C$ over a period of time
ΔT	Temperature anomaly
P	Precipitation
h_s	Ice surface topography
h_b	Bedrock topography
H	Thickness of the ice

Chapter 1 Introduction and Objectives

The Greenland Ice Sheet (GrIS) and Antarctic Ice Sheet (AIS) are fundamental components of the global climate system. These only two currently available ice sheets, are losing mass and contributing an estimated 1.2 mm/year to global mean sea level rise (SLR) over the past decade (IPCC, 2019). The rate of sea level rise is expected to increase further into the future in response to climate warming (Figure 1.1; IPCC, 2019). GrIS holds enough water to raise global sea levels by ca. 7 m (Bamber et al., 2001). Glacier melt processes are understood fairly well and have been included in global climate/ice sheet models, but uncertainties remain with respect to ice sheet-ocean interactions, snow/ice-albedo feedback processes, and resolution of all of the relevant mass balance processes. As a result, there is significant uncertainty in projections of ice sheet sensitivity to temperature changes, and its contribution to SLR, due to melting ice sheets.

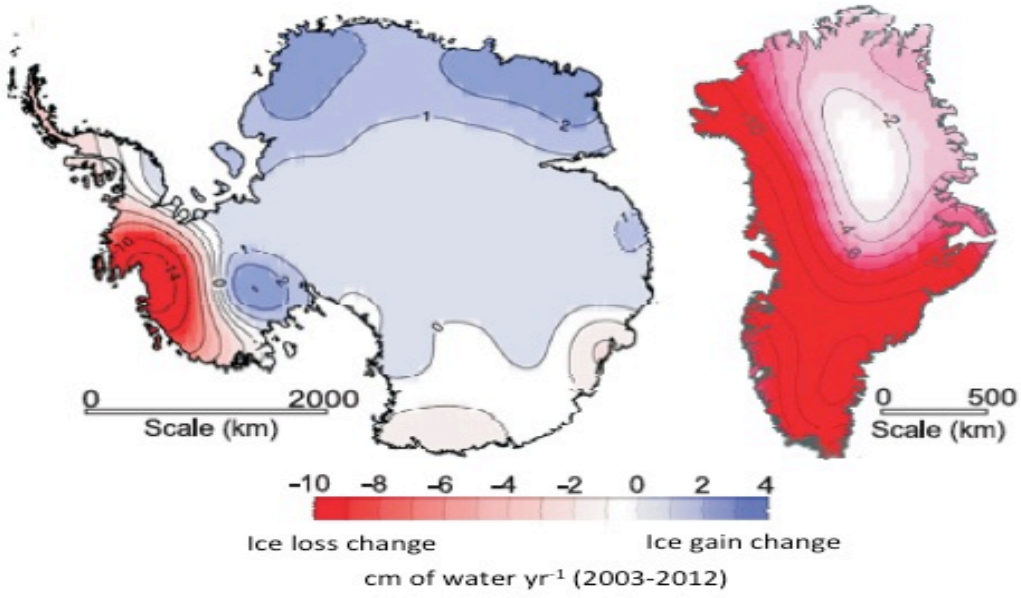

Figure 1.1. Ice sheet mass loss over (a) Antarctica (b) Greenland shown in centimeters of water per year (cm of water yr^{-1}) from 2003 to 2012 (IPCC, 2013).

Past studies have examined how stable GrIS is in a warmer climate by employing ice sheet models, exploring a wide range of uncertainty in the model parameters (e.g., Letréguilly et al., 1991; Huybrechts et al., 1991; Huybrechts and de Wolde, 1999; Cuffey and Marshall, 2000; Lhomme et al., 2005; Otto-Bliesner et al., 2006; Gregory and Huybrechts, 2006; Robinson et al., 2012; NEEM Community Members, 2013; Otto-Bliesner et al., 2013; Dutton et al., 2015; Yau et al., 2016).

Letréguilly et al. (1991) estimated that it would take a temperature increase of 3°C for the margins of the GrIS to melt with the central part of the ice sheet unaffected. The ice sheet divides into two part with an increase of 4°C. The central and northern parts as well as an ice cap on the southern mountains remain intact. According to this model, the GrIS disappears with a temperature increase of 8°C. On the other hand, Huybrechts et al. (1991) determined that a 1°C temperature rise could increase the global sea level 0.22 mm/yr. According to Huybrechts and de Wolde (1999) GrIS would likely contribute 10 cm and a few meters to global sea level rise by the year 2100 and 3000, respectively. Robinson et al. (2012) simulated a 60% reduced volume of the GrIS after 1200 years when forced with an applied constant temperature anomaly of 6°C. In addition, Dutton et al. (2015) states that currently the assessment of a threshold of 1-4°C above preindustrial levels could mean irreversible GrIS retreat. It needs to be noted however that with Arctic amplification of warming, approximately +1.5°C for the Northern Hemisphere means +5°C for Greenland (Otto-Bliesner et al., 2013).

Arctic temperatures were several °C warmer than present during the last interglacial (LIG) period (Letreguilly et al., 1991; Turney and Jones, 2010; McKay et al., 2011), also known as the Eemian period (129 to 116 ka), resulting in notably smaller GrIS (Figure 1.2). In addition, the LIG period is the penultimate warming period in Earth's history and at the moment Earth has a

comparable climate regime to that of the early Eemian (Nature, 2013). As a result, the LIG is considered an instructive period to investigate to understand how the ice sheet will react to future, warmer conditions. While the climate forcing in the LIG was different than today, orbital variability vs. greenhouse gasses, modelling research shows an intensified summer warming through similar albedo and water vapour feedbacks obtained in future and LIG climate simulations over Greenland (Lunt et al., 2013). Eemian climate warming was driven by an Earth-Sun orbital configuration that focused more summer insolation at high northern latitudes (Otto-Bliesner et al., 2006). However, Otto-Bliesner et al. (2013) also concludes that the Eemian should not be considered as an exact resemblance of future warming.

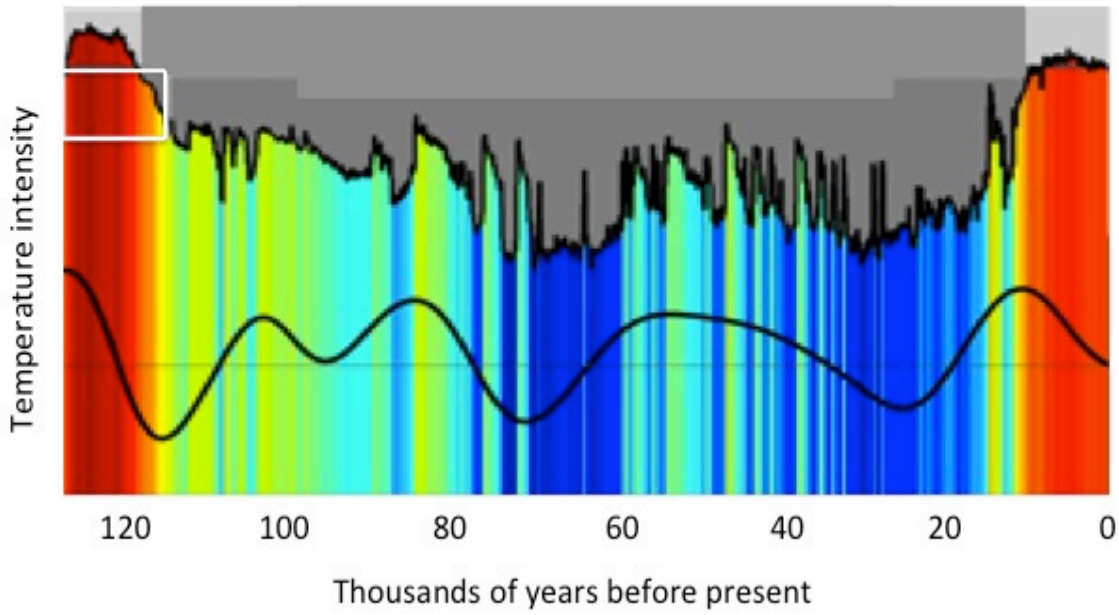

Figure 1.2. Temperature from the Eemian (left) through the last glacial cycle (darker grey background from ~115 to 10 ka) to present. The red colour indicates ice from a warm period, the blue from a cold period, and the rest of the colours from periods in between (adapted from University of Copenhagen, 2013).

It should be noted that high latitudes of both hemispheres were significantly warmer during the last interglacial period than the pre-industrial era (Church et al., 2013), with peak

warmth from 129 to 122 ka. Climate reconstructions of the Northern Hemisphere reveal maximum anomaly temperatures of +2 to +5°C early in the LIG (Bakker et al., 2014), leading to substantial melting of ice sheets. The increased melting of the GrIS caused the ice sheet to lose mass and reduce in height during the Eemian. Based on interpretations from the North Greenland Eemian ice core (NEEM Community Members, 2013), the NEEM ice core site thinned at a mean rate of 7 ± 6[1] cm per year between 128 and 122 kyr BP and stabilized at this thickness until 117-114 kyr BP. The NEEM group also reconstructed local (north Greenland) temperature anomalies of up to +8°C at this time (Figure 1.3). The temperature inference comes from $\delta^{18}O$ values in Eemian ice near the base of the core.

Despite the warm temperatures and the high rate of melting, the ice sheet did not disappear; older ice has been found in central Greenland (Centre for Ice and Climate, 2019a) and at the base of the NEEM core. Reconstructions of paleo ice sheet elevation can be derived from the total gas content in ice-core air bubbles (which is a proxy for air pressure, hence altitude; Raynaud et al., 1997). Using this method, air pressure reconstructions from the NEEM ice core indicate that surface elevation of the 128-ka ice depositional site was 540 ± 300 m higher than NEEM surface elevation at present (NEEM Community Members, 2013). The present surface elevation at the 128-ka ice depositional site is 330 ± 50 m higher than present at NEEM. The 210 m ± 350 m surface elevation decrease is the difference between the elevation 128 ka and present. At about 122 ka, the surface elevation was estimated to have decreased to 130 ± 300 m below the present elevation, resulting in an ice thickness change of ~340 m (400 ± 350 m after accounting for isostatic rebound) (NEEM Community Members, 2013). Figure 1.4 plots the LIG elevation

[1] NEEM reports 7 ± 4, which is an error. As 7*6000 years= 42,000 cm = 420 (or 400) m is correct, but 4*6000 would give 240 m. It should be 6 cm/yr for the error.

reconstruction for the ice sheet based on these data. Based on this, the NEEM group concludes that GrIS geometry did not change much during the LIG, and GrIS could not have caused more than ~2 m of sea-level rise during the Eemian.

Surface melting during the warm Eemian period can be seen in the ice core as layers of refrozen meltwater (NEEM Community Members, 2013). Surface meltwater percolated into the snow below and refroze. This site does not experience melting today, so there is no question that the Eemian climate was considerably warmer. However, the whole ice sheet inferences from the NEEM ice core are more difficult to validate, as the climatic and ice-sheet elevation records from this core are specific to this sector of the ice sheet.

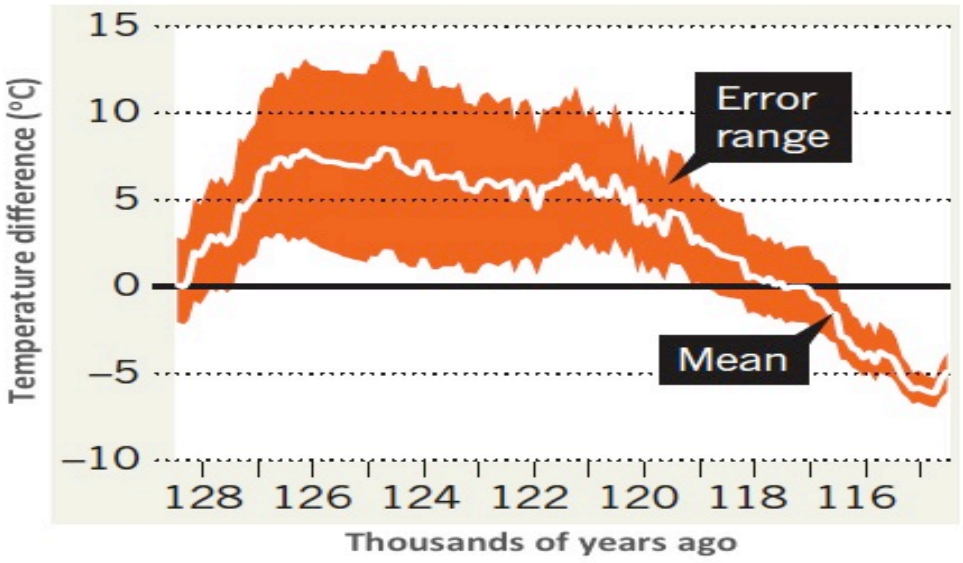

Figure 1.3. Temperature (°C) difference during the Eemian period relative to mean of past millennium (adapted from Nature, 2013).

Paleoceanographic data and a coupled atmosphere-ocean climate model were used to investigate global ocean surface temperatures of the LIG period (Figure 1.5), in order to provide an estimate of ocean thermal expansion SLR during the LIG, which most probably did not

exceed 0.4 ± 0.3 m (McKay et al., 2011). Kopp et al. (2009) estimate that during the last interglacial, sea level rose above 6.6 m, yet not exceeding 9.4 m. If the NEEM Community Members (2013) are correct that melting of the Greenland Ice Sheet caused less than 2 m of sea-level rise during the LIG, then most of the Eemian sea-level rise must have originated in Antarctica (Nature, 2013; Quiquet et al., 2013). This is possible, but the contributions of the two ice sheets remain uncertain, with a wide range of reconstructions from modelling studies.

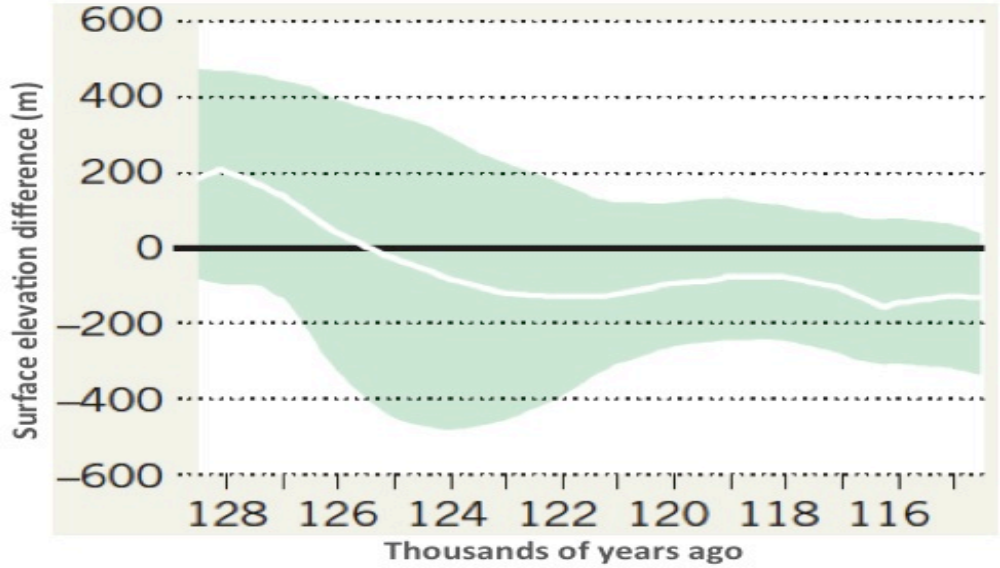

Figure 1.4. Surface elevation (m) difference during the Eemian period relative to past millennium (adapted from Nature, 2013).

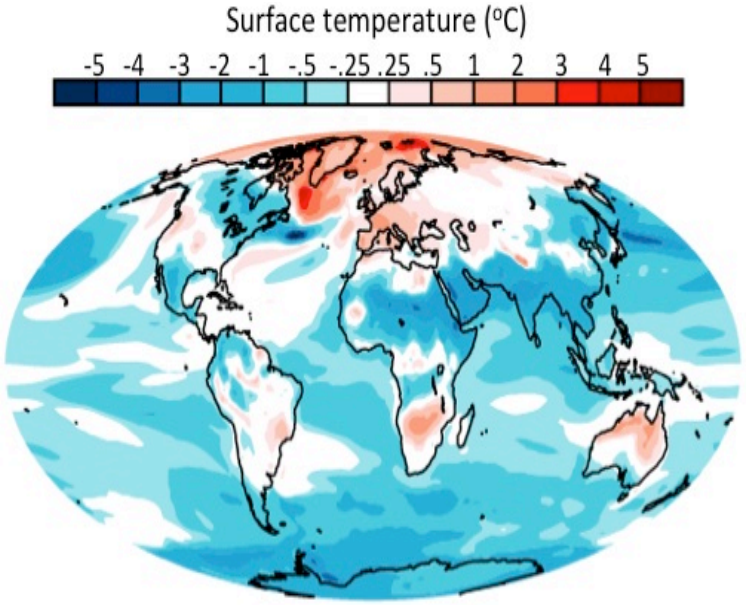

Figure 1.5. Annual LIG surface air temperature (°C) simulation minus preindustrial anomalies in a global climate model (adapted from McKay et al., 2011).

Estimates of Eemian global sea level rise associated with GrIS retreat range from 0.5 to 7 m, with no conclusive data available to better constrain this number. A contribution of 0.3 to 3.6 m from GrIS is supported by modelling studies of the LIG (Otto-Bliesner et al., 2006; Stone et al., 2013). Other researchers believe that GrIS contributed at least 5 m of SLR during the Eemian (Cuffey and Marshall, 2000; Nature, 2013). The conclusions from the NEEM Community Member (2013) are on the other end of the spectrum, arguing that GrIS was resilient to 8°C or more of regional warming in the Eemian, experiencing only minor retreat at this time. This was reinforced by the perspective piece that accompanied the publication of the NEEM results in *Nature News*, titled "Greenland Defied Ancient Warming" (Nature, 2013).

The interpretation of the isotope record and paleo-elevation history in the NEEM core requires reconstruction of source ice trajectories and ice sheet geometry in the Eemian period through to present day; it is necessary to know the age, location, and isotopic values of snow

falling on the ice sheet, which eventually flowed to the site of the present-day NEEM core. Another interesting question is associated with evidence of ice-core melting during the Eemian (NEEM Community Members, 2013). This melting is assumed not to have impacted the $\delta^{18}O$ values or total gas content, such that these proxies give valid estimates of Eemian air temperatures (Figure 1.3) and ice sheet elevations (Figure 1.4). My main research questions stem from the ability to examine these assumptions and reinterpret the results of NEEM Community Members (2013), with the aid of isotopic tracing in ice sheet modelling. The study expands current understanding of past and present-day ice sheet dynamics and GrIS sensitivity to climate change.

The paleo record draws attention to the sensitivity of ice sheets and sea level to increased global temperatures (Figure 1.6). It even highlights a major sea-level response to less severe global warming than what is predicted for future climate. The high SLR sensitivity related to greater warming at high latitudes results from powerful cryosphere-climate feedbacks (Church et al., 2013).

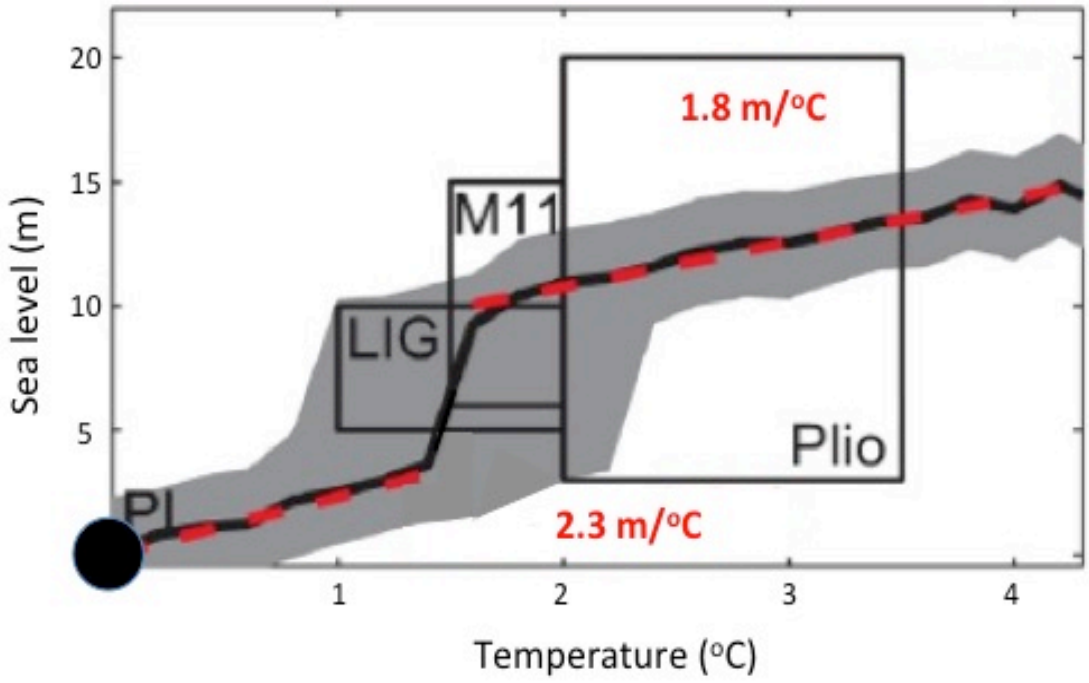

Figure 1.6. Multi-millennial equilibrated sea level (m) per °C of warming (x-axis) above preindustrial (PI) levels (y-axis). Resulted from physical models (black lines/grey shading) and proxy-data estimates from past warm periods (black boxes). PI = pre-industrial, LIG = last interglacial period, M11 = Marine Isotope Stage 11, Plio = Mid-Pliocene. M11 is marine isotope stage 11, another interglacial period ca. 400 kyr BP. Plio is another warm interval ca. 3.3 to 3.0 Ma (Ma equals million years ago) with about 400 ppmv CO_2 and global mean surface temperature of 1.9°C to 3.6°C higher than pre-industrial values. Shading represents the uncertainty range. Red lines indicate fitted relationships (adapted from Church et al., 2013, fig. 13.14).

My research explores GrIS reconstructions during the last interglacial period, approximately 128,000-116,000 years ago (128 to 116 ka) and through the last glacial cycle, from 116 ka to present. Modelled ice sheet reconstructions offer an opportunity to understand how GrIS reacted to a warmer Arctic, with less sea ice, longer summers, and increased energy available for melt. I use the University of Calgary (U of C) ice sheet model (Marshall and Cuffey, 2000; AMAP, 2009), and the isotope tracer models within the ice sheet model (Clarke and Marshall, 2002; Lhomme et al., 2005), to carry out long-term coupled ice-sheet/climate simulations in order to investigate the susceptibility of the GrIS and sea level to higher

temperatures. The simulations of the LIG period will be benchmarked against ice core observations to provide a validation of model performance in warm past climate states. I employ these new modelling capabilities to re-examine the history of the GrIS and its sensitivity to climate change. I also build on this work through examination of post-depositional isotopic modifications within the GrIS during the Eemian. This research is becoming ever more relevant as high northern latitudes are facing substantial warming.

The U of C ice sheet model has been developed by Dr. Shawn Marshall over many years, and has the ability to trace stable water isotopes of precipitation ($\delta^{18}O$) through the ice sheet system. These isotope-tracing capabilities in the ice sheet model allow predictions of 3D $\delta^{18}O$ fields (Clarke and Marshall, 2002; Lhomme et al., 2005), which are compared with modern observed fields (in ice cores) to better understand and constrain past climates and ice-sheet changes. A challenge of this approach is that precipitation isotopes in the past are unknown, and can only be roughly estimated.

My specific hypotheses are:

H1: 3D isotope tracers in a GrIS model can be used in conjunction with ice-core records to better constrain the Eemian extent of the GrIS.

H2: The isotopic signal in Eemian ice in Greenland has been modified by melting; this requires a re-interpretation of the temperature and elevation history of the ice sheet.

New understanding concerning these two hypotheses will inform reinterpretation of the Eemian climate and ice sheet history in Greenland. This in turn will provide a revised estimate of

the GrIS's climate sensitivity. Future climate warming in the Arctic is projected to exceed that of the Eemian. My results will better constrain estimates of GrIS stability and future sea level rise.

Chapter 2 of this thesis is a literature review that discusses early and recent investigations of ice cores and ice sheets during the last interglacial period, stable water isotopes, and ice sheet/climate models (mainly the U of C ice sheet model), as well as summarizes the affect of post depositional modifications, especially melting, on stable water isotopes. My methodology and analysis are described in Chapter 3. The results are presented in Chapter 4. Chapter 5 discusses the isotopes and post depositional modifications on Greenland in the context of larger literature. The thesis is concluded in Chapter 6.

Chapter 2 Literature Review

In its recent special report on the oceans and the cryosphere, IPCC (2019) reports that global mean sea level was at least 5 m higher than present during the Eemian, and that modelling studies have come to the conclusion that GrIS withdrew between approximately 1 and 6 m, but still demonstrate a small contribution to the global mean sea level around 129 ka; most of Greenland's sea-level contribution likely came later in the Eemian. Like mountain glaciers, it is clear that the Greenland Ice Sheet is sensitive to warm temperatures. Greenland mass loss in recent decades is caused by increased surface melting and the acceleration of large outlet glaciers (van den Broeke et al., 2009). Satellite gravity measurements indicate that the GrIS is currently losing mass at an average rate of 278 ± 11 Gt/yr (IPCC, 2019). A mass loss of 360 Gt is equal to global SLR of 1 mm (Lipscomb, 2010).

The main contributions to global sea level are from land ice retreat and ocean thermal expansion, adding to the sea level at a rate of roughly 3.2 mm per year (IPCC, 2019). The IPCC (2013) suggests that these processes account for about 75% of recent SLR, but the value fluctuates from year to year (Figure 2.1). Estimates of 21st century ice-sheet mass loss and SLR are extremely uncertain (IPCC, 2019). Therefore, there has been a great urgency for modelling of land ice, and the need for a number of improvements in ice sheet models.

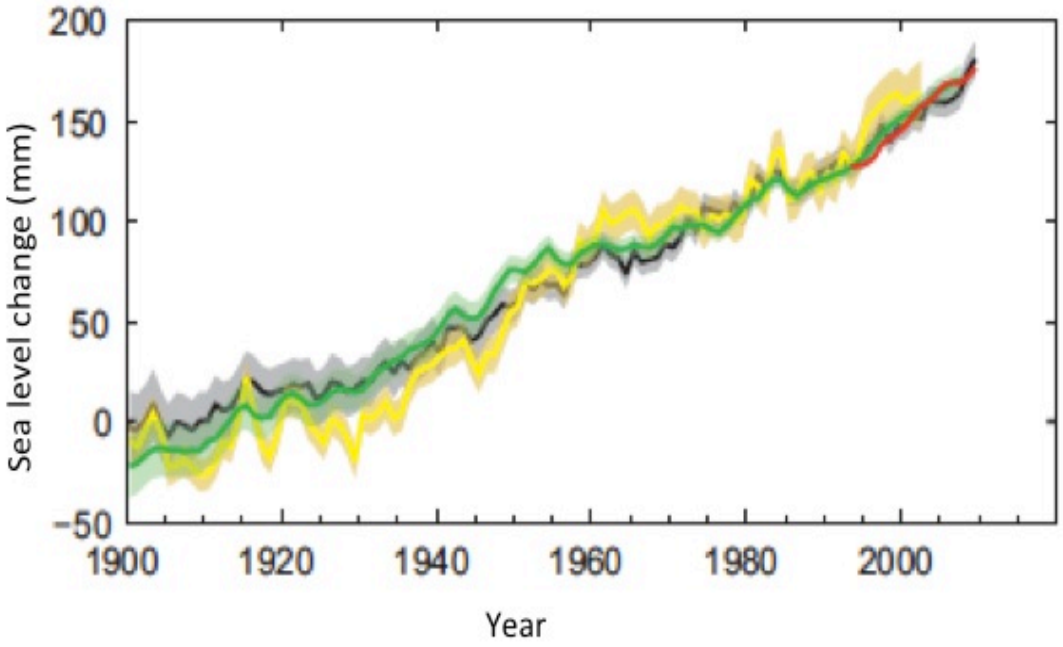

Figure 2.1. Global mean sea level change accompanied by coloured lines (of annual values) indicating different data sets. Shadings represent uncertainty (IPCC, 2013).

2.1. Ice sheets

Ice sheets are glaciers that cover an area of at least 50,000 square kilometers, and are in constant motion, due to gravitational stresses that cause ice deformation (National Snow and Ice Data Center, 2018). They move faster at the coastline since the ice flows through channelized outlets glaciers, ice streams, and ice shelves (National Snow and Ice Data Center, 2018). Ice sheets will remain in equilibrium as long as they gain the same mass in snowfall as they lose through melting and calving (Figure 2.2) (National Snow and Ice Data Center, 2018).

An ice sheet can be divided into a number of zones (Figure 2.2). Within the GrIS accumulation zone, which is where an ice sheet gains mass through snowfall, there are four other zones: the dry-snow zone, the percolation zone, the wet-snow zone, and the superimposed ice zone (Nolin and Payne, 2007). Within the dry zone, there is no melting as the air temperature is always below freezing. The dry zone is located at the highest elevations of the ice sheet. In the

percolation zone, there is partial surface melting, which percolates into the snow and refreezes (Nolin and Payne, 2007). The percolation zone is below the dry-snow zone, next in elevation (Figure 2.2). The meltwater that has penetrated the whole snowpack creates the wet-snow zone and as widespread refreezing occurs the superimposed ice zone is created (Nolin and Payne, 2007). Melting and refreezing of the current year's snow creates the superimposed ice; therefore, this zone is considered part of the accumulation area of the ice sheet. The lowest elevation zone is the bare-ice zone, which designates the ablation zone (Figure 2.2) (Nolin and Payne, 2007).

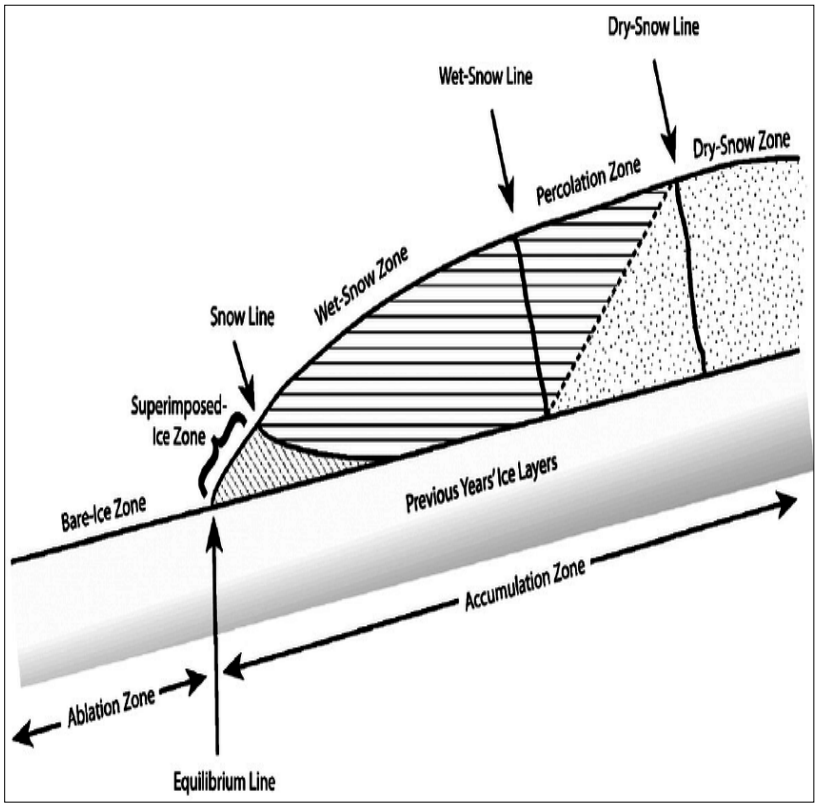

Figure 2.2. An image of the different glacier zones on Greenland ice sheet (Nolin and Payne, 2007, fig. 1).

An ice sheet experiences mass loss through snow and ice melt, evaporation, sublimation, wind erosion, or when ice is detached through calving. These mechanisms are collectively

referred to as ablation (Nolin and Payne, 2007). Calving is an effective ablation mechanism for glaciers and ice sheets that are exposed to the ocean. Enormous amounts of ice are removed by iceberg calving (Marshall, 2012, Chapter 6). Calving of icebergs to the ocean explains 40-50% of annual mass loss in Greenland, which makes it an important factor to consider (Marshall, 2012, Chapter 6). Most melting happens at the glacier surface. However, melting also occur englacially and subglacially (Marshall, 2012, Chapter 6). Melting that leads to run off and is removed from the system cause ablation, as some surface meltwater can percolate into the snowpack and refreeze (Marshall, 2012, Chapter 6). About 50% of the annual ablation occurs by surface melting (Marshall, 2012, Chapter 6) in Greenland, which also makes it a crucial factor (Nolin and Payne, 2007). This varies from year to year; in warm summers, such as 2012 and 2019, mass loss due to surface melting can account for as much as 75% of annual ablation.

2.1.1. Greenland Ice Sheet.

According to Alley et al. (2010), the Greenland ice sheet covers approximately 1.7 million km^2 and has a volume of 2.9 million km^3, with a maximum ice thickness of 3367 m and an average ice thickness of 1600 m. It extends 2200 km from north to south (Figure 2.3). The ice load has resulted in some bedrock below sea level, due to isostatic depression. However, with ice removal the bedrock would slowly rebound, with only a little staying below sea level. If all of the ice that rests on bedrock above sea level melted completely, it would contribute a globally averaged SLR of 7.3 m (Alley et al., 2010).

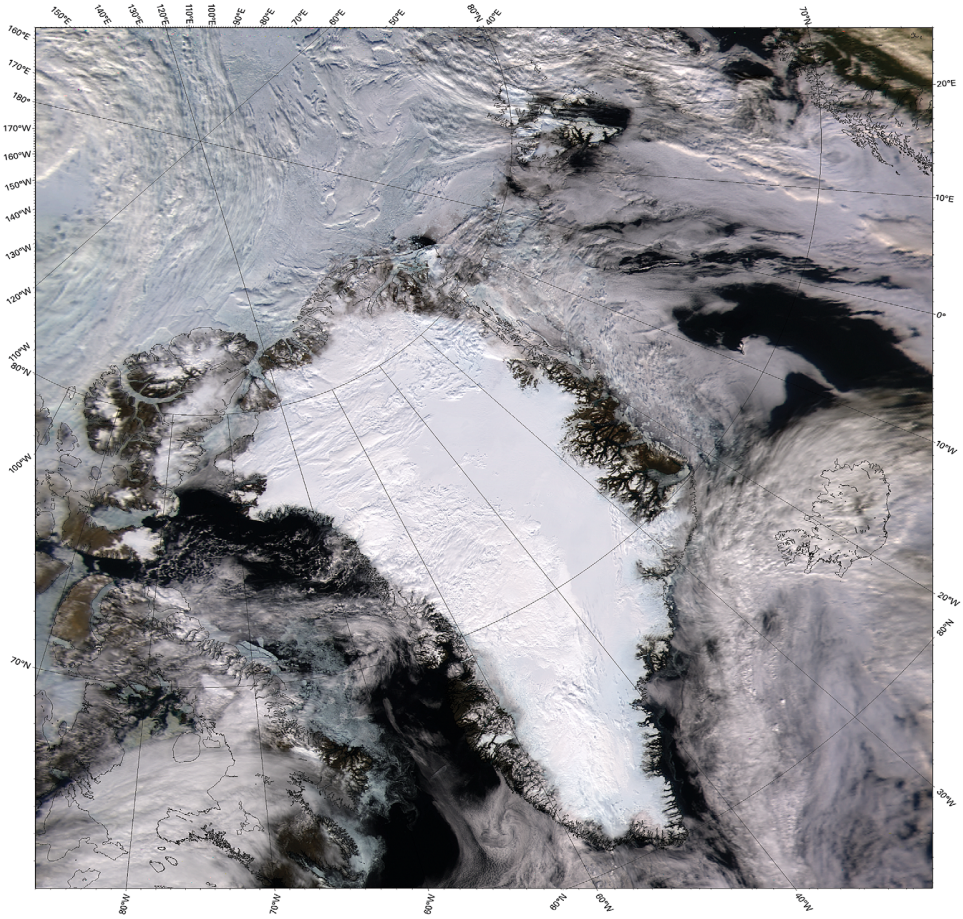

Figure 2.3. Satellite image (SeaWiFS) taken of the Greenland Ice Sheet on July 15, 2000 (Alley et al., 2010, fig. 1).

2.2. Stable water isotopes

Isotopes are variations of a chemical element, which contain a different number of neutrons, resulting in a different atomic mass. Water consists 99.7% of $H_2{}^{16}O$ but also contains $H_2{}^{18}O$, $H_2{}^{17}O$, and $HD^{16}O$ (Jouzel et al., 2013). Oxygen has the most commonly measured isotopes in glaciology. The most abundant oxygen isotope, ^{16}O, has eight neutrons and eight protons, while ^{18}O consists of ten neutrons and eight protons, making it heavier than ^{16}O. Similarly, deuterium (^{2}H or D) is heavier than ^{1}H. As a result, the slight differences in the physical properties of these stable isotopic molecules lead to fractionation at each phase change

of the water cycle, except sublimation and melting of compact ice (Gat, 1996; Jouzel et al., 2013), due to the different saturation vapour pressure and molecular diffusivities of the heavier and lighter water molecules (Schlosser et al., 2008). This causes variations in the distribution of water isotopes, both spatially and temporally in the atmosphere and in precipitation (Figure 2.4; Jouzel et al., 2013). As a result, the ratios of ^{18}O to ^{16}O ($\delta^{18}O$), and ^{2}H to ^{1}H (δD) provide excellent proxies for temperature and environmental conditions at the time of rain or snow deposition (Gat, 1996).

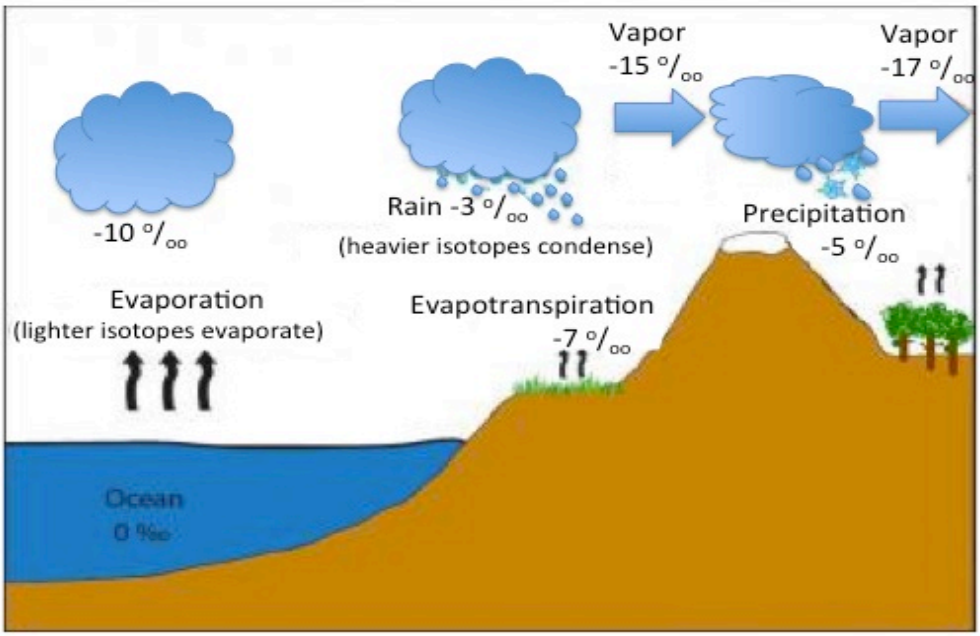

Figure 2.4. The isotopic fractionation process at each phase change with hypothetical ^{18}O values (adapted from Bruckner, 2019).

Isotopic concentrations are given with respect to a standard:

$$\delta = (R_{sample} - R_{SMOW}) / R_{SMOW} \quad (1)$$

where R_{sample} and R_{SMOW} are the isotopic ratios of the sample (e.g. $[^{18}O]/[^{16}O]$) and Vienna Standard Mean Ocean Water, respectively, with δ typically expressed in parts per thousand (per mil) (Jouzel et al., 2013).

The water cycle connects evaporation of oceanic water, cloud formation, vapour and cloud transfer by wind, precipitation, and the isotopes of the run-off water back to the ocean (Gat, 1996; Sokratov and Golubev, 2009; Brady et al., 2019). Stable water isotope distribution in precipitation is strongly related to climatological parameters (Sokratov and Golubev, 2009). The measured isotopic content of solid precipitation and its variations in land ice and snow are considered to represent climate variations (Sokratov and Golubev, 2009). Annual values of $\delta^{18}O$, δD, and annual mean air temperatures at observed precipitation sites are linearly related in middle and high latitudes (Dansgaard, 1964; Jouzel et al., 1983; Jouzel et al., 2013). Despite this, measurements indicate that only under relatively uniform meteorological conditions is it possible to construct a temperature-isotope relationship (Jouzel et al., 1983).

During evaporation, initial fractionation takes place in thermodynamic equilibrium (Jouzel et al., 1997). This equilibrium occurs only in a very thin layer at the water–air interface (Schlosser et al., 2008). The kinetic effect (i.e. the non-equilibrium effect) happens during molecular diffusion in the water layer right above (Schlosser et al., 2008), causing the lighter and heavier isotopes to behave differently (Jouzel et al., 1997). The amount of kinetic fractionation

during evaporation depends on sea surface temperature, relative humidity, and wind speed (Masson-Delmotte et al., 2006).

After water evaporates from the ocean or from inland water bodies, it can be carried to higher latitudes and altitudes, where the vapour condenses due to cooling, forming precipitation (Gat et al., 2001). Due to kinetic effects, the isotopic fractionation during evaporation is larger than the fractionation during the condensation process, which in turn results in the depletion of heavy isotopes in vapour and precipitation (Figure 2.4; Gat et al., 2001). As the distance from the ocean increases, the $\delta^{18}O$ in the precipitation becomes more and more depleted, which is called the continental effect or the distance-from-coast effect (Gat et al., 2001). The continental effect depends on the topography and the climate of the region, as well as the temperature gradient (Gat et al., 2001). The $\delta^{18}O$ in the precipitation gets more depleted at higher altitude, as well as higher latitudes (the altitude and latitude effect, respectively). The altitude and latitude effects are also temperature related, since temperature controls condensation (Gat et al., 2001).

As a result of these processes, the isotopic composition of precipitation is strongly correlated with the temperature at which the precipitation occurs (Dansgaard, 1964). The lower the temperature is, the lower the $\delta^{18}O$ (Dansgaard, 1964; Jouzel et al., 1983). Therefore, winter precipitation at a specific location is isotopically lighter than its summer values (Figure 2.5; Jouzel et al., 1983). This seasonal effect is especially noticeable in higher latitudes and therefore is of special interest in the snow layers over the ice caps of polar regions, where precipitation is preserved for long periods of time in its original order of deposition (Jouzel et al., 1983). Annual snow layers can be recognized by periodic seasonal variations of $\delta^{18}O$ (Figure 2.5; Gonfiantini et al., 1963).

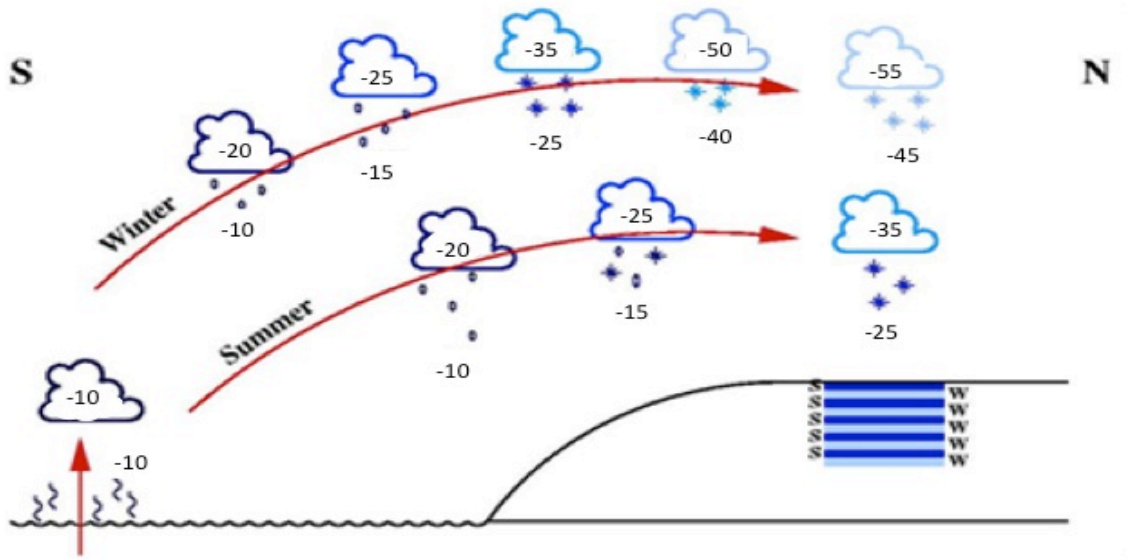

Figure 2.5. Stable water isotopic value depletion during fractionation processes by comparing summer and winter seasons with the distinguishable summer and winter layers within the ice (adapted from Centre for Ice and Climate, 2019).

Past changes in evaporation conditions or atmospheric transport might cause biased temperature reconstructions of $\delta^{18}O$ (Masson-Delmotte et al., 2006). In fact, the temperature at the time and height of condensation is the main control on isotopic composition of snowfall and not the surface temperature (Masson-Delmotte et al., 2006). Masson-Delmotte et al. (2006) noted that in central Antarctica, the condensation temperature is almost the same as the temperature in the inversion layer, which is linearly related to the surface temperature. However, the same should not be assumed for coastal Antarctica or Greenland, as convective activity takes place episodically in these locations. For that reason, changes in the vertical temperature profiles might impact past temperature reconstructions. In addition, changes in the seasonality of precipitation, as well as post-depositional effects might also cause biases in temperature reconstructions from ice cores (Masson-Delmotte et al., 2006).

Anderson et al. (2016) concluded that temperature is well correlated with the majority of $\delta^{18}O$ variations for some individual storms, locations, and years. However, local temperature can sometimes have little or no influence on $\delta^{18}O$, meaning that other factors must be in control (Anderson et al., 2016). Water vapour source, transport history, and post-depositional processes within the snowpack could be among the controlling factors (Sinclair and Marshall, 2009; Anderson et al., 2016).

Isotopic data retained in individual precipitation events can be modified by a number of different processes, such as meltwater percolation, wind scour, depositional sublimation, meltwater refreezing, and vapour diffusion (Moran and Marshall, 2009). As a result, the interpretation of $\delta^{18}O$ profiles in these records requires a crucial evaluation of the impact of post-depositional processes on the isotope stratigraphy. On a seasonal timescale, these processes smooth the isotopic variability recorded in the snowpack stratigraphy. This reduces the interannual variability retained in the ice cores, which makes it difficult to use stable water isotopes as paleothermometers on longer timescales (Moran and Marshall, 2009).

2.3. Post-depositional isotopic modifications

Stable water isotopes in precipitation, such as $\delta^{18}O$, are dominated by the advective transport and condensation history of precipitation, and especially the temperature in the cloud system during condensation (Dansgaard, 1964). Solid-phase precipitation represents these characteristics in such a way that accumulated snow and ice record the history and environmental conditions during precipitation events. Snowpacks that survive summer melting can preserve the annual isotopic cycle, enabling the reconstruction of high-resolution temperature records from ice cores.

In general, it is assumed in ice-core research that there is negligible post-depositional isotopic modification, as long as the near-surface snow remains cold and dry (i.e., below freezing). However, several processes can modify the isotope stratigraphy. “The most significant post-depositional process is probably wind scour or loading but they also include sublimation, frost and rime condensation, vapor circulation, and basal melt” (Anderson et al., 2016). Post-depositional modifications compromise the interpretation of precipitation isotopes as thermometers both on a seasonal timescale and in longer-term analyses (Sinclair and Marshall, 2008), and it is important to consider whether such processes occurred at ice-core sites. “Each of these mechanisms is non-linear, highly local, and can only be studied effectively with process modeling validated by monitoring” (Anderson et al., 2016).

2.3.1. Effects of vapour diffusion.

Sublimation effects occur in the near-surface snow and could deprive the snowpack of light isotopes, specifically during extended dry periods (Anderson et al., 2016). If phase changes remove light isotopes, then the remaining snow will be more enriched (Anderson et al., 2016). Fractionation has been documented in snowpacks in association with the non-equilibrium processes related to water-vapor diffusion (Sinclair and Marshall, 2008). At the ground–snow interface of alpine snow-packs, cold atmospheric conditions combined with the input of geothermal heat can create strong temperature (hence vapour pressure) gradients, promoting vapour transport, recrystallization, and depth-hoar formation (Sinclair and Marshall, 2008). This has shown to be associated with increased heavy isotopic concentration in the lowest layers of the snowpack (Sinclair and Marshall, 2008; Anderson et al., 2016), since heavy isotopes are the first to condense or be deposited from the vapour. Solid diffusion may be neglected in the

snowpacks; however, vapour-phase diffusion within the snow matrix is 1000 times faster and reduces isotopic gradients in times of sublimation and redeposition in snow and firn (Sinclair and Marshall, 2008).

2.3.2. Effects of wind scouring.

Wind scouring may mainly impact low-density (i.e. winter) snowfall, leaving the remaining snow enriched in heavy isotopes (associated with warmer conditions), in contrast to wind-loaded areas, which may be biased toward lower isotope values (Anderson et al., 2016). In addition, spring and summer precipitation on glaciers and ice sheets would also enrich the snowpack (Sinclair and Marshall, 2008).

2.3.3. Snow isotopic content change by melts.

Snowpack enrichment may also be due to mass loss from erosive sublimation, evaporation, or meltwater runoff, if these processes are associated with fractionation and preferential removal of heavy or light isotopes from the snowpack (Sinclair and Marshall, 2008). Field studies by Moran and Marshall (2009) indicate that meltwater percolation may affect the accuracy of palaeoclimatic reconstructions. It can decrease seasonal isotopic signals and cause isotopic enrichment, as well as initiate time gaps. The isotopic fractionation resulting from refreezing and evaporation of meltwater in the snowpack could influence the ability of isotopic values to be used as accurate proxies of environmental change. Hence, this should be noted when interpreting climatic information from ice cores drilled in areas with high amounts of summertime melt.

Pohjola et al. (2002) acknowledge the reduction of seasonal range in isotopic values that occurs with meltwater percolation. However, Pohjola et al. (2002) conclude that due to the

similarity between annual $\delta^{18}O$ values from an ice core site and modified coastal values for a geographical gradient, water isotopes appear to be only slightly affected. There were indications of smoothing of the record as well as some diffusion, yet atmospherically deposited signals were preserved in their depositional layer. This is in contrast to the significant evidence of $\delta^{18}O$ signal modifications Goto‐Azuma et al. (2002) found due to melting, which restricts the use of $\delta^{18}O$ signals as a temperature proxy.

Moran and Marshall (2009) investigated the modification of snow temperature, water content, density and stable water isotopes of $\delta^{18}O$ at four Arctic snow-pit sites during early-season melt. The goal was to understand the impact of melt on snowpack stratigraphies and seasonal isotopic signals. Moran and Marshall (2009) associated isotopic changes observed at the four Arctic snow-pit sites to temperature reconstructions that were obtained from a 33-year firn-core record drilled on the same icefield, and came to the conclusion that preservation of annual isotopic signals does not mean that isotopic values are preserved.

Positive degree-day (PDD) values can be used as proxies for melt-induced isotopic correction (Moran and Marshall, 2009). It is based on Braithwaite's (1995) assumption that PDD values are linearly related to melting of snow and ice. PDD is defined as the summation of all temperatures above $0^{o}C$ (melting point) over a period of time. Moran and Marshall (2009) used empirically obtained linear relationships between PDD and isotopic modification to extrapolate between the amount of isotopic enrichment, which were estimated to be +0.08 ‰ $(PDD)^{-1}$. A temperature-isotope relationship is then required to be able to relate isotopic modifications to errors in the isotopic temperature estimates. There is a wide range of temperature-isotope relationships in literature. However because this study focuses on temperature reconstructions on

Greenland and especially NEEM, the reported value of 2.1 ± 0.5 °C $‰^{-1}$ in the NEEM research paper (2013) is considered to be appropriate.

2.4. The last interglacial period (Eemian)

High latitudes of both north and south hemispheres were warm during the last interglacial period (129 to 116 ka) compared to the pre-industrial era, primarily due to greater Earth axial tilt and eccentricity in the Earth-Sun orbit, which combined to give increased summer insolation at high latitudes (Turney and Jones, 2010; McKay et al., 2011). Surface temperatures during the last interglacial period are estimated to have peaked at 8 ± 4^{o}C above the mean temperature of the past millennium at NEEM, based on stable water isotopes (Figure 1.3; NEEM Community Members, 2013). Substantial amounts of surface melting occurred at NEEM during the last interglacial period (NEEM Community Members, 2013).

As mentioned above, based on the NEEM Community Members (2013) results, temperatures were estimated to have reached 8°C above present. During the summers of 2012 and 2019 it was not this warm; nevertheless, the entire interior plateau of the GrIS experienced melting (Arctic Report Card, 2019). Isotopic fractionation due to melting and refreezing may have affected the isotopic records, and accounting for this could improve isotope-temperature reconstructions in Greenland ice cores. This would result in revised estimates of peak LIG warming; peak warming in Greenland may have actually been less than 8°C, due to meltwater effects that lead to isotopic enrichment in firn and ice.

There has been no simulation of the LIG period with an atmospheric general circulation model that includes the water isotopic composition (Masson-Delmotte et al., 2006). Analysis of the temperature-isotope relationships in LIG climate simulations of GCMs with stable water

compositions would shed some light on the above estimates (Masson-Delmotte et al, 2006), by including both potential changes in the vapour source region and changes in air-mass trajectory.

2.5. Ice cores

Ice cores are paleoclimate archives that contain important physical and chemical information about past climate and atmospheric changes (Masson-Delmotte et al., 2006). Of particular interest for my study are stable isotope records of the ice cores, because they are proxies for the temperature and precipitation history in a region (Figure 2.6).

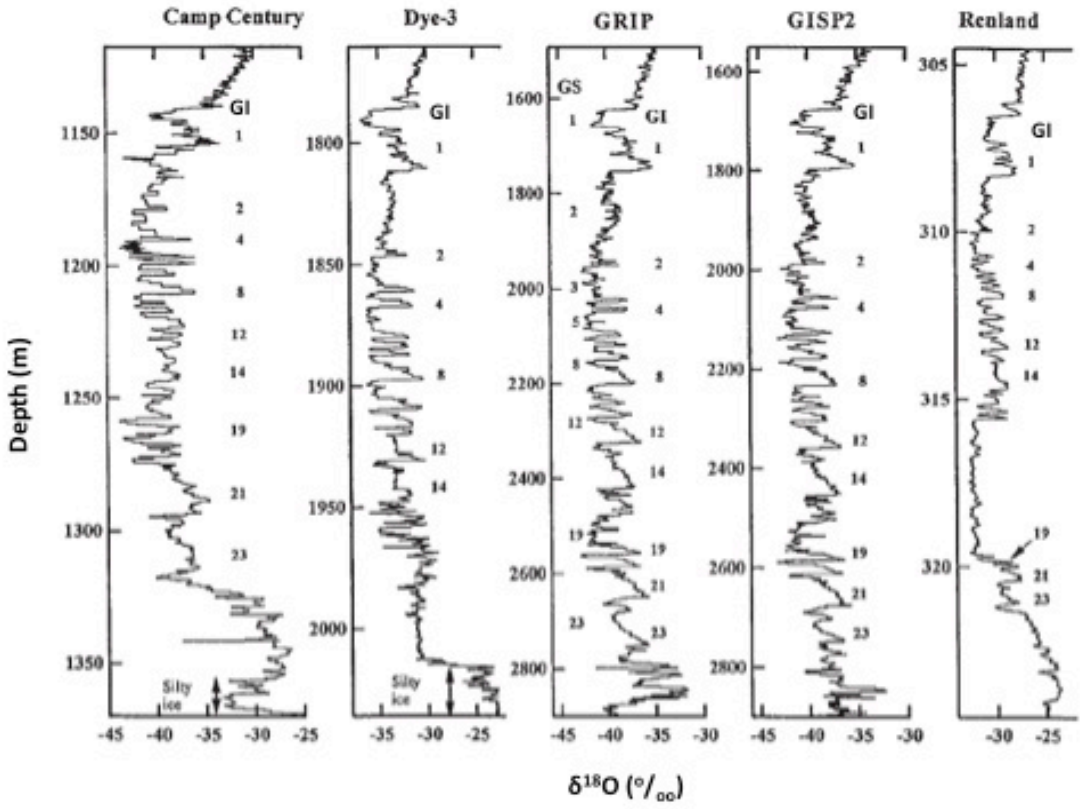

Figure 2.6. $\delta^{18}O$ profiles of five Greenland deep ice-cores that extend from the present to some period before the beginning of the last glacial stage. Warm Greenland Interstadials (GI) and cold Greenland Stadials (GS) are numbered to the right and left of some profiles, respectively (Johnsen et al., 2001, fig. 2).

The flow of ice over uneven bedrock topography has resulted in folding of ice older than 105,000 years ago, and disturbed layers of ice about 300 m above at the bottom of both Summit ice cores (GRIP and GISP2) (Figure 2.7). Due to the disturbed ice deposition during the Eemian period, researchers sought for a new drill site with undisturbed Eemian ice, which resulted in the North Greenland Ice Core Project (NGRIP) and NEEM ice core (University of Copenhagen, 2019). It should be noted however that the NGRIP only contains the last part of the Eemian (University of Copenhagen, 2019), and NEEM ice core is also folded for the Eemian period (NEEM Community Members, 2013).

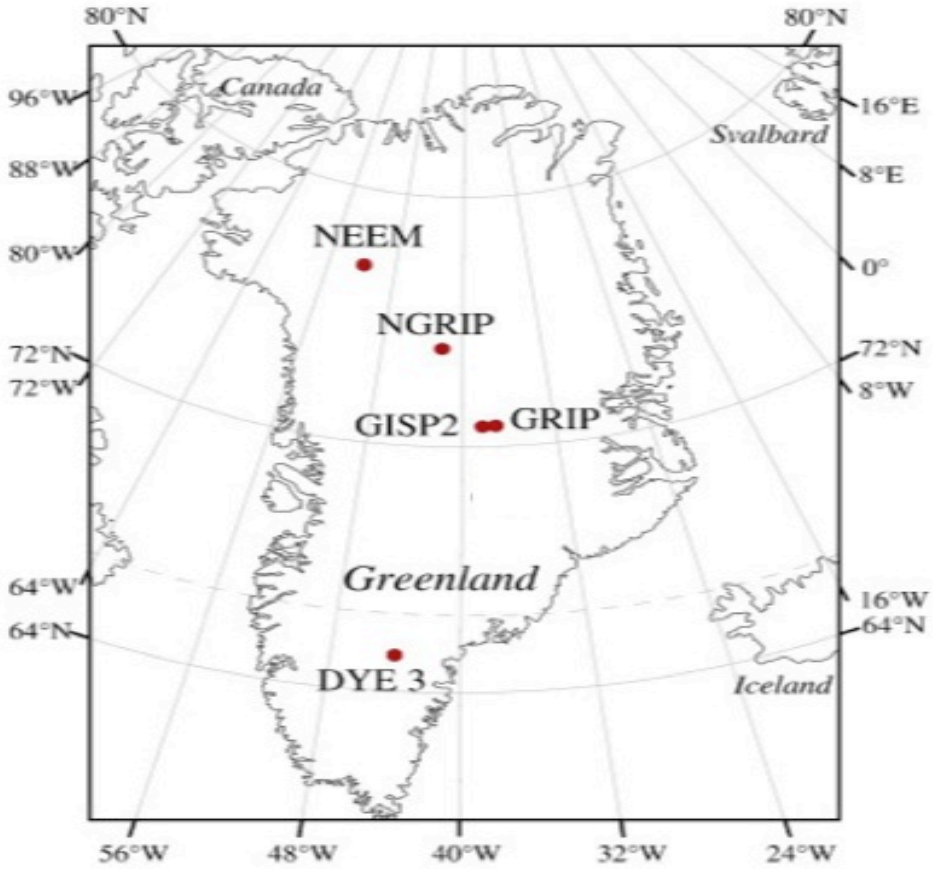

Figure 2.7. The location of five deep drilling sites in Greenland (adapted from Abbott and Davies, 2012).

Quantitative temperature reconstructions are vital to be able to compare ice core records and climate models (Masson-Delmotte et al., 2006). Masson-Delmotte et al. (2006) obtained quantitative information on past temperature changes and concluded that to reproduce the observed magnitude of polar temperature changes, the glacial-interglacial temperature intensity evaluated from deep ice core sites could be used to study the capability of climate models (Figure 2.8). Climate models systematically underestimate the magnitude of temperature change in comparison to the ice-core values. One limitation of this kind of comparison could be due to change in the ice sheet topography that are not well understood and are incorrect in the model simulations (Masson-Delmotte et al., 2006).

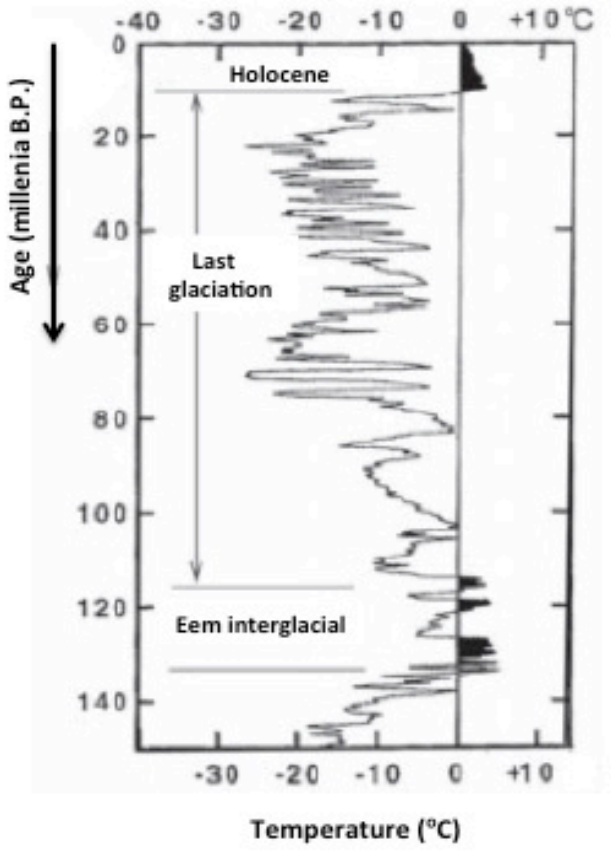

Figure 2.8. Greenland temperature (^{o}C) deviations compared to present time calculated from the GRIP ice core (Dansgaard, 2005).

2.6. Coupled ice-sheet/climate models

Ice sheet models are numerical tools that are used to simulate the mass balance and flow dynamics of ice sheets. Given a certain climate forcing and assumptions about the ice rheology, these models predict how the three-dimensional ice sheet velocity and temperature structure will evolve. This in turn influences how the ice sheet geometry (thickness, area, and volume) changes for a given climate history. Ice sheets have a long memory; the deep ice in Greenland is 10s of 100s of kyr in age. Simulation of the present-day GrIS therefore requires one to carry the model back through the last glacial cycle. Lhomme et al. (2005) recommend a simulation of at least the last 200,000 years in order to examine the internal structure of the present-day ice sheet.

Scientists have recognized that developing coupled ice-sheet/climate models and their application to simulate past and future coupled system behavior is crucial to scientific and policy-relevant goals (Hanna et al., 2013). Uncoupled ice sheet simulations can produce physical inconsistencies and therefore using coupled ice-sheet/climate models are highly beneficial and allows consideration of coupled feedbacks (e.g., Ridley et al., 2010). However, there are contrasting timescales and technical complexities, which have delayed modellers to implement full ice-sheet/climate coupling. In a ‘one-way’ coupled simulation of ice sheets, surface mass balance (SMB) is calculated within a climate simulation and directed to the ice sheet model, with no feedbacks (e.g., Gregory and Huybrechts, 2006; Otto-Bliesner et al., 2006). Topography and surface types of the land and atmosphere models are fixed. On the contrary, in ‘full’ or ‘two-way’ coupling, the surface types, surface elevation, and albedo fields evolve as the ice sheet grows and retreats. One-way coupling can be valid for timescales of about 100 years or less, as the surface elevation and areal coverage of the major ice sheets in Greenland and Antarctica is

not expected to change much over this timescale (CESM Land Ice CESM2.0 documentation, 2018).

2.6.1. The U of C ice sheet model.

The U of C ice sheet model is a 3D coupled-ice-and-heat-flow model of Marshall and Clarke (1997), including a tracer model for oxygen isotopes (Clarke and Marshall, 2002; Lhomme et al., 2005). Ice sheet dynamics and thermodynamics are solved on vertically transformed co-ordinates with linear interpolation between grids. The ice sheet model is also based on the shallow ice approximation, with simple higher-order treatments of floating ice and iceberg calving fluxes. I will work with this model because of its existing tracer model and experience tracking stable water isotopes through the ice sheet system.

The model has been applied to past reconstructions and future projections of the Greenland Ice Sheet in several different studies (e.g., Marshall and Cuffey, 2000; Otto-Bliesener et al., 2006; AMAP, 2009). The mass balance calculation in the ice-sheet model uses the positive degree-day (PDD) method. The usage of the PDD method for exploring ice sheet evolution in climate change studies has been criticized, as it does not account for all of the physics involved in snow and ice melt, but a full surface energy balance is difficult to apply in paleoclimate studies, as it requires detailed information of a large number of meteorological fields (e.g., cloud cover, wind, humidity). The PDD model is simpler to implement, requiring estimates of past temperature on monthly or annual timescales. These can be distributed over the ice sheet topography using a prescribed lapse rate. Precipitation fields are also required to estimate snow accumulation over the ice sheet.

Different climate forcing can be applied where sufficient climate information is available. For recent historical runs (i.e., on decadal time scales), these can be acquired from climate reanalyses, and a full surface energy balance is possible. Similarly, future climate simulations on century timescales could be forced by climate models, although with less skill than climate reanalyses as models of future climate change are not constrained by observations. For paleoclimate simulations, however, it is conventional to apply climate perturbations from present-day spatial patterns (ΔT, ΔP), based on ice-core records. Ice cores in central Greenland give a good idea of ΔT, based on isotope thermometry, while ΔP is inferred from the change in annual layer thickness of net accumulation in ice cores. Central Greenland contains an intact record of these two proxies for the past ~110 kyr, but no clean records exist prior to that. Hence, simple ΔT scenarios are needed to extend simulations to the last 200 kyr, typically based on a splice of Antarctic and Greenland ice core reconstructions (Cuffey and Marshall, 2000). I will work with this model because of its existing tracer model and experience tracking stable water isotopes through the ice sheet system. The next chapter provides details on how I applied the U of C ice sheet model to study the NEEM core and explore Eemian reconstructions of GrIS.

Chapter 3 Methods

To address the contribution of Greenland to past SLR, I use the U of C ice sheet model, running on the WestGrid and Compute Canada platforms. WestGrid and Compute Canada, in partnership, gather advanced computing facilities, research data management services, and technical experts for innovative researchers (WestGrid, 2016). They also employ advanced research computing systems, software and storage solutions (Compute Canada, 2016).

The ice sheet model was used to run from 200 ka till present using 10 different temperature scenarios based on the NEEM and Summit ice cores (Cuffey and Clow, 1997; NEEM Community Members, 2013). As noted above, an initial time of 200 kyr BP is needed to allow for an appropriate model spinup going into the LIG, i.e. with a realistic internal (3D) temperature and isotope structure in the model (Lhomme et al., 2005). The climate scenarios produce a range of scenarios for GrIS geometry in the LIG, and I use ice core reconstructions to examine model output against the NEEM ice core. The isotope tracer model allows me to trace stable water isotopes ($\delta^{18}O$) of precipitation through the ice sheet (Figure 3.1), which can be used to better understand the ice sheet history and to validate (or invalidate) different model reconstructions. Temperature modification was also investigated to analyze the potential effects of ice core enrichment due to melting.

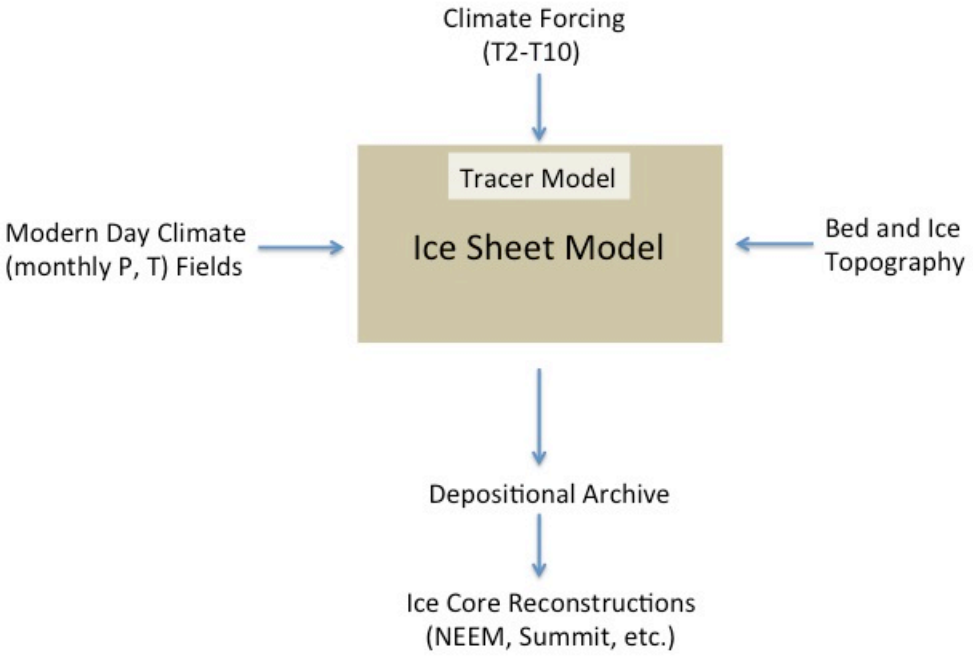

Figure 3.1. Schematic diagram illustrating the big picture behind the ice sheet modelling, and reconstruction of ice cores.

3.1. Paleoclimate data

To be able to construct a climatic temperature history, a time dependent temperature perturbation (ΔT $(t)_{paleo}$) is added as a perturbation onto the prsent-day temperature fields, T $(x,y)_{pres}$ (e.g., Quiquet et al., 2013). By assuming a uniform lapse rate of $\beta = -0.006°C\ m^{-1}$ over Greenland, the impact of changing ice sheet surface topography, Δh (x,y,t) is also taken into consideration: ΔT $(x,y,t)_{topo} = \beta \Delta h$ (x,y,t). The air temperature at any point and time on the ice sheet is then:

$$T(x,y,t) = T\,(x,y)_{pres} + \Delta T\,(t)_{paleo} + \Delta T\,(x,y,t)_{topo} \quad (1)$$

The paleotemperature comes from the climate proxy data, inferred from $\delta^{18}O$ at NEEM or GISP2, which is converted to temperature with the following formula:

$$\delta^{18}O(t) = \alpha T(t)_{paleo} + b \quad (2)$$

The α coefficient is the isotopic slope and b is the $\delta^{18}O$ intercept (Cuffey and Clow, 1997; Jouzel et al., 1997; Quiquet et al., 2013). The $\Delta T\,(t)_{paleo}$ perturbation is then calculated from $\Delta T(t)_{paleo} = T(t)_{paleo} - T_{pres}$

at the relevant ice core site.

3.1.1 Temperature Scenarios.

To obtain a long-term climate history, I take $\Delta T(t)_{paleo}$ from the temperature calibration of the GISP2 project ice core $\delta^{18}O$ record for the most recent 97.8 ka, and extend the GISP2 $\delta^{18}O$ ice core reconstruction with temperature estimates from the NEEM $\delta^{18}O$ record (NEEM community, 2013) from 97.8 to 128 ka. For times older than this, no Greenland ice core data is available, so the Vostok ice core $\delta^{18}O$ record is mapped onto Greenland from 128 to 200 ka, after Marshall and Cuffey (2000).

Specific to the NEEM record, I use a dataset of 18,000 isotope temperature records/entries (nine different temperature scenarios; Figure 3.2) compiled by Kurt Cuffey (personal communication, 2016), using the NEEM isotopic record with isotope-temperature relationships based on Cuffey and Clow (1997). The goal of using this compilation is to provide a range of anomalies that span the potential temperature conditions during the LIG for the region of northwest Greenland that is of particular interest in my study.

To obtain a long-term climate history for Summit (Figure 3.3), I use Marshall and Cuffey's (2000) the temperature calibration of the GISP2 project ice core $\delta^{18}O$ record for the most recent 102 kyr. And for times older than 102 ka, the Vostok ice core $\delta^{18}O$ record is mapped onto Greenland to 200 ka, after Marshall and Cuffey (2000).

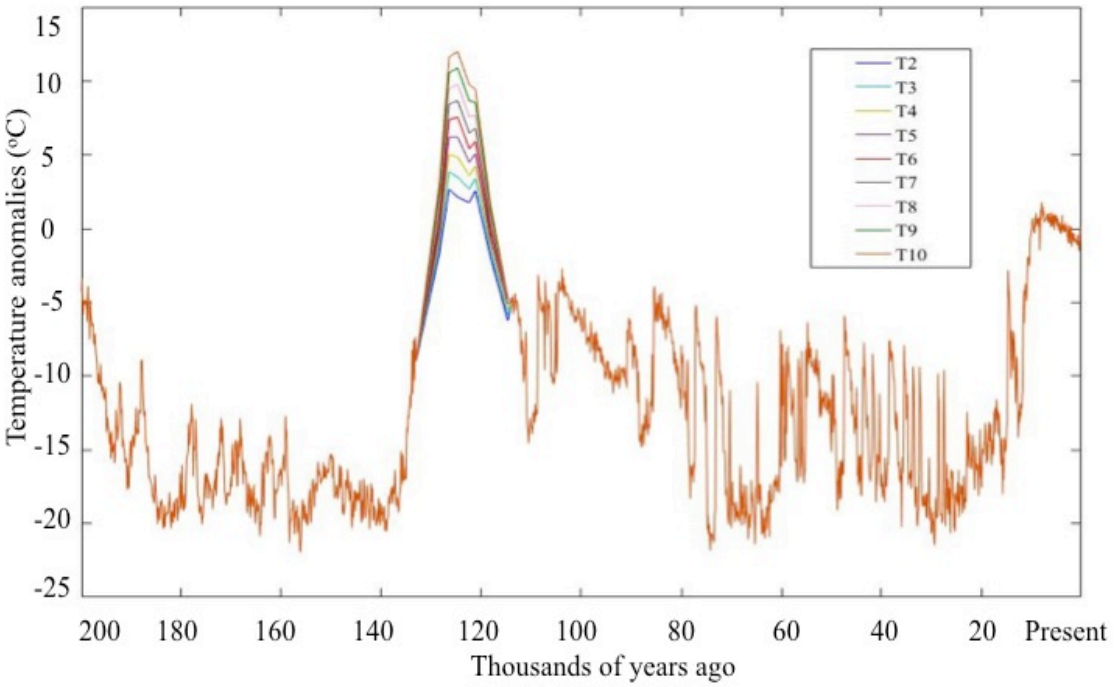

Figure 3.2. Temperature forcing anomalies (T2-T10) over the past 200 kyr.

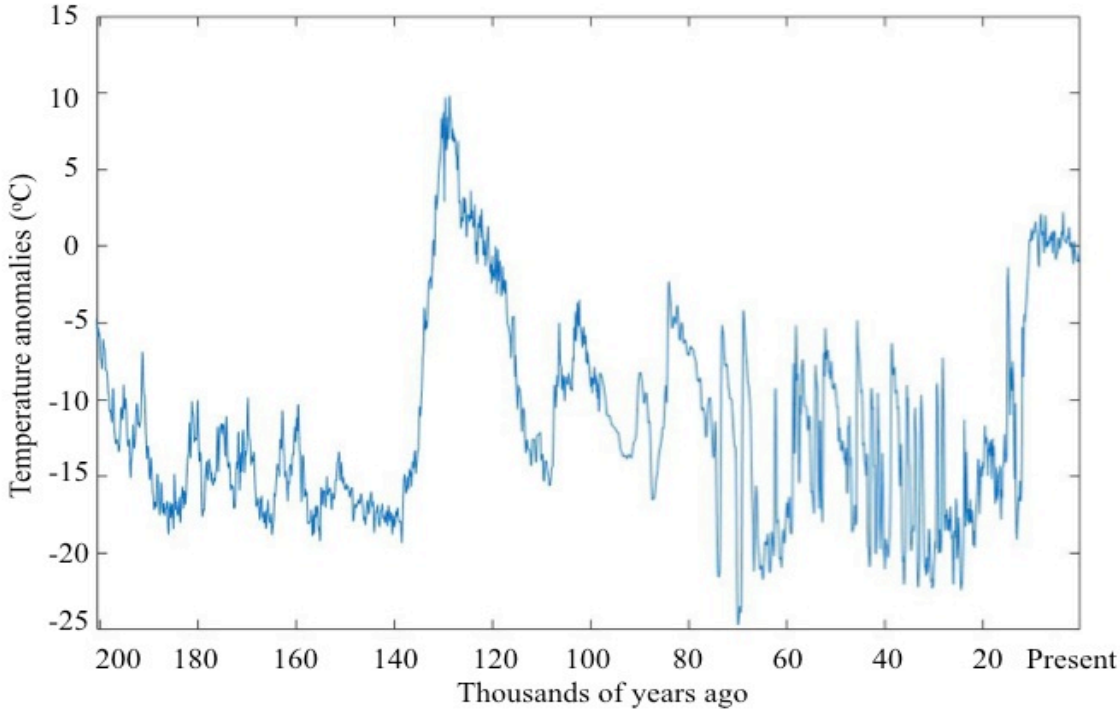

Figure 3.3. Summit temperature forcing anomalies over the past 200 kyr.

3.1.2. NEEM ice core.

The GICC05 model-extended time scale is taken from the NGRIP core using linear interpolation between 740 match points of the NEEM and NGRIP ice core records, which starts from the surface down to the depth of 2203.6 m (108.17 ka). Below this depth, ice has been folded (NEEM community members, 2013). Between 108.17 ka and 122 ka (NEEM depth of 2203.6-2398.2 m), global methane (CH_4) and $\delta^{18}O_{air}$ records from NGRIP and Antarctica, cross-dated via the EDML time scale, as well as NGRIP $\delta^{18}O_{ice}$, were used to match NEEM records back to the oldest NGRIP record i.e. 122 ka. Since that does not cover the entire Eemian record, the lower section of the NEEM core between 2398.2 m and 2432.2 m is matched to the global CH_4 and $\delta^{18}O_{air}$ records from Antarctica, cross-dated via the EDML time scale (NEEM community members, 2013), to extend back to 128 ka. More on the time scale is described in detail in the Supplementary Information of NEEM community members (2013).

3.2. Defining present and LIG target intervals

To be able to consistently compare both reconstructed and simulated present and LIG period temperature trends, I need to define target intervals. The main criterion in defining these intervals is that the Eemian ice sheet needs to be compatible with available constraints on its past elevation and extent. To meet this criterion the minimum ice volume was examined for each temperature scenario. For this purpose, we identified the timing of the maximum change in the ice sheet in the LIG period at 125 ka for cases T2-T5 and 125.5 ka for T6-T10. This is consistent with the approach of the NEEM Community Members (2013), who defined the peak surface temperature at 126 ka. There can be a lag between the peak of temperature and minimum ice sheet volume, as the ice sheet geometry responds to cumulative periods of negative mass

balance, which causes thinning and retreat of the ice sheet margins. These defined intervals do not cover the whole LIG period.

3.3. The ice sheet model

The U of C ice sheet model is a 3D coupled thermomechanical model developed by Marshall and Clarke (1997), with 0.8° longitudinal resolution, 0.2° latitudinal resolution, and 20 layers in vertical in the default model over Greenland. The model uses spherical co-ordinate (a latitude-longitude grid), with grid cells roughly equivalent to 22.2 km North-South and 44.5, 30.4, and 15.5 km at 60°, 70° and 80°N. The model also includes elevation changes as a result of isostatic response of the crust.

As thermomechanical coupling is invoked, the vertical dimension is added in the dynamic solution and 3D velocity fields are calculated. Thermodynamics are solved after Jenssen (1977) in the style of Huybrechts (1986). Dynamics and thermodynamics are solved on vertically transformed co-ordinates with linear interpolation between grids. User inputs are required for numerical/physical option flags, and model integration limits. Global parameters and dimensions are set at run-time. A degree-day mass balance treatment table-look up (Wake and Marshall, 2015), and a uniform geothermal heat flux are set for the ice sheet. PDD are calculated from the monthly temperature data and ice elevations at each point in the grid.

Present-day precipitation rates over the ice sheet, $P\,(\mathrm{x,y})_{\mathrm{pres}}$ are taken from the gridded dataset of Bales et al. (2001, updated in 2009), which is based on historical station data and ice core records, interpolated onto the model grid. Precipitation is adjusted in time through a simple scaling factor $f_P\,(\mathrm{t})$: $P\,(\mathrm{x,y,t}) = f_P\,(\mathrm{t})\,P\,(\mathrm{x,y})_{\mathrm{pres}}$. The scaling factor is based on the ratio of past to present-day annual accumulation in the GISP2 ice core for the past 97.8 ka (Cuffey and Clow,

1997, 1999); this is assumed to apply to the whole ice sheet. In earlier periods, changes in past precipitation rates are assumed to scale with the temperature anomaly, ΔT, following $f_P(t) = \exp(0.0693\Delta T)$ when $\Delta T \geq 0°C$ and $f_P(t) = \exp(0.115\Delta T)$ when $\Delta T < 0°C$. This is modelled after Cuffey and Clow (1997), and is related to the change in saturation vapour pressure with temperature (the Clausius-Clapeyron effect) as manifest at the GISP2 site in central Greenland.

The ice sheet model tracks the spatial and temporal evolution of the bedrock topography (h_b) and the ice surface topography (h_s), following:

$$h_s(x,y,t) = H(x,y,t) + h_b(x,y,t) \quad (3)$$

where H stands for thickness of the ice. The evolution of the ice sheet with time follows

$$\frac{\partial h_s}{\partial t} = -\nabla \cdot q + b(x,y,t), \quad (4)$$

where q is the ice sheet flux (m^2/yr) and b is the surface mass balance (m/yr): the net annual accumulation minus ablation of ice. The notation $\nabla \cdot q$ refers to the ice flux divergence, which is essentially representing the flow of ice into and out of a grid cell. For surface mass balance, surface accumulation and ablation are calculated using the PDD method based on monthly temperature and precipitation values. Further details on the model physics are described in full in Marshall and Clarke (1997).

3.4. Climate forcing

3.4.1. Present day climate forcing.

The evolution of the GrIS for the last 200,000 years was modelled using the U of C ice sheet model, using the ice-core based climate forcing described above. Present-day temperature over the ice sheet is prescribed after Reeh (1991), based on a sinusoidal annual temperature

cycle. The annual sinusoid is sampled monthly, to give a monthly resolution of the climate forcing, and stochastic variability is superimposed on the monthly mean temperature following Wake and Marshall (2015). The climate forcing is updated every 100 years, including a perturbation for climatic change and local elevation change (lapse rate feedbacks).

The climatic forcing for the model consists of nine NEEM temperature scenarios and an additional simulation forced by the GISP2 ice core record, after Cuffey and Marshall (2000). For the Eemian warming from the NEEM scenarios, minimum, mean, and maximum temperatures are represented by cases T2, T6, and T10 (Cuffey and Clow, 1997), respectively, at all grid points on the ice sheet surface, as functions of time. The temperature forcing time series spans 200,000 presenting the penultimate glacial period, the Eemian interglacial, the last glacial period, and finally the Holocene period and post-industrial warming. Time '0' nominally refers to the year 1950.

3.4.2. Model initialization.

I initialize the model by starting with present-day bed and surface topography as initial conditions and running a 100-kyr simulation (i.e. from 300 ka to 200 ka) with a fixed climate 10^{o}C colder than present. There are pockets of deep ice in Greenland as much as 200,000 years old today, but the climate 'memory' for the overall ice sheet geometry is mostly dictated by the internal temperature structure, which has a memory of about 35,000 years; effects of the initial geometry and temperature structure are erased after 35,000 years due to diffusive processes (Clarke and Marshall, 2002). By initiating the glacial cycle runs at 200 ka, this should eliminate effects of the initial condition on the Eemian ice sheet reconstruction. The age of the ice is traced throughout the 3D ice sheet structure. The Eemian is my main focus; however the model is run to

the present to evaluate whether particular model settings give an accurate reproduction of the modern GrIS.

3.5. The tracer model

The tracer code is adapted from Clarke and Marshall (2002), and Lhomme et al. (2005). It is coupled with the ice sheet model and is called with a time step of 100 years, chosen to match the climate update. Provenance markers identify time and location (latitude and longitude) of deposited snow on the surface of the ice sheet. The trajectory of these depositional provenance markers is tracked with the tracer code, based on the 3D velocity fields. This means that as snow falls on the surface of the ice sheet, the depositional location of that snow has a birth marker, which will be carried throughout the ice sheet as that snow turns to ice, migrates, melts, or calves from the ice sheet. The time evolving 3D structure of the provenance markers provides a depositional archive, which can be interpolated to provide a detailed stratigraphic reconstruction of the marker of interest. The provenance markers do not directly provide the isotopic stratigraphy of the ice, but this can be constructed if one knows the isotopic ratio of snowfall at a given time and location (e.g., through ice core records, the isotope-temperature relationship (Lhomme et al., 2005), or isotope-enabled climate models (e.g., Brady et al., 2019)).

3.6. Reconstructing the ice cores

Using the depositional archive, the modelled stratigraphy at the NEEM and Summit ice core sites can be reconstructed to compare model output to the observed ice cores (Lhomme et al., 2005). Tracer provenance markers include values for latitude, longitude, elevation, air temperature, and time of origin for every point in the 3D ice sheet grid. The spatial values are not

positioned column-like within the depositional archive. The points are located within quadrilateral regions that are approximated by bilinear interpolation (Clarke and Marshall, 2002). Isotopic stratigraphies can be reconstructed through the application of a temperature-isotope relationship, e.g. after Cuffey and Clow (1997).

3.7. Temperature modifications and data analysis

Melt estimates based on positive degree-day (PDD) values are used as proxies for melt-induced isotopic correction, after Moran and Marshall (2009). Based on field studies of isotopic modifications during melt, Moran and Marshall (2009) derived a linear relationship between PDD and $\delta^{18}O$ enrichment, equal to $+0.08\,^{o}/_{oo}\,(PDD)^{-1}$.

A $\delta^{18}O$–temperature relationship must also be assumed, in order to link isotopic modification to temperature change estimates. A wide range of $\delta^{18}O$–temperature relationships is available in different research and reports. However, because this study focuses on temperature reconstructions on Greenland and especially NEEM, I use the reported value of $2.1 \pm 0.5\ °C\ ^{o}/_{oo}{}^{-1}$ from the NEEM research paper (2013).

Chapter 4 Results and analysis

4.1. Greenland Ice Sheet over the last 200 kyr

The purpose of this section is to give a sense of the complete model simulation over the last glacial cycle in Greenland. I present the results of the model for the last 200 ka, before focusing in on the Eemian period. Figure 4.1 plots modelled ice sheet volume over the full time frame, in response to the temperature scenarios shown in Figure 3.2.

The volume of the ice sheet is stable with some fluctuations from 200-145 ka, but increases as temperature increases at around 140 ka (Figure 3.2 and Figure 4.1), in response to an initial increase in snow accumulation in the warmer early-Eemian atmosphere. Volumes then decrease in response to the Eemian warmth, with the magnitude of the ice sheet decline dependent on the extent of Eemian warming (i.e., from T2 through to T10). The temperature scenarios (T2 to T10) differ markedly during the Eemian, with peak warming of between 2.5 and 12°C at about 126 and 125 ka, respectively (Figure 3.2). This period is examined in greater detail in section 4.2.

The ice sheet recovers after the Eemian warmth, starting into the last glacial cycle at about 115 ka. There is only a small influence of the Eemian ice sheet extent through the glaciation, which lasted from ~110 to ~11 ka. Ice sheet volume fluctuates between 3 and 3.7 × 10^6 km^3 through this period, equivalent to ~7.4 to 8.9 m of global sea-level equivalent. Peak volume occurs at the last glacial maximum at about 18 ka, with a temperature of about −18°C colder than present. At this time, the ice sheet is extended to the edge of Greenland's continental shelf and there is mass loss by iceberg calving, but negligible surface melting. GrIS comes out of the glacial period relatively abruptly from ~12 to 10 ka, reaching its early Holocene volume of about 3.0 × 10^6 km^3 in these simulations. The ice sheet grows slightly from the early Holocene through to the present, reaching a modelled present-day volume of ~3.15 × 10^6 km^3 (Table 4.1). This is

about 8.6% greater than the observed present-day ice sheet volume, although the model also implicitly includes peripheral glaciers and ice caps in Greenland, which are not part of the primary ice sheet.

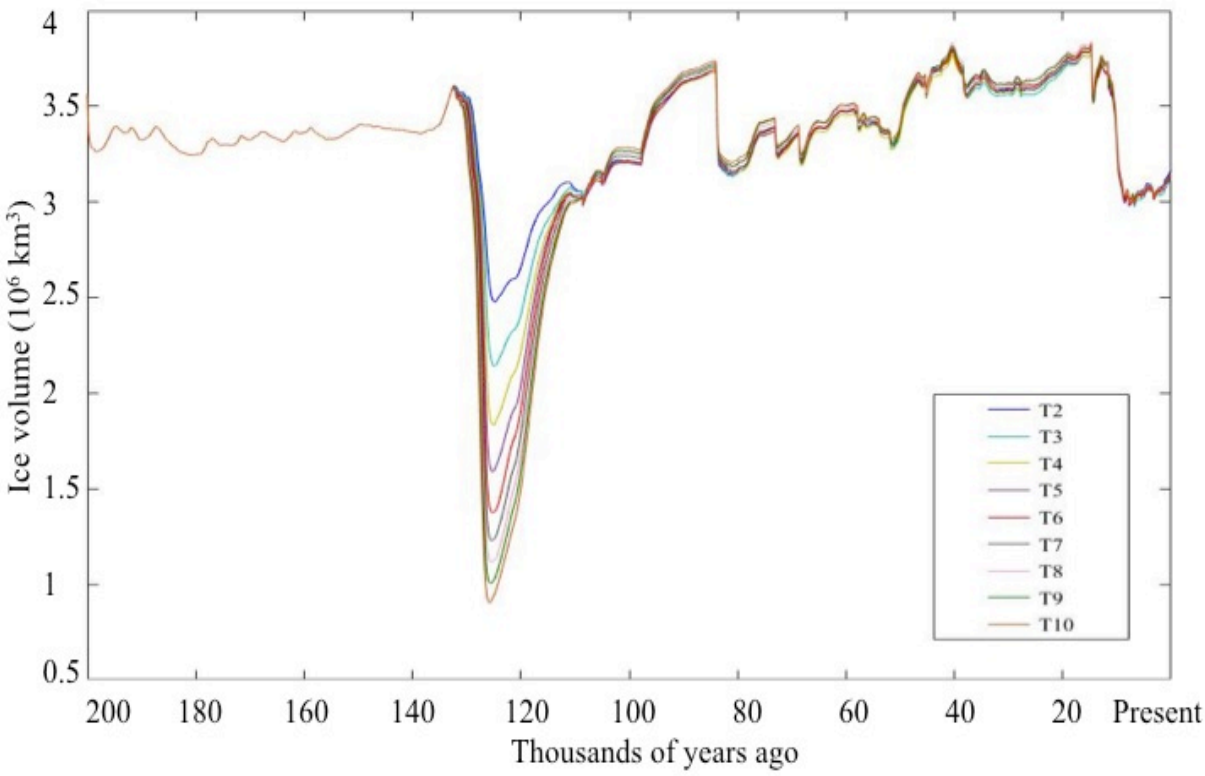

Figure 4.1. Ice volume change over the past 200 kyr using T2-T10 temperature forcing.

Table 4.1. Observed and modelled present-day ice area, volume, and sea level equivalent for the T2, T6, and T10 temperature scenarios.

	obs	T2	T6	T10
Ice area (10^6 km^2)	1.71	1.75	1.73	1.73
Ice volume (10^6 km^3)	2.90	3.16	3.12	3.14
Sea Level Equivalent (m)	7.30	7.88	7.77	7.82

Modelled present-day ice area, volume and sea level equivalent do not differ significantly (within 9% deviation) as a function of the Eemian temperature scenarios (Table 4.1). As a more local point of comparison, Table 4.2 shows observed vs. modelled ice sheet elevation, thickness, and air temperature at two critical ice core sites, NEEM and Summit. Counter-intuitively, the warmer Eemian scenarios produce slightly thicker ice at NEEM ice core site. This may be associated with the deep ice temperature and viscosity structure in these scenarios, which result in different present-day ice deformational velocities. In addition, the modelled present-day ice elevation is higher than the observations at both ice core sites, with colder surface temperature. At the Summit ice core site, elevation and ice thickness reduce slightly for warmer scenarios as surface temperature decrease slightly (Table 4.2).

Modelled present-day ice elevation, thickness, and temperature do not differ significantly as a function of the Eemian temperature scenarios at the Summit ice core site (Table 4.2). Values at Summit are in good accord with the observations. Results are more variable at the NEEM core site, where the modelled ice sheet is from 120 to 170 m too thick compared to the observations, with the excess elevation making it slightly too cold. The ice thickness at NEEM is also sensitive to the temperature scenario, with ice at NEEM about 70 m thicker for the T10 scenario compared to T2 and T6. This increases the deviation from the observations for the T10 scenario. The modelled present-day results in Table 4.2 are also within 10% of the observations at the Summit and NEEM ice cores.

Table 4.2. Observed and modelled present-day elevation (h_s), ice sheet thickness (H) and air temperature (T_a) for T2 (minimum T forcing), T6 (mean T forcing), and T10 (maximum T forcing) temperature scenarios at the Summit and NEEM sites.

		Summit				NEEM		
	obs	T2	T6	T10	obs	T2	T6	T10
h_s (m)	3203	3241	3236	3232	2450	2565	2567	2617
H (m)	3053	3037	3035	3033	2542	2666	2668	2736
T_a (°C)	-31	-31.6	-31.6	-31.5	-29	-29.7	-29.7	-30

4.2. Model Reconstructions in the Eemian Period

The purpose of this section is to evaluate my output during the Eemian against available observations. No direct observations or proxies for ice sheet volume are available from the Eemian period, but several constraints are available from the NEEM Community (2013) research findings and the Summit reconstructions of Yau et al. (2016).

Figures 4.2 and 4.3 provide a detailed view of the modelled temperature forcing and ice sheet volume in the Eemian period. T10 is the warmest scenario and has the lowest ice sheet volume during the Eemian, while T2 has the lowest temperature anomaly and the highest ice volume. The ice sheet volume starts to decline at ~130 ka for all of the temperature scenarios, reaching a minimum at ~125 ka and recovering after ~124 ka (Figure 4.3). The ice sheet volume reaches its minimum of ~2.4 10^6 km^3 for T2 and ~0.9 10^6 km^3 for T10, equivalent to ~6 and ~2.2 m of global sea-level equivalent (i.e., a global sea-level rise of 1.3 and 5.1 m, respectively, relative to the present-day ice sheet volume of 7.3 msl). The minimum occurs at approximately 125 ka in the T2-T5 scenarios and 125.5 ka for T6-T10 (Figure 4.3 and Table 4.3). The ice sheet collapses more quickly with the stronger temperature forcing.

Figure 4.4 plots contour maps of ice sheet elevation for several Eemian warming scenarios near the time of minimum ice sheet volume. The maximum ice sheet elevation decreases from T2 to T10, to a point where the entire ice sheet lies below ~3000 m in T10 (Figure 4.4e). The central ice sheet dome persists in all scenarios, but it is considerably retracted with the warmer temperatures; the minimum Eemian ice sheet area is 1.4×10^6 km^2 for T2 and 0.6×10^6 km^2 for T10 (Table 4.3).

Table 4.3 presents summary values of Eemian ice sheet geometry and climate conditions in Greenland. The temperature is highest at 126 ka for T2-T5, but reaches its Eemian maximum about 1000 years later for T6-T10 (Figure 4.2 and Table 4.3). This is likely due to the more extensive ice sheet collapse in T6-T10, along with the associated elevation (lapse rate) feedbacks on temperature. The timescale of ice sheet geometric responses to climate forcing is of order 1000s of years.

Figure 4.5 provides the evolution of the ice sheet surface elevation for Summit, NEEM source, and NEEM ice core sites over Eemian. Summit is located at the highest elevation of about 3203 m, and NEEM site at the lowest elevation of 2450 m (Table 4.2). During the Eemian all ice core elevations initially increase, then decrease after they reach the peak elevation. However, for the T2 temperature scenario the ice sheet surface elevation does not decrease more than it has increased, in contrast to the T6 and T10 temperature scenarios that plummet much more than they increase early in the Eemian (Figure 4.5). The T2 elevation decrease is less than 100 m at all ice cores, whereas T10 elevation decreases by ~1100 m at Summit (Figure 4.5a) and NEEM source (Figure 4.5b) and 1700 m at NEEM (Figure 4.5c). Summit is at its peak elevation late in the Eemian for the T2 and T3 scenarios, but early in the Eemian for the rest of the temperature scenarios (Table 4.3).

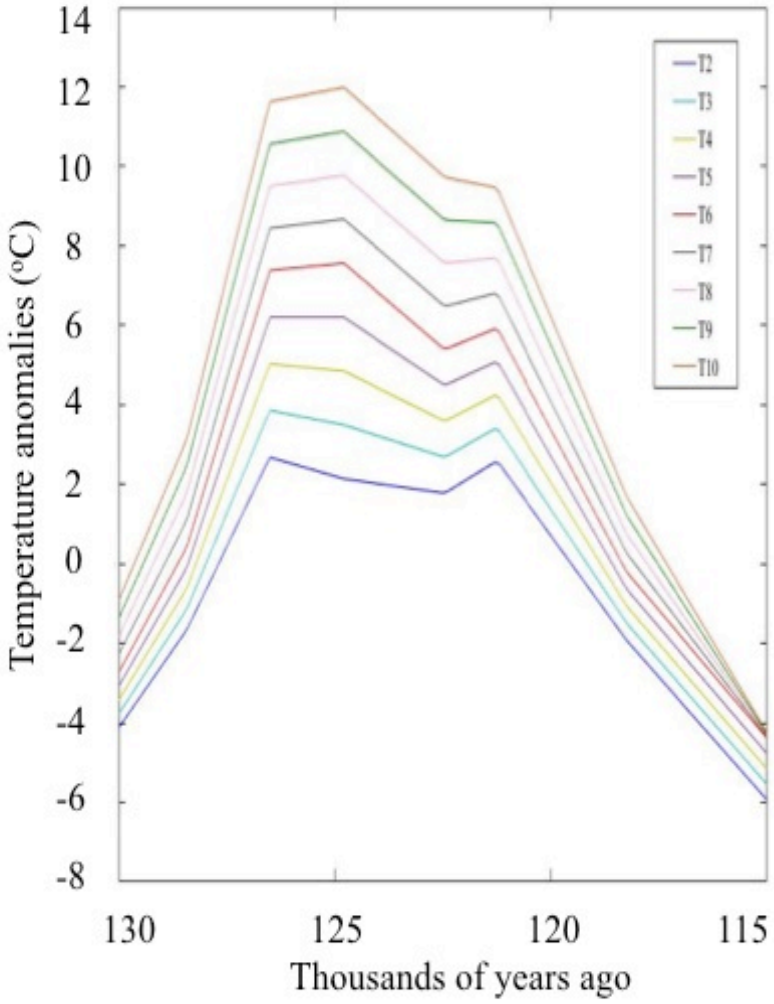

Figure 4.2. Temperature forcing anomalies during the Eemian (130-115 ka) for scenarios T2 to T10.

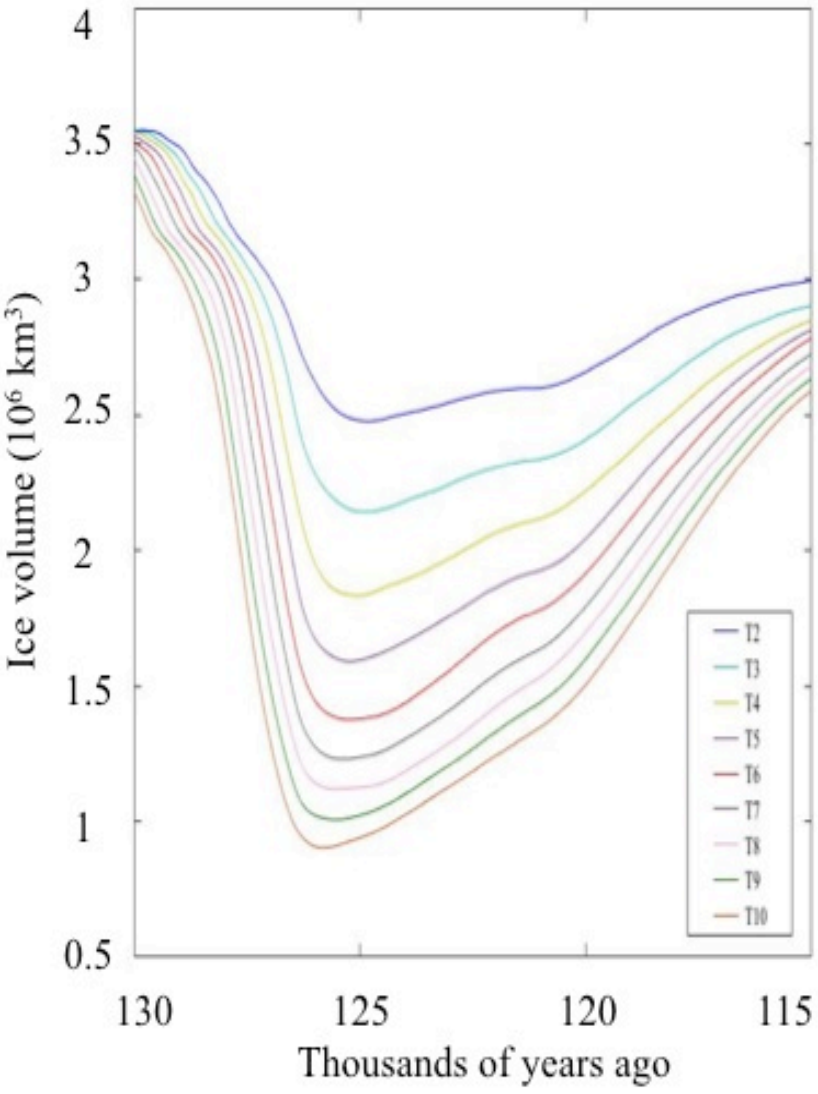

Figure 4.3. Ice volume change over the Eemian (130-115 ka) for scenarios T2-T10.

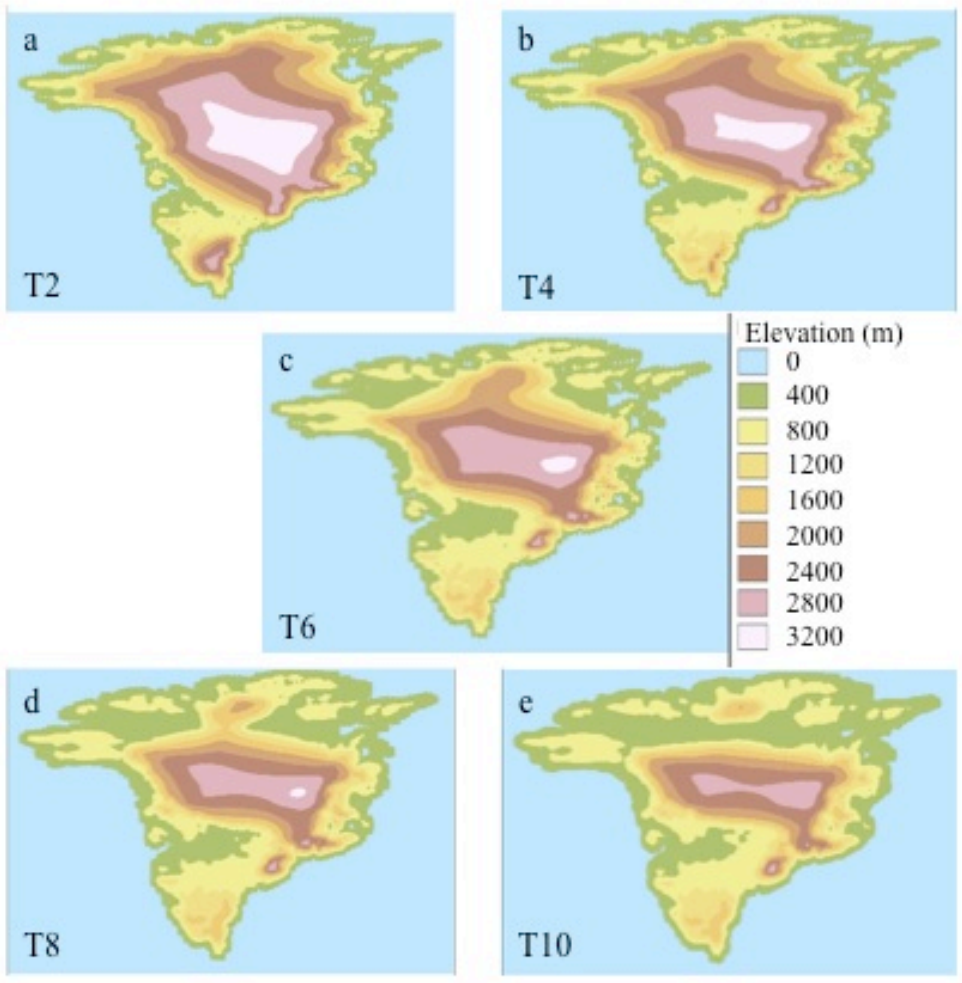

Figure 4.4. Ice surface topography showing elevation over Greenland. The legend shown in (c) applies to all ice sheet scenarios. The ice sheet is shown at 125 ka for scenarios (a) T2 and (b) T4 and 125.5 ka for (c) T6, (d) T8, and (e) T10.

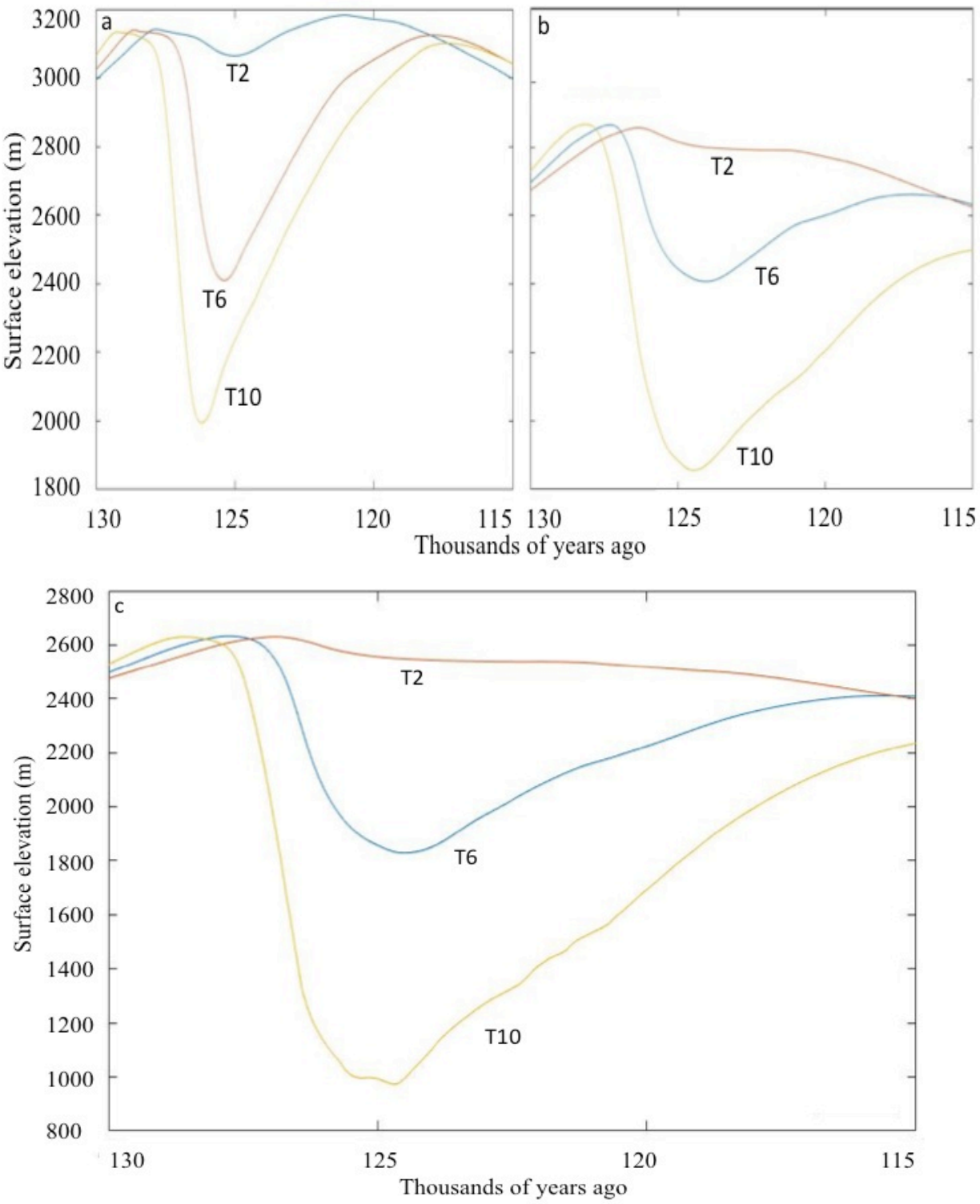

Figure 4.5. Evolution of the ice sheet surface elevation over Eemian (130-115 ka) for T2, T6, and T10 scenarios at (a) Summit, (b) NEEM source, and (c) NEEM.

Table 4.3. Modelled minimum ice volume and area (10^6 km^3), sea level equivalent of this volume, maximum temperature change (ΔT), maximum NEEM source surface temperature, maximum Summit elevation (h_s), and the time they occur (ka) for all temperature scenarios during the Eemian.

	T2	T3	T4	T5	T6	T7	T8	T9	T10
Min vol (10^6 km^3)	2.4	2.1	1.8	1.5	1.3	1.2	1.1	1	0.9
Time of min vol (ka)	124.8	124.9	125	125.2	125.3	125.5	125.6	125.6	125.8
SLR at this time (m)	1.3	2.1	2.8	3.6	4.1	4.3	4.6	4.8	5.1
Min area (10^6 km^3)	1.39	1.22	1.06	0.94	0.85	0.79	0.74	0.69	0.63
Time of min area (ka)	124.3	124	124.5	125.1	125.2	125.5	125.4	125.6	125.7
Max Eemian ΔT (°C)	2.6	3.8	5	6.2	7.5	8.6	9.7	10.8	11.9
Time of max ΔT (ka)	126.4	126.4	126.4	126.4	124.7	124.7	124.7	124.7	124.7
NEEM source max Eemian T_s (°C)	-27.8	-26.7	-25.7	-24.9	-24.3	-23.9	-23.6	-22.9	-22.3
Time of max T_s (°C)	126.4	126.4	126.4	126.4	126.4	126.4	126.4	124.7	124.2
Max Summit h_s (m)	3182	3147	3141	3141	3139	3138	3136	3133	3133
Time of max Summit h_s (ka)	121.1	118.7	128.3	128.5	128.6	128.8	129	129.1	129.2

Table 4.4. Elevation (h_s) at NEEM, NEEM source, and Summit at 126 ka, as well as PDD for NEEM source for all temperature scenarios.

		T2	T3	T4	T5	T6	T7	T8	T9	T10
NEEM	h_s **(m)**	2594	2553	2451	2280	2068	1839	1589	1352	1132
NEEM source	h_s **(m)**	2852	2836	2787	2706	2603	2485	2356	2220	2086
	PDD (°Cd)	0.83	1.44	2.23	3.16	4.08	4.89	5.8	7.2	9.52
Summit	h_s **(m)**	3097	3047	2920	2722	2514	2333	2200	2097	2007

Table 4.4 shows that NEEM source is at a higher elevation than NEEM at 126 ka. However, Summit is at the highest elevation except for the warmer scenarios (T6-T10) where NEEM source is actually higher than the modern Summit at 126 ka. This indicates northward mobility of the central ice sheet dome during the Eemian ice sheet retreat. Deep Eemian ice at the present-day NEEM site has flowed in from a location near to the Eemian ice sheet divide, in proximity to the present-day summit (see Section 4.5). The elevation difference between T2 (minimum T forcing) and T6 (mean T forcing) is almost half the elevation difference between T6 and T10 (maximum T forcing) at NEEM source and NEEM. PDD ranges from 0.83 to 9.52°C d at NEEM source at 126 ka (Table 4.4).

4.3. Melting modifications

The purpose of this section is to examine the potential effects of partial melting on Eemian isotopes at NEEM, and the associated implications for Eemian temperature and ice sheet volume reconstructions. Based on the PDD–$\delta^{18}O$ linear relationship and the $\delta^{18}O$–temperature relationship described in section 3.7, as well as the modelled Eemian PDD, I adjusted the isotopic (temperature) record during the LIG and ran an additional model simulation to account for the effects of meltwater modification. As melting results in enrichment of the isotopic ratios

in snow (higher $\delta^{18}O$), this adjustment corrects for that and effectively decreases the LIG $\delta^{18}O$ and temperature anomalies. The Eemian temperature anomaly reaches its maximum during the same time after the modifications for scenarios T2 to T7 (Table 4.5). The T2 temperature anomaly is modified to a maximum of 0.1°C, but the T10 temperature anomaly is reduced by more than 2°C during the Eemian (Figure 4.6). This in return results in higher ice volume revisions for T10 compared to T2 (Figure 4.7), compared to the initial simulations. The ice sheet volume reaches its minimum of ~$2.5x10^6$ km^3 at T2 and ~$1x10^6$ km^3 at T10 at about 125 ka after the modifications, which is a $0.1x10^6$ km^3 volume increase for all scenarios (Table 4.5). By modifying the $\delta^{18}O$ values for the meltwater enrichment affect, the temperature values are reduced, resulting in higher ice volume and thickness. While this is a systematic result, it does not strongly alter the modelled Eemian ice sheet reconstructions.

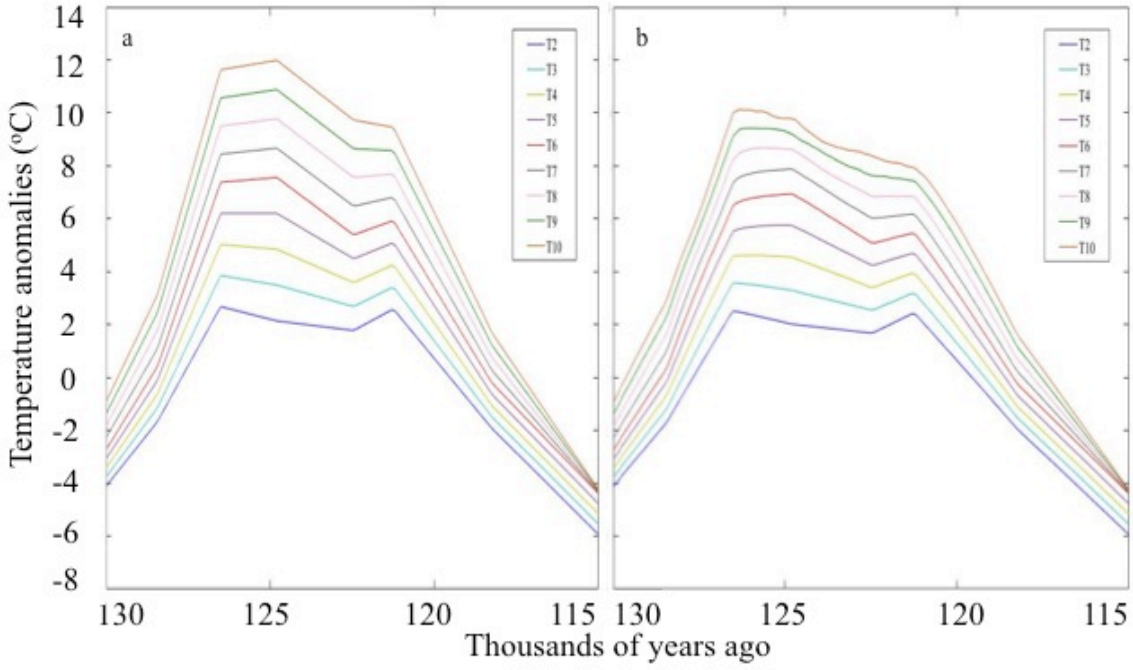

Figure 4.6. Temperature forcing anomalies (a) before and (b) after modifications for meltwater enrichment over the Eemian (115-130 ka).

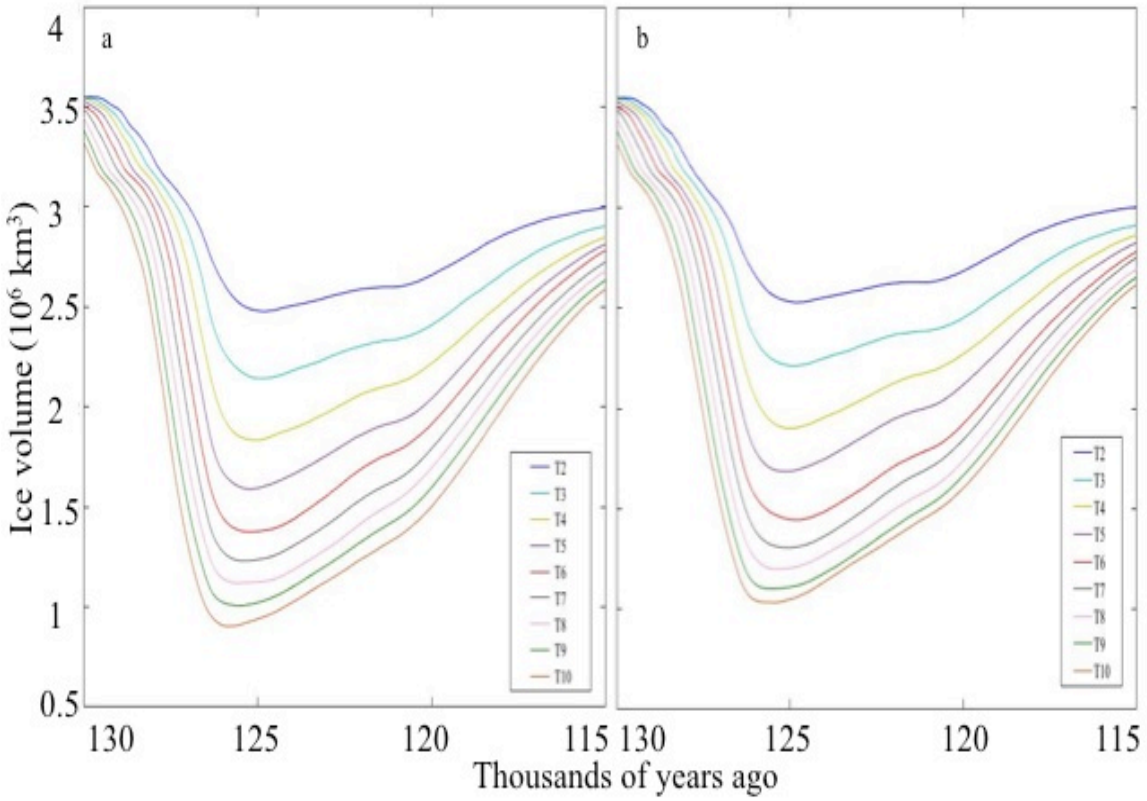

Figure 4.7. Ice volume change (a) before and (b) after the modifications for meltwater enrichment over the Eemian (130-115 ka) using T2-T10 scenarios.

Table 4.5. Modelled Eemian maximum temperature anomalies, minimum ice sheet volume and their time of occurrence after modifications for all the scenarios. Where dT and dV are the changes from before modifications.

	T2	T3	T4	T5	T6	T7	T8	T9	T10
Max Eemian ΔT (°C)	2.5	3.5	4.6	5.7	6.9	7.8	8.6	9.4	10.1
dT (°C)	-0.1	-0.3	-0.4	-0.5	-0.6	-0.8	-1.1	-1.4	-1.8
Time of max ΔT (ka)	126.4	126.4	125.6	125.1	124.7	124.7	125.6	126	125.9
Min vol (10^6 km^3)	2.5	2.2	1.9	1.6	1.4	1.3	1.2	1.1	1.0
dV (10^6 km^3)	+0.1	+0.1	+0.1	+0.1	+0.1	+0.1	+0.1	+0.1	+0.1
Time of min vol (ka)	124.8	124.9	125	125.1	124.9	125.1	125.4	125.5	125.5

Table 4.6. Modelled elevation (h_s) of NEEM source and Summit, as well as PDD of NEEM source for the T2, T6, and T10 scenarios after modifications compared with the initial simulations for 126 ka.

		T2	T6	T10
NEEM source	**h_s (m)**	2851 (-1)	2672 (+69)	2275 (+189)
	PDD (°Cd)	0.79 (-0.04)	3.67 (-0.41)	6.42 (-3.1)
Summit	**h_s (m)**	3100 (+3)	2618 (+104)	2090 (+157)

Table 4.6 shows the impact of melting modifications on surface elevation at NEEM source and Summit, as well as and PDD at NEEM source for the T2, T6, and T10 scenarios. As the temperature increases from T2 to T10 at the NEEM source and Summit locations, the impact on the elevation and PDD increase as well. For T2, elevation and PDD decreased by 1 m and 0.04°Cd, respectively (Figure 4.8 and Table 4.6). For T10, on the other hand, elevation increases by 189 m and PDD decreases by 3.1°Cd. At Summit, surface elevation increases 3 m, 104 m, and 157 m for T2, T6, and T10 scenarios, respectively (Table 4.6). As the temperature values decrease after the modifications, PDD and melt values decrease slightly, resulting in higher elevations (Figure 4.6, Table 4.6, and Figure 4.8). The modifications impact PDD and melt from ~128 ka until ~120 ka.

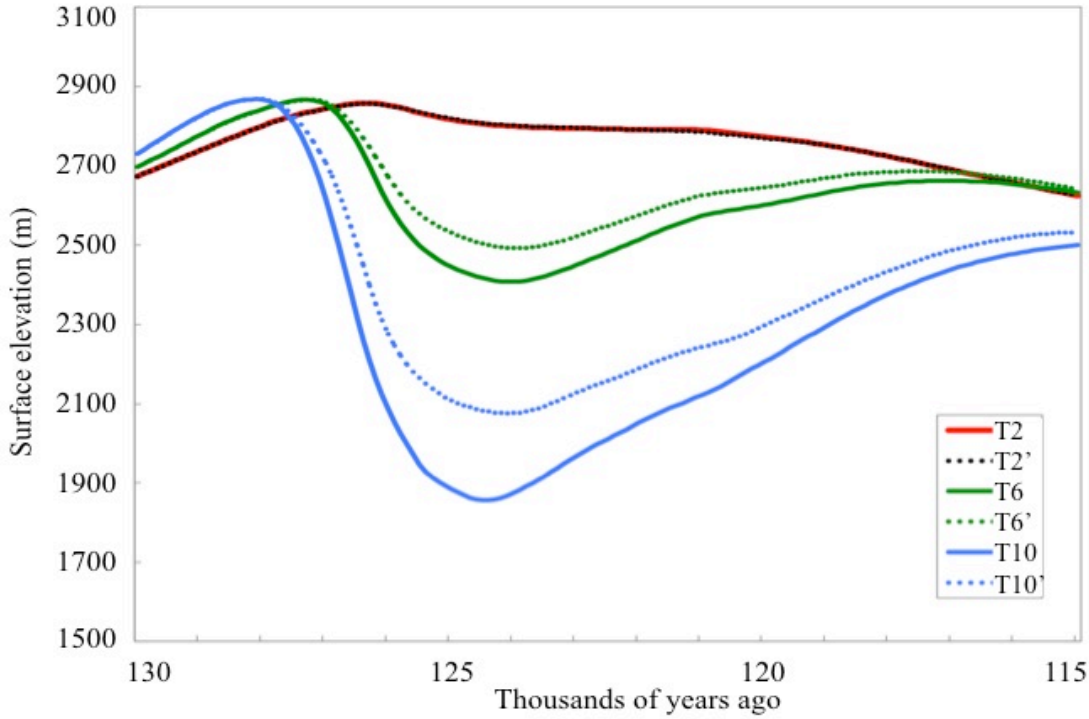

Figure 4.8. Surface elevation before (T2, T6, and T10) and after (T2', T6', and T10') melting modifications at NEEM source ice core site over the Eemian (130-115 ka) using T2, T6, and T10 scenarios.

4.4. Summit

Figure 4.9 shows the impact of melting modifications on Summit surface elevation during the Eemian for T2, T6, and T10 scenarios. Summit surface elevation fluctuates slightly over the Eemian for the T2 scenario, however it increases early in the Eemian and around 124 ka for T6 and T10 scenarios. Table 4.7 shows that Summit hits its lowest elevation 125 and 126 ka for T6 and T10, respectively. Summit reaches its minimum surface elevation of 2994 m around 130 ka for T2 scenario, which is an increase of 110 m after the modifications (Table 4.7).

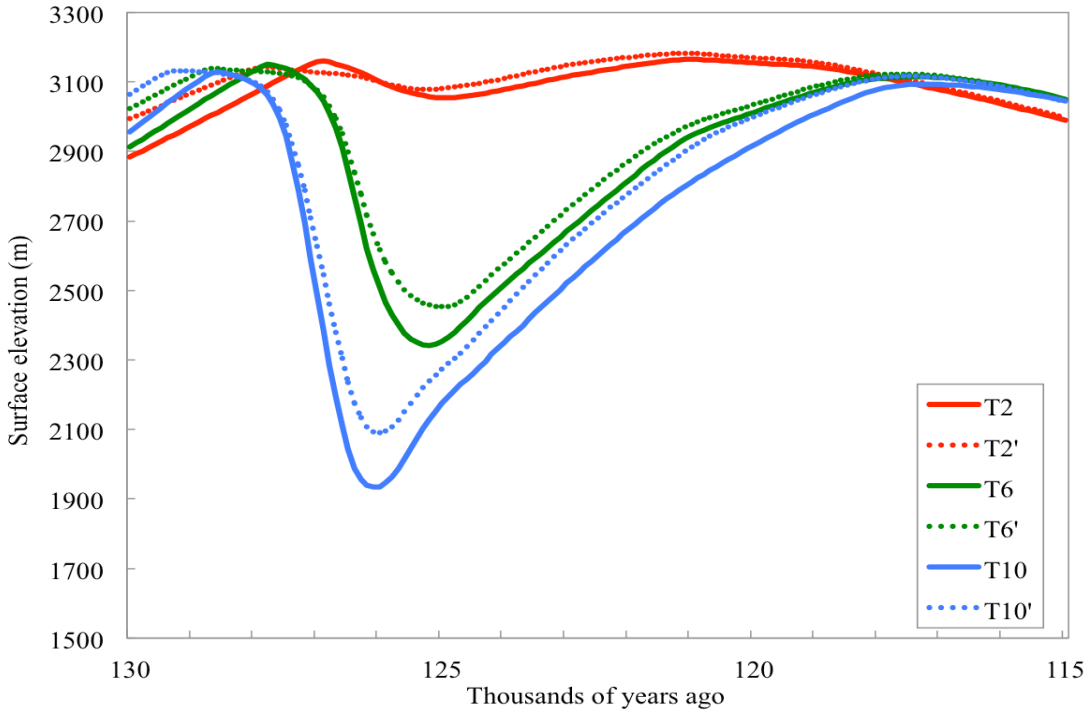

Figure 4.9. Surface elevation before (T2, T6, and T10) and after (T2', T6', and T10') melting modifications at the Summit site over the Eemian (130-115 ka) using T2, T6, and T10 scenarios.

Table 4.7. Modelled Eemian minimum surface elevation (h_s) and time of occurrence after melting modifications for T2, T6, and T10 scenarios, where Δh is the change from the initial simulation.

	T2	T6	T10
Min h_s (m)	2994	2453	2090
Δh (m)	+110	+112	+157
Time of min h_s (ka)	130	125	126

4.5. Tracing

The purpose of this section is to display the results of the tracing of the snow deposition over GrIS in the past 200 kyr with the different temperature scenarios. Figure 4.10 plots the tracing of the snow deposition over time on GrIS for T2, T5, T7, and T10. The source ice at the

NEEM ice core site moves in from the southeast. For the higher temperature anomaly (T10), no ice older than 160 ka exists. However, ice as old as 180 ka exists in the lower part of the NEEM core for T2, T5, and T7 (Figure 4.10).

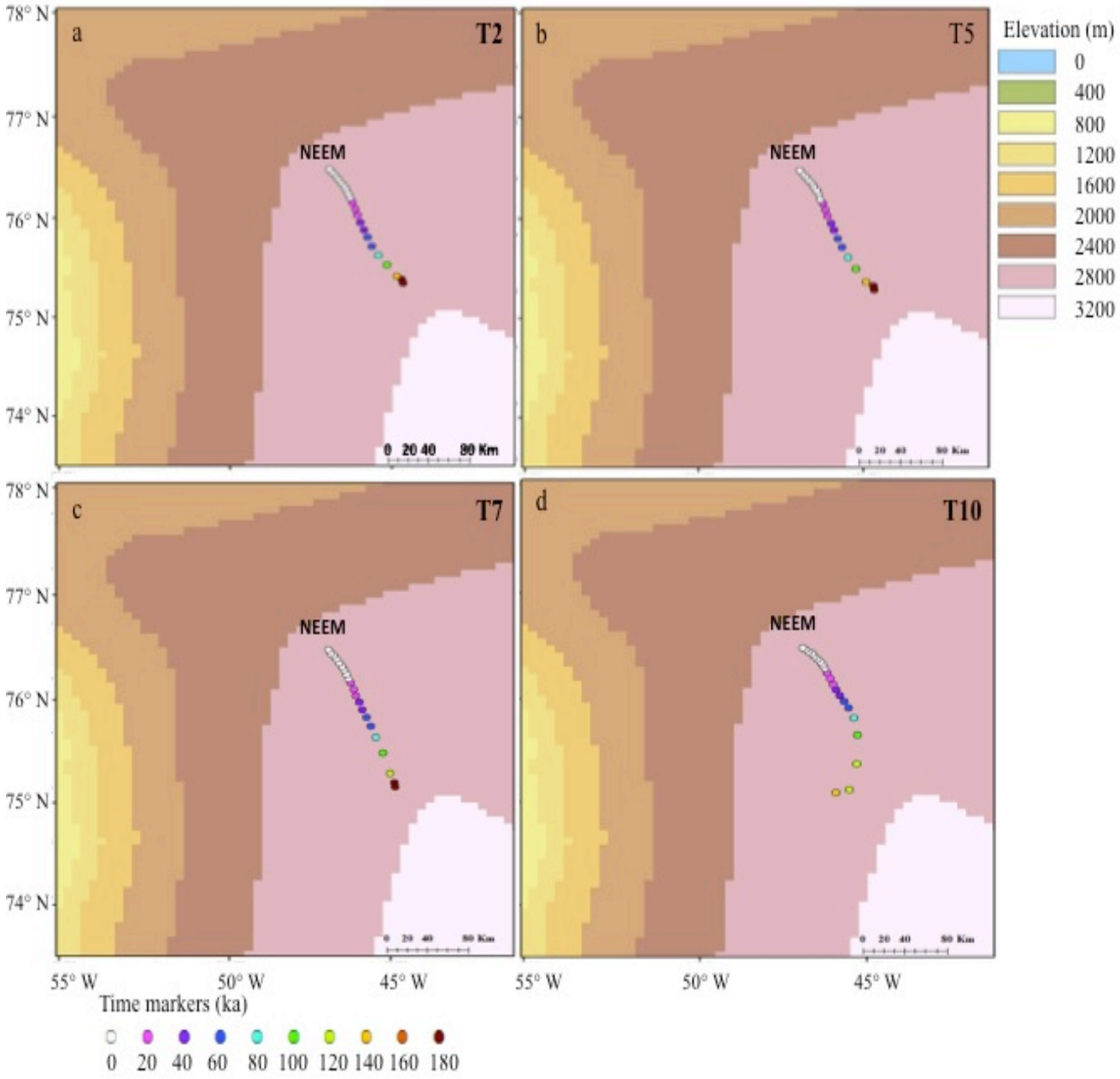

Figure 4.10. Surface elevation map of the position of the NEEM ice core site with the tracing of the snow deposition over time on GrIS is shown for (a) T2, (b) T5, (c) T7, and (d) T10.

Figure 4.11 shows NEEM and Summit ice core provenance trajectories for different temperature scenarios. NEEM ice immigrates from the southeast. It moves more than 90 km west and less than 140 km north with the T2 scenario, but more than 140 km north with the T6 scenario. The T10 scenario ice moves slightly (less than 10 km) east before it changes direction and moves west like the other scenarios (~80 km). It moves more than 160 km north. The ice of the Summit ice core however, moves in from the north, about 30 km south and 20-30 km west, before it moves slightly east again to where it is now located.

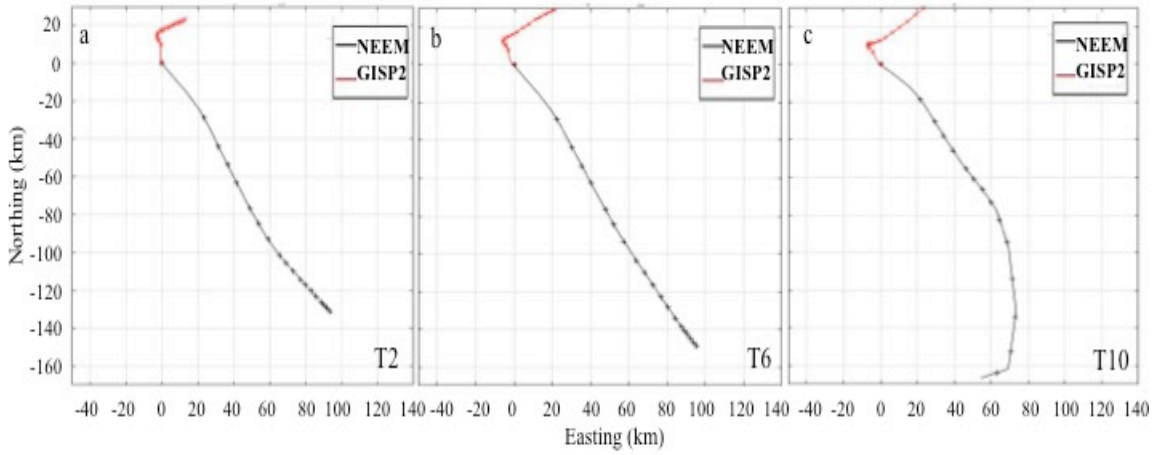

Figure 4.11. NEEM and Summit ice core provenance trajectories for (a) T2, (b) T6, and (c) T10 scenarios.

4.6. Ice core reconstructions

With the ice core reconstruction model (Clarke and Marshall, 2002), it is possible to fabricate any ice core record of depositional tracers at any drill hole location and time (e.g., Lhomme et al., 2005). Figure 4.12 shows the reconstruction of ice age in the NEEM ice core using the modelled depositional data. The depositional age decreases smoothly from sea level, which happens to be close to ice sheet bed at NEEM, with time starting from 200 ka to present

(aka time zero), which is at the surface of the ice (Figures 4.12). With the T10 temperature forcing, the bed of the ice sheet is slightly below sea level with the oldest ice having an age of ~150 ka (Figure 4.12). In this case, isostatic depression has moved the ice below sea level. Ice older than 150 ka has melted in this case, but there is still Eemian ice. With the T2 and T6 scenarios, the bed of the ice is at about the sea level with ice as old as 200 ka.

Temperature is the lowest with T2, but still warmer than the highest elevation (Figure 4.13a), and highest with the T10 scenario (Figure 4.13c) close to the bed of the ice linking it to the Eemian. At higher elevation with the younger ice to about 1700 m elevation, temperature is around -30ºC for all temperature scenarios similar to the Holocene. With this ice core reconstruction model, it is possible to fabricate any ice core record of depositional tracers at any drill hole location and time. The paleo-temperature can in turn be converted to other tracers such as $\delta^{18}O$ to be compared with observational $\delta^{18}O$ ice core records.

Figure 4.14 shows the elevation differences of the surface paeleo-elevation. Major fluctuations can be seen in the surface elevation at different layers of the ice column, which are linked to changes to the ice thickness and warmer temperatures linking it to the Eemian warming, especially in Figure 4.14c close to the bed of the ice.

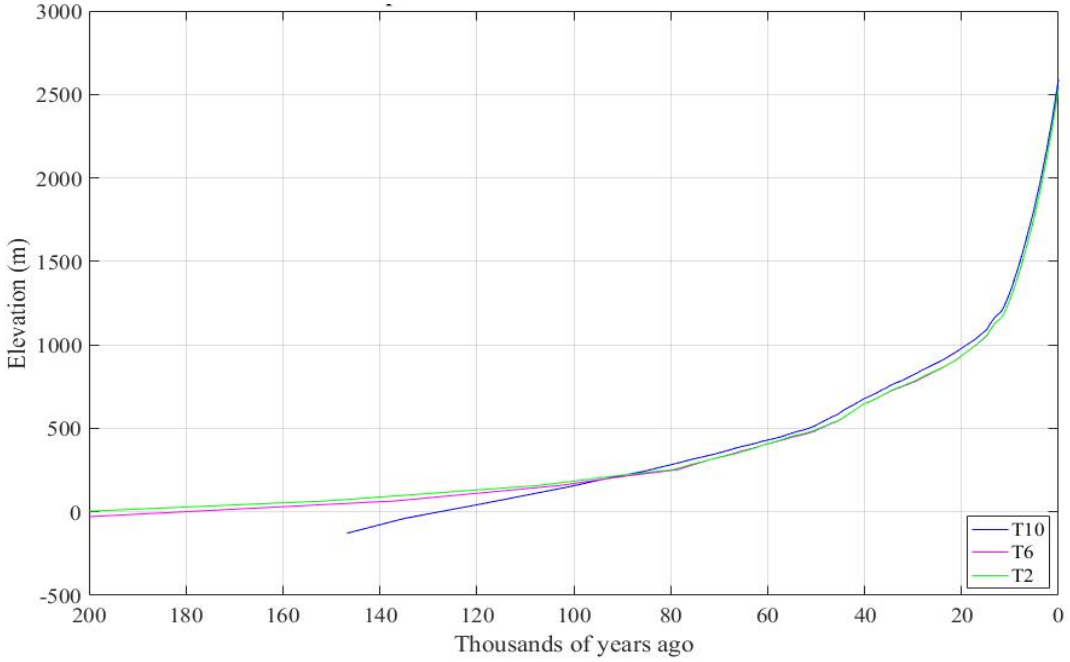

Figure 4.12. Deposition depth and time for NEEM ice core site for T2, T6, and T10 scenarios (to compare with observations).

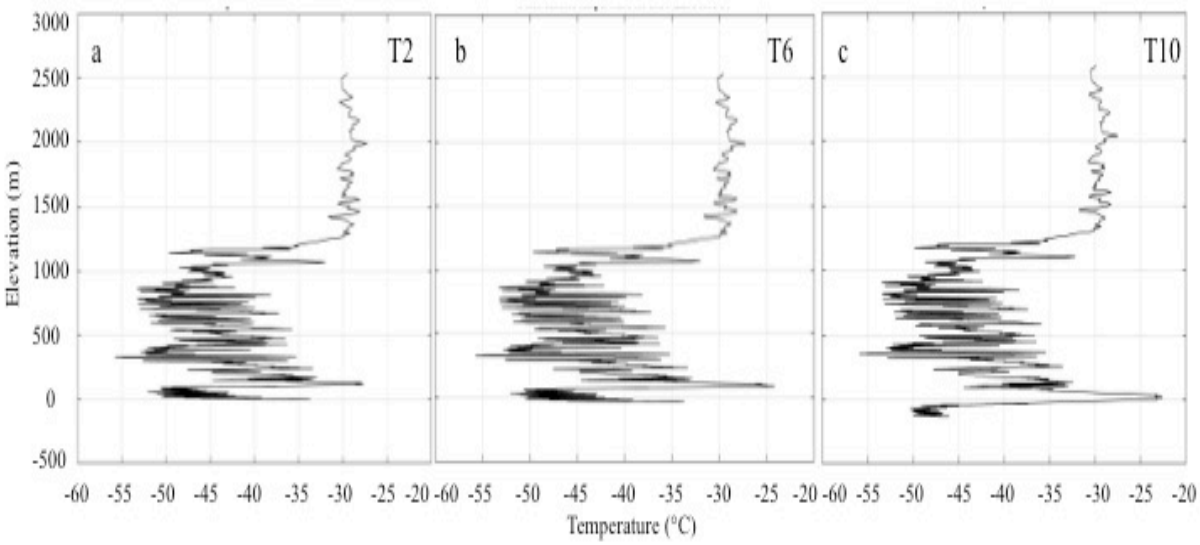

Figure 4.13. Surface paleo-temperature for NEEM ice core site for (a) T2, (b) T6, and (c) T10 scenarios.

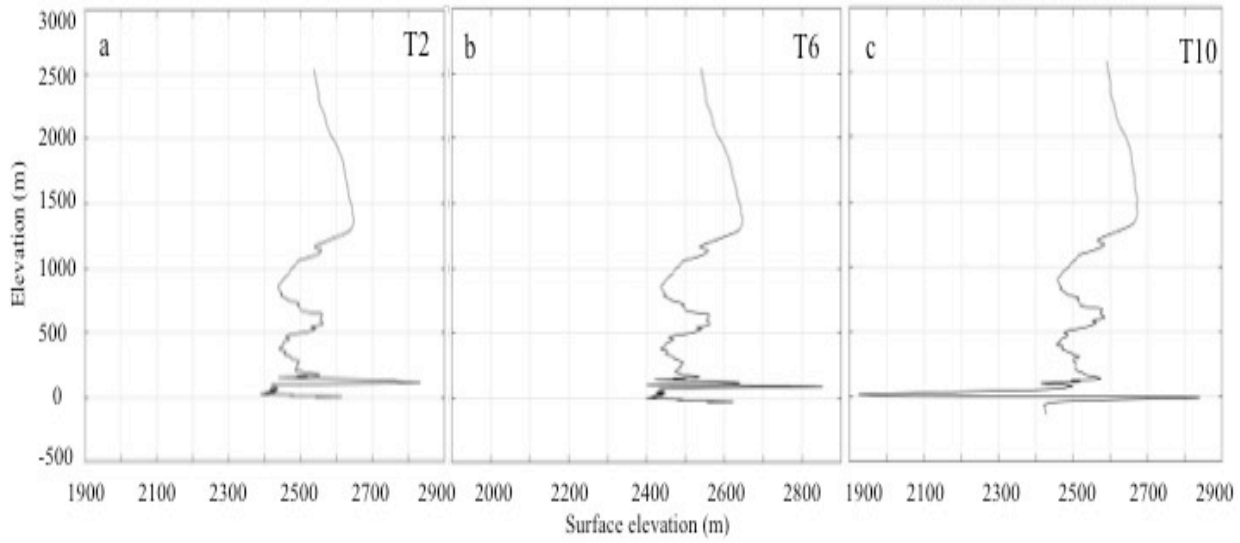

Figure 4.14. Surface paleo-elevation for NEEM ice core site for (a) T2, (b) T6, and (c) T10 scenarios.

Figure 4.15 illustrates modelled ice age in vertical cross sections of the ice sheet near the NEEM drill site. The top row of figures shows west-east transects for cases T2, T6, and T10, and the lower row plots south-north transects for these three scenarios. Younger (Holocene) ice is found in the upper ~1500 m of the ice sheet. With time, ice is buried, compressed, and thinned by flow. This creates thinner layers in the deeper, interior regions of the ice sheet. Ice from the Eemian period, ~120-130 ka is modelled to occur a few 100 metres above the bed for most of the W-E and S-N transects through NEEM, but old (pre-Eemian) ice is best-preserved in the deep ice of central Greenland. In the model, no ice of Eemian age (or older) is found in southern Greenland or on the ice sheet flanks.

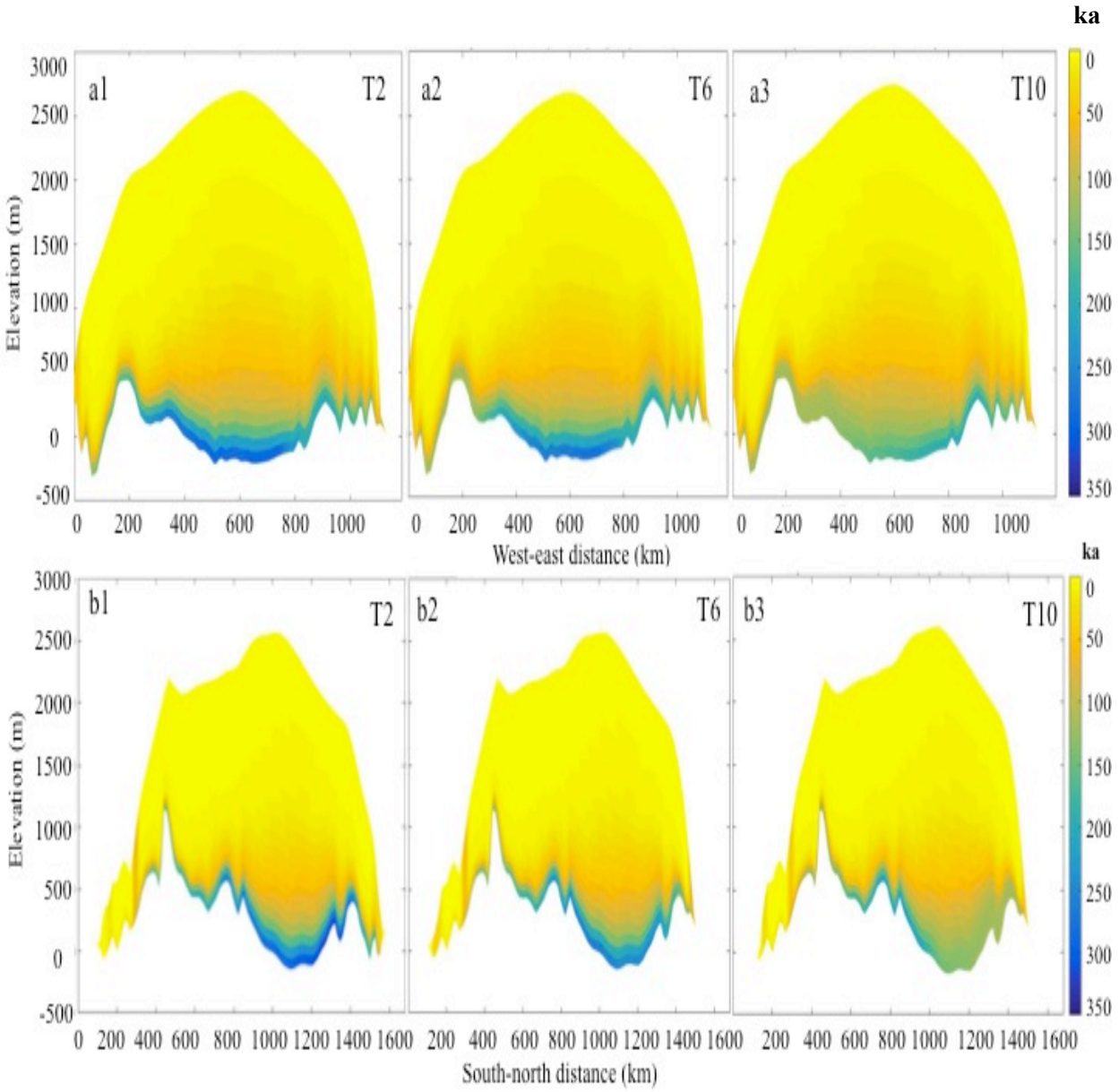

Figure 4.15. Modelled ice age for west-to-east (a1-a3) and south-to-north (b1-b3) profiles through the NEEM site for T2, T6 and T10. a1-a3: ice age vs longitude from 70º to 20ºW at a latitude of 77.45ºN. b1-b3: ice age vs. latitude from 68º to 83ºN at a longitude of 51.06ºW.

At Summit, the depositional elevation increases smoothly from approximately 200 m above the sea level with time starting about 190, 160, 150 ka to present, which is at the surface of the ice, for T2, T6, and T10 scenarios, respectively (Figure 4.16). Eemian ice exists in all temperature scenarios. With the T2 scenario ice as old as 190 kyr exist. Figure 4.17c shows the

temperature being the highest, about -21ºC, close to the bed of the ice. That is about 10ºC warmer than present Summit temperature. At higher elevation with the younger ice to about 1400 m elevation, temperature is around -32ºC for all temperature scenarios similar to the Holocene (Figure 4.17).

Figure 4.18 is a fabricated ice core reconstruction at the Summit ice core site for the past 200 ka. It shows Holocene down to the depth of ~1700 m containing $\delta^{18}O$ of about -35 ‰ and the Eemian at the depth of around 2900 m containing $\delta^{18}O$ of about -32 ‰.

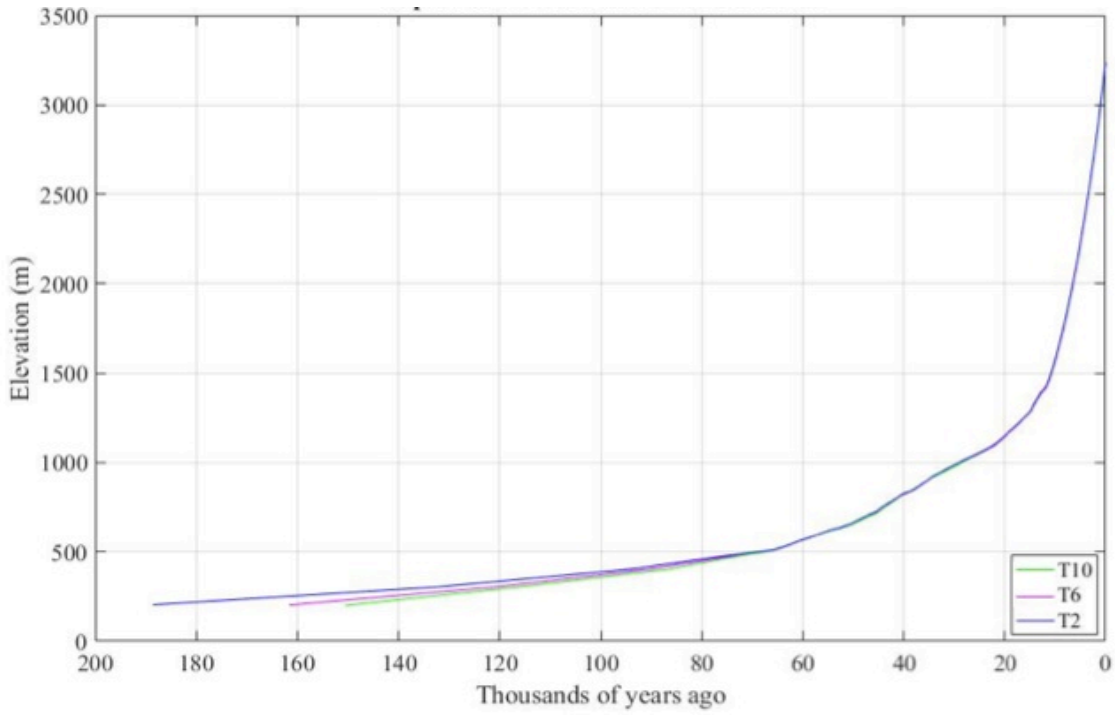

Figure 4.16. Deposition depth and time for the Summit site for T2, T6, and T10 scenarios (to compare with observations).

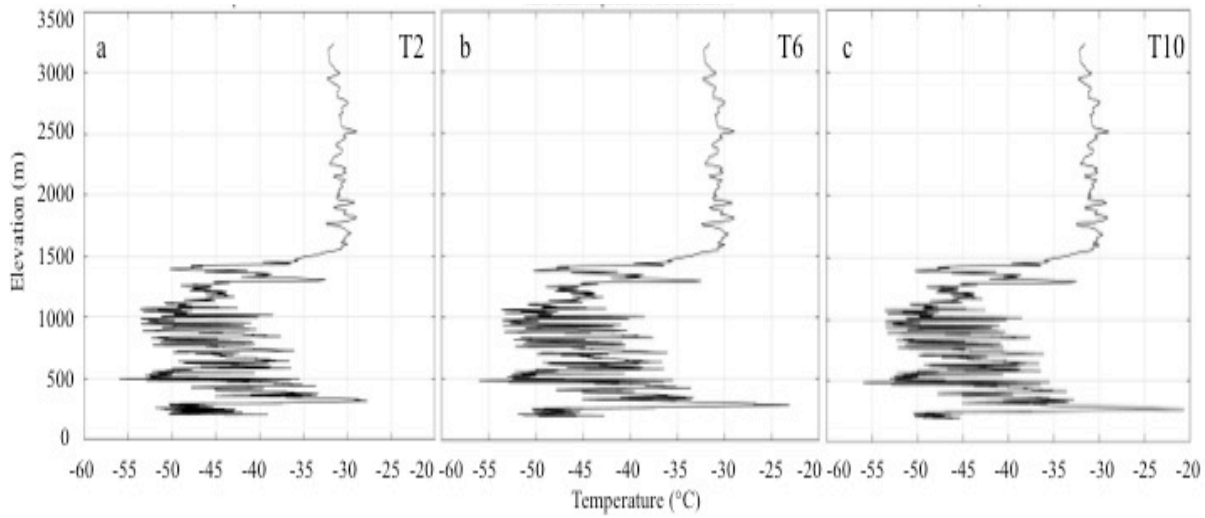

Figure 4.17. Paleo-surface temperature for the Summit site for (a) T2, (b) T6, and (c) T10 scenarios.

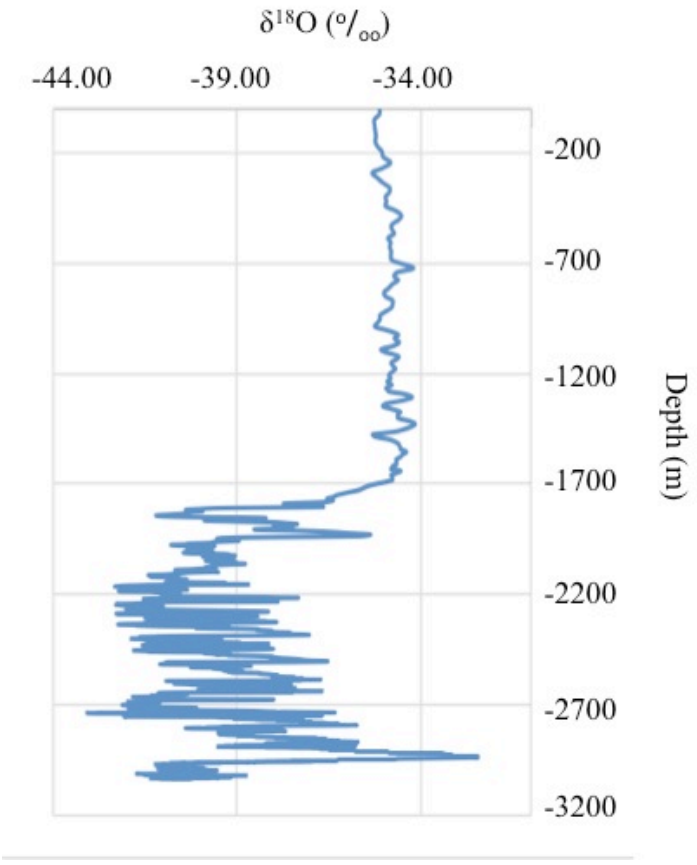

Figure 4.18. Modelled Summit ice core of $\delta^{18}O$ (‰) versus depth (m).

Chapter 5 Discussion

5.1. Summary of the Ice Sheet Reconstructions

This chapter discusses the results from each subsection of the previous chapter (chapter 4). I used the U of C 3D coupled-ice-and-heat-flow model (Marshall and Clarke, 1997) including a tracer model for oxygen isotopes (Clarke and Marshall, 2002; Lhomme et al., 2005) using nine different temperature scenarios based on the NEEM ice core (Cuffey and Clow, 1997; NEEM Community Members, 2013) to examine how stable GrIS is in a warmer climate by running simulations of the past 200 kyr. I especially focus on the Eemian warming with the intent of reconstructing source ice trajectories and ice sheet geometry from that period to today. I also build on that model to examine post-depositional isotopic modifications within the GrIS during the Eemian.

Past studies have used several ice sheet/climate models reconstructing LIG Greenland geometry. Some studies have used surface mass balance (SMB) based on modelled climate fields, while others use temperature forcing based on ice-core proxy data. Cuffey and Marshall (2000) used surface temperature forcing from Summit ice core temperature reconstructions to drive a coupled 3D ice-and-heat flow model. Lhomme et al. (2005) used a similar surface temperature forcing on a coupled 3D ice-and-heat-flow model containing a provenance transport model. To reconstruct GrIS during the Eemian warming, Otto-Bliesner et al. (2006) used modelled climate fields from the NCAR general circulation model (GCM), coupled with an ice sheet model using one-way forcing. “One-way” coupling refers to simulations in which SMB is calculated within the coupled climate simulation and sent to the ice sheet model, but the topography and surface types of the land and atmosphere models are fixed, whereas with “full” or “two-way” coupling, the surface types and surface elevation can evolve within the climate

model as the ice sheet advances and retreats (CESM Land Ice CESM2.0 documentation, 2018). Quiquet et al. (2013) used ice-core based surface temperature forcing with a thermomechanically coupled ice sheet model to conduct long-term simulations of the GrIS. The measurements of GrIS contributions to the global mean sea level rise during the Eemian range from 2.2 m to 5.5 m among these studies. Meanwhile, another study has suggested SLR levels as low as 0.4 m (Robinson et al., 2011). My simulations result in SLR of 1.2 m (T2 scenario) to 5 m (T10 scenario). This range will be more constrained, as more probable temperature scenarios during the Eemian are determined within this chapter.

My model resulted in similar present-day simulations for the NEEM and Summit sites for all the temperature scenarios (Table 4.1 and 4.2). The present-day ice sheet area and volume are also insensitive to the temperature scenario; while there is pervasive old (pre-Eemian) ice in the present-day ice sheet, which has some impact on modern-day ice sheet flow, the present-day ice sheet geometry is not sensitive to the extent of ice sheet retreat during the Eemian period. The modelled glacial cycle in Greenland is similar in all scenarios following recovery from the Eemian ice sheet retreat, with a peak volume at about 18 ka (the last glacial maximum). The temperature was ~18°C colder than present at this time (Figure 3.2), similar to the Greenland temperature anomaly of -20°C at the last glacial maximum reported by Johnsen at al. (2001).

The maximum Eemian temperature change occurs at ~126 ka for the T2-T5 scenarios (Figure 4.2). The rest of the scenarios have the maximum Eemian temperature change at ~125 ka (Figure 4.2). In addition, the T2-T8 scenarios have the highest surface temperatures at NEEM source ~126 ka, which is in agreement with the NEEM community members' (2013) research findings (Table 4.3). Ice sheet volume changes increase with temperature (Figure 4.3), and exceeds 4.3 m of sea level rise for scenarios T7 and above. Snapshots of the simulated GrIS ice

extent during its lowest ice sheet volume are offered in Figure 4.4. The T10 forcing presents the most retracted ice sheet on Greenland during the Eemian, although the central ice sheet dome persists in all scenarios. As the temperature gets warmer, from T2 to T10, the pattern of retreat is strongest in the northeastern and southwestern parts of GrIS. Ice is preserved at the NEEM and Summit ice core sites during the Eemian in all temperature scenarios (Figure 4.10). These findings are all compatible with Quiquet et al. (2013). Nonetheless, the minimum ice sheet volume is at ~125 ka in the simulations, which disagrees with the Quiquet et al. (2013) estimate of 121 ka.

5.2. Effects of meltwater on the NEEM isotope-temperature reconstructions

I also looked at possible modification of $\delta^{18}O$ values in the NEEM ice core that could have been caused by melting during the Eemian warming period. As per Moran and Marshall (2009) and Moran et al. (2011), meltwater percolation during warming periods may impact the accuracy of palaeoclimatic reconstructions, by causing isotopic enrichment within the ice sheet, jeopardizing accurate interpretations of the climatic information. The enrichment of heavy isotopes in the snowpack due to either refreezing of meltwater (assuming that some meltwater leaves the system) or evaporation of liquid meltwater could influence the ability of isotopic values to be used as accurate proxies (Moran and Marshall, 2009). This may have affected the ice core record at NEEM, given the evidence for melting during the Eemian (NEEM community members, 2013).

Thus, I used PDD values, at the NEEM ice source location during the Eemian period, which were outputs of the ice sheet model, as a proxy for melt-induced isotopic correction. The melt-adjusted isotopic record may provide a more accurate climate reconstruction for the GrIS. I

used a linear relationship between PDD and isotopic modification to extrapolate the amount of isotopic enrichment, which Moran and Marshall (2009) estimated to be 0.08‰ $(PDD)^{-1}$. A $\delta^{18}O$–temperature relationship of 2.1 ± 0.5 °C $‰^{-1}$, derived from the NEEM community members (2013), was assumed at times when melting occurred during the Eemian, in order to link the isotopic modification to temperature change estimates. The modification reduced the original temperature anomalies, resulting in higher elevation, ice thickness and ice volume.

On the whole, water isotopes and temperature reconstructions appear to be only slightly affected by the Eemian warming on the GrIS. This is compatible with the findings of Pohjola et al. (2002), who argue for minimal effects of a small amount of melting. In contrast, Goto_Azuma at al. (2002) argue for significant post-depositional melting modifications to $\delta^{18}O$ signals within Arctic ice cores. Melting during the Eemian reduced the T2 to T10 temperature anomalies from a minimum of 0.1°C to a maximum of 2°C (Figure 4.6 and Table 4.5), which slightly increases the reconstructed Eemian ice volume over Greenland (Figure 4.7). Whether or not melting has a significant impact on the climate interpretation coming from water isotopes on the GrIS depends on the magnitude of the warming during the Eemian. Even in the T10 scenario, there is only a small amount of melting predicted at the NEEM source site, which remains above an elevation of 2000 m, so the isotopic modification is modest (Figure 4.8).

5.3. Tracer Modelling

Tracer transport modelling is used to model stratigraphic records within ice sheets. According to Clarke et al. (2005), as ice moves the stratigraphic records within ice cores are disfigured, and tracer transport modelling can be used to overcome such limitations. Flow modelling is especially useful for the validation of climate and ice sheet models, as it can be used

to reconstruct the layers of an ice core from any drilling site. I ran the tracer transport model simultaneously within my ice sheet model to track the flow of the provenance markers from the time the snow is deposited on the ice to the time it arrives at the ice core site.

Tracing of the snow deposition over GrIS in the past 200 kyr with the different temperature scenarios indicates that the ice at the NEEM site flowed in from the southeast (Figure 4.10 and 4.11), which is in agreement with the tracing results of the NEEM community members (2013). The NEEM community members (2013) modelled the locations of the depositional sites of the Eemian ice using nested 3D flow models, which estimates the depositional site of the 128-ka ice to be located 205 ± 20 km upstream from the NEEM site at present. My simulations resulted in the depositional site of the 128-ka ice to be located approximately 150 km upstream of the NEEM site; hence, the southeasterly source is consistent, but my modelling indicates that the source ice was less far-travelled. In my simulations the depositional site of the 128-ka, 126-ka, and 124-ka ice were all within one grid cell in the ice sheet model.

Consistent with the conclusions of the NEEM community members (2013), I find that even higher temperature scenarios such as T9 and T10 produce ice older than the Eemian at the bottom of the NEEM ice core site (Figure 4.10). In other words, the presence of old (Eemian and pre-Eemian ice) in the NEEM core is consistent with a greatly retracted ice sheet at this time.

In Figure 4.12, according to the model simulations of T2, T6, and T10 scenarios, 1400 m below the surface of the ice sheet at NEEM site is from the current interglacial, the Holocene, which is compatible with the observations in the NEEM ice core of the top 1419 m ice belonging to the Holocene (NEEM community members, 2013). Figure 4.15 displays the severe thinning of the bottom ice (i.e. older ice layers) in comparison to the younger ice closer to the surface. Older ice is buried and compressed by flow, and the younger ice covers the top ~half of the ice sheet.

The model predicts existing ice even older than the Eemian (Figures 4.12-4.15), which is in agreement with the research findings of the NEEM community members (2013). If melting had occurred from the bottom, older ice would not exist (Clarke and Marshall, 2002). Basal melting occurs within my model, if temperatures reach the pressure melting point, but I will underestimate the basal melting in geothermal hot spots under Greenland (e.g., Martos et al., 2018), since I use a uniform value for the geothermal heat flux that is typical of mature shield rock, rather than the higher heat fluxes associated with geothermal hot spots.

Figure 4.14 displays major fluctuations in the source-ice surface elevation in different layers of the ice column, especially close to the bed of the ice, which are linked to changes to the fluctuations in ice thickness during the Eemian warming. The NEEM community members (2013) mention ice down at about 2480 m at NEEM being from the Eemian warming, which also agrees with my results (Figure 4.12). The T2 and T6 scenarios have Eemian ice between depths of ~2400 m and ~2500 m. The T10 scenario has Eemian ice from ~2450 m to 2600 m. These results are in agreement with the high $\delta^{18}O$ values found near the bed of Summit ice indicating a warmer climate than the present, most likely the Eemian (Yau et al., 2016).

The modelled time-elevation curve for Summit shows that the ice sheet bed dates to around 190, 160, and 150 ka for the T2, T6, and T10 scenarios, respectively (Figure 4.16). Clarke et al. (2005) arrived at a simulation that dated the basal ice at Summit back to 380 ka. Nonetheless, the paper states that one should be doubtful of the predicted deep ice sheet bed age, as the ice flow model does not consider flow-induced disturbance of the deep ice. Indeed, disrupted and folded stratigraphies in both the NEEM and Summit cores are consistent with the rapid fluctuations in Eemian source ice elevation predicted by the model, which will be associated with shifts in the

flow direction. However, while the physics of folding are not in the ice sheet model (and are not well understood), this cannot be quantitatively tested.

Figure 4.18 is a fabricated ice core reconstruction at the Summit ice core site for the past 200 ka, which can be compared with the observed $\delta^{18}O$ within the Summit ice cores (Figure 2.6). At the depth of ~1500 m $\delta^{18}O$ concentration is about -35 ‰, which is consistent with the modelled Summit ice core reconstruction. However, at the depth of ~1700 m $\delta^{18}O$ concentration reaches to about -40 ‰, which disagrees with the modelled results. The Holocene section is about 200 m thicker in the model, implying too high an accumulation rate through this period. This discrepancy should be further investigated within the coding and parameterization of the U of C ice sheet model. While the transition from the Holocene to the glacial period is offset, the glaciation and underlying Eemian and pre-Eemian ice look similar between the observed and modelled ice cores.

5.4. Comparison with observations

I compare several features of the model simulations against available observations to assist evaluating the different models and examining the most plausible model, as well as the implausible models. Based on the suite of observational criteria summarized in Tables 5.1 and 5.2, the model results are similar to observations and inferences from the NEEM ice core. There are some exceptions. The NEEM community members (2013) estimated an ice thickness decrease of 400 ± 350 m from 128 to 122 ka (an average 7 ± 6 cm/yr reduction) after considering the isostatic rebound, which the model also accounts for. According to the same research, the air content within the ice core suggests a surface elevation of the 128-ka ice depositional site to be 540 ± 300 m higher than NEEM surface elevation at present (2450 m), estimating the 128-ka

depositional site surface elevation to be at 2990 ± 300 m (Table 5.1). All the temperature scenarios agree with this, however only the T4-T7 scenarios agree with the lowered ice thickness every 2000 years (Table 5.1). The Summit forcing produces surface elevation results that are compatible with the observations, but it fails to produce a lowered ice thickness from 128-122 ka (Table 5.1).

In the present-day ice sheet, the elevation of the Eemian (128 ka) source ice location in the NEEM core is 2780 ± 50 m (Table 5.2) (NEEM community members, 2013). Therefore, the surface elevation at this location on the ice sheet is 210 ± 350 m lower at present compared to the depositional time. It is considered that 128 ka was the onset of the Eemian warming. A surface elevation increase may have occurred at the onset of a warming period such as the Eemian due to an initial increase in precipitation and mass balance, before the ice sheet can adapt to the warmer conditions and increase the rate of ice flow, which subsequently thins the ice (NEEM community members, 2013).

In addition to the stratigraphic evidence, the modelled thickness of the ice itself can be compared with the observations (Table 5.2). The NEEM ice core is 2540 m long (NEEM community members, 2013), which is ~100-200 m lower than the simulated ice cores produced for all the temperature scenarios as well as when forced by the Summit (GISP2) ice core. The T10 scenario produces a thicker ice sheet in northwest Greenland, with a NEEM ice core about 2735 m long. The modelled results of Table 5.2 are within 10% of the observations, which is consistent with the passing criteria.

On the other hand, most of my modelled Summit results when forced by the Summit (GISP2) ice core are not compatible with the observational results estimated by Yau et al. (2013). None of the temperature scenarios pass the observations (Table 5.3), which is most

probably due to the reason that I forced the model with temperature scenarios adjusted from the observed NEEM temperature range. This can produce modelled results similar to NEEM observations, but less similar to observations at Summit, especially for the Eemian simulations due to the large uncertainty for that period.

Table 5.1. Observations versus model results (T2-T10 and Summit forcing) of ice thickness change (ΔH) from 128-122 ka and elevation (h_s) for every 2000 years from 128 ka to 122 ka at the NEEM source location. Crosses indicate failed scenarios of the model to produce the observed data.

Time (ka)		128	126	124	122	128-122	Fail
Observations	ΔH **(m)**					-400 ± 350 (-7 ± 6 cm/yr)	
	h_s **(m)**	2990 ± 300	2850 ± 420	2710 ± 540	2570 ± 660		
Models:							
T2	$H/\Delta H$ **(m)**	2799	2885	2849	2849	+50	x
	h_s **(m)**	2801	2852	2799	2791		
T3	$H/\Delta H$ **(m)**	2815	2870	2802	2826	+11	x
	h_s **(m)**	2814	2836	2757	2776		
T4	$H/\Delta H$ **(m)**	2826	2822	2716	2770	-56	
	h_s **(m)**	2824	2787	2682	2734		
T5	$H/\Delta H$ **(m)**	2838	2740	2596	2664	-174	
	h_s **(m)**	2835	2706	2577	2652		
T6	$H/\Delta H$ **(m)**	2848	2632	2403	2488	-360	
	h_s **(m)**	2843	2603	2407	2513		
T7	$H/\Delta H$ **(m)**	2860	2510	2240	2299	-561	
	h_s **(m)**	2853	2485	2267	2359		
T8	$H/\Delta H$ **(m)**	2870	2372	2066	2120	-750	
	h_s **(m)**	2860	2356	2118	2218		x
T9	$H/\Delta H$ **(m)**	2879	2227	1903	2005	-874	x
	h_s **(m)**	2868	2220	1982	2135		x
T10	$H/\Delta H$ **(m)**	2879	2080	1768	1893	-986	x
	h_s **(m)**	2866	2086	1874	2052		x
Summit forcing	$H/\Delta H$ **(m)**	2759	2694	2803	2828	+69	x
	h_s **(m)**	2746	2714	2773	2784		

Table 5.2. Present-day observations versus model results (T2-T10 and Summit forcing) of temperature (T_a), elevation (h_s), and ice thickness (H) at the NEEM site, total ice sheet volume and area, plus elevation (h_s), and time (ka) of highest temperature of the NEEM source ice site.

	NEEM T_a (°C)	Volume (10^6 km^3)	Area (10^6 km^2)	NEEM divide elevation, h_s (m)	NEEM ice sheet thickness, H (m)	NEEM source ice elevation, h_s (m)	Time (ka) - source highest T_a
Observations	-29	2.9	1.71	2450	2540	2780 +/- 50	126
Models:							
T2	-29.7	3.1	1.75	2565	2665	2811	126.4
T3	-29.7	3.1	1.74	2563	2663	2812	126.4
T4	-29.7	3.1	1.74	2565	2665	2813	126.4
T5	-29.7	3.1	1.74	2566	2666	2814	126.4
T6	-29.7	3.1	1.73	2567	2667	2813	126.4
T7	-29.8	3.1	1.73	2575	2679	2818	126.4
T8	-29.9	3.1	1.74	2587	2695	2822	126.4
T9	-29.9	3.1	1.73	2599	2712	2824	124.7
T10	-30	3.1	1.73	2616	2735	2828	124.2
Summit forcing	-30	3.0	1.73	2569	2672	2809	128.4

Table 5.3. Summit observation versus model results (T2-T10) of temperature changes over the Eemian, and present temperature. Crosses indicate failed scenarios of the model to produce the observed data.

Time (ka)		127.6-126.6	121.8-118	126-122	127	Present	Fail
Observations	ΔT/T (ºC)	Increase (6 ± 1.5)	Decrease (3 ± 1)	4-8 higher than recent	= recent (-31)	-31	
Models:							
T2	ΔT/T (ºC)	+2.5	-4.2	2-3.4	-28.8	-31.6	x
T3	ΔT/T (ºC)	+2.7	-4.9	3-4.6	-27.8	-31.6	x
T4	ΔT/T (ºC)	+3	-5.5	4-6	-26.8	-31.6	x
T5	ΔT/T (ºC)	+3.3	-5.7	4.5-7.4	-25.8	-31.6	x
T6	ΔT/T (ºC)	+3.8	-5.7	4.6-8.6	-24.8	-31.6	x
T7	ΔT/T (ºC)	+4.1	-6.1	3.2-4.4	-23.8	-31.5	x
T8	ΔT/T (ºC)	+4.2	-6.2	4.8-9.7	-22.7	-31.5	x
T9	ΔT/T (ºC)	+4.1	-6.5	5-10	-21.6	-31.5	x
T10	ΔT/T (ºC)	+3.8	-6.8	5.7-10.4	-20.4	-31.5	x

5.5. Implications for the stability of GrIS

When comparing simulated results with observations at NEEM and NEEM source, T4-T7 scenarios pass, which can mean peak temperature anomalies between 5 to 9ºC during the Eemian, compatible with the NEEM community members (2013) temperature peak of 8 ± 4ºC. Temperature anomalies of 5-9ºC can mean Greenland contribution to the SLR of 2.8-4.3 m between 125-125.5 ka, which does not agree with Yau et al. (2016) 4.1-6.2 m Greenland SLR contributions by 121 ka. My results imply that GrIS can lose 1.2-1.8 10^6 km^3 ice volume over such warm periods.

My results are not narrowed enough to support or contradict the suggested resilience of GrIS to a warmer climate and the large Antarctic ice sheet contribution to the global mean sea level rise during the LIG by NEEM community members (2013) and Quiquet et al. (2013). However, it does not agree with Yau et al. (2016) that by the end of Eemian GrIS contributed 5.1

m to the global sea level rise. On the contrary, it confirms that the GrIS contributed to SLR most likely early in the Eemian ~125 ka, and that Antarctica is a much stronger candidate than Greenland for the SLR later in the Eemian.

Finally, despite the fact that the results suggest a large contribution of Greenland to the SLR at ~125 ka, there are still discrepancies left to be explained between the modelled and observed relative changes between the ice core sites. Furthermore, this and other studies are limited by the accuracy of the climate/ice sheet models available (Yau et al., 2013), and the underestimation of temperature change magnitude when compared to evaluations based on ice cores (Masson-Delmotte et al., 2006).

Chapter 6 Conclusions

The aim of this study was to investigate the susceptibility of the Greenland ice sheet to higher temperatures during the Eemian warming, by combining an ice dynamics model and an isotope tracer model to carry out long-term ice-sheet simulations. Another objective was to build on that model to examine the potential impact of Eemian melting on isotopic modifications and temperature, and reconstructions in the NEEM ice core. Using nine different temperature scenarios based on the NEEM ice core and one scenario based on the Summit ice core, I ran simulations of the past 200 kyr and came to the following three conclusions:

I. Even for peak Eemian warming up to 12ºC higher than present, there is a persistent ice dome in central Greenland and old ice (pre-Eemian and Eemian) is preserved at the NEEM site.

II. Greenland's contribution to sea level rise due to Eemian warmth most likely ranges between 2.8 to 4.3 m, associated with temperature anomalies from 5-9ºC.

III. Melting during warmer periods can cause an overestimation of 0.1 to 2ºC in proxy records of Eemian warming. The impact on the climate interpretation coming from water isotopes depends on the magnitude of the warming and the extent of Eemian melting, which is not well constrained.

The available data and model results are broadly consistent, creating confidence in the conclusion above and the model's ability to reconstruct ice core records of depositional tracers at the NEEM drill hole location. There is more confidence in predicting characteristics of ice core records closer in time to present, rather than Eemian ice, due to the folding of ice near the ice sheet base and uncertain affects from Eemian ice sheet melting. Thus, I disagree with the

statement that Greenland defied ancient warming. Only the central ice sheet dome seems to be persistent with ancient warming. Greenland ice sheet caused more SLR during the Eemian (while still being consistent with the NEEM ice core record) than the implied ~2 m by the NEEM community members (2013) and Nature (2013).

6.1. Recommendations for future work

I looked carefully at the NEEM ice core site, but comparisons of modelled versus observed ice core stratigraphy could also be carried out at several other sites (e.g., NGRIP, Camp Century, Dye 3), to better constrain the ice sheet history and provide a more rigorous test of the model. Other proxies such as dust and deuterium excess can also provide valuable information. Deuterium excess does not depend on condensation temperature like $\delta^{18}O$, but the climate conditions of source water when vapour is created (Hoffman and Jouzel, 2001).

I also looked at the potential effects of partial melting on Eemian isotopes at NEEM, but meltwater effects on the isotope records of other ice core sites could also be examined to understand the implications better. Other post depositional modifications (such as wind scouring) to water isotopes could also help quantify the magnitude of post depositional effects on isotopic records within the ice cores (Anderson et al., 2016).

Most important is understanding the precipitation isotopes in the Eemian, as these may have changed with the open Arctic oceans and retreating ice sheets. Eemian warming could have changed the moisture source and air mass trajectories, creating uncertainty in the isotope-temperature relationship in Greenland.

Additionally, the ice sheet model should also be coupled to water isotope enabled atmospheric and ocean models, to focus on the coupled evolution of the climate and the GrIS for

the LIG as well as the future. The Community Earth System Model (CESM) and the Community Ice Sheet Model (CISM) at NCAR (National Center for Atmospheric Research) have recently enabled a full two-way coupling of ice sheets with the atmosphere and land surface allowing the new "CESM-CISM" model to be used to simulate climate/ice-sheet interactions on scales of centuries to millennia (Vizcaíno et al., 2008; Fyke et al., 2011; CESM Land Ice CESM2.0 documentation, 2018). A future project would be to include the full hydrological isotope cycle in the "CESM-CISM" climate model and focus on the coupled evolution of the climate and the GrIS for the LIG and the last glacial cycle. This would provide diagnostic models of precipitation isotopes over Greenland and their variations in time and space, accounting for differences in air mass trajectory, seasonality of precipitation, and source characteristics during the Eemian period.

Simulations of the LIG period in such a study should be benchmarked against paleoclimate observations to provide a robust validation of model performance in warm past climate states. This validation would in turn provide the basis for assessing the future climate simulations and the impacts of global warming on GrIS and sea level in the coming centuries. The Eemian, being warmer than today, contributes as a learning tool to anticipate the future warming. These findings will serve as a baseline for future projects to investigate the sensitivity of the ice sheet to climate change. This study assists the scientific effort to understand the impact that global warming will have on the Greenland ice sheet.

References

Abbott, P.M. & Davies. S.M. (2012). Volcanism and the Greenland ice cores: The tephra record. *Earth Science Reviews, 115*(3), 173-191. doi.org/10.1016/j.earscirev.2012.09.001

Alley, R.B., Andrews, J.T., Brigham-Grette, J., Clarke, G.K.C., Cuffey, K.M., Fitzpatrick, J.J., … White, J.W.C. (2010). History of the Greenland ice sheet: Paleoclimatic insights. *Quaternary Science Reviews, 29*(15-6), 1728-1756. doi:10.1016/j.quascirev.2010.02.007

AMAP. (2009). *The Greenland ice sheet in a changing climate: Snow, water, ice and permafrost in the Arctic (SWIPA) 2009.* By: Dahl-Jensen, D., Bamber, J., Bøggild, C.E., Buch, E., Christensen, J.H., Dethloff, K., … van der Veen, C.J. Arctic Monitoring and Assessment Programme (AMAP), Oslo. 115 pp.

Anderson, L., Berkelhammer, M., & Alisa Mast, M. (2016). Isotopes in North American Rocky Mountain snowpack 1993-2014. *Quaternary Science Reviews, 131*, 262-273.

Arctic Report Card. (2019). 2019 Artic report card: Visual highlights. Retrieved from https://earthsky.org/earth/2019-arctic-report-card-visual-highlights-video

Bakker, P., Masson-Delmotte, V., Martrat, B., Charbit, S., Renssen, H., Groger, M., ... Varma, V. (2014). Temperature trends during the present and last interglacial periods - a multi-model-data comparison. *Quaternary Science Reviews, 99*, 224-243.

Bales, R.C., Guo, Q., Shen, D., McConnell, J.R., Du, G., Burkhart, J.F., … Cappelen, J. (2009). Annual accumulation for Greenland updated using ice core data developed during 2000-2006 and analysis of daily coastal meteorological data. *Journal of Geophysical Research, 114*, 1-14. doi:10.1029/2008JD011208

Bales, R. C., J. R. McConnell, E. Mosley-Thompson, and G. Lamorey. (2001). Accumulation map for the Greenland ice sheet: 1971–1990, *Geophysical Research Letters, 28*(15), 2967–2970, doi:10.1029/2000GL012052

Bamber, J.L., Layberry, R.L., & Gogineni S.P. (2001). A new ice thickness and bed data set for the Greenland ice sheet 1. Measurement, data reduction, and errors. *Journal of Geographical Research, 106*(D21), 33773-33780.

Brady, E., Stevenson, S., Bailey, D., Lui, Z., Noone, D., Nusbaumer, J., … Zhu, J. (2019). The connected isotopic water cycle in the community earth system model version 1. *Journal of*

Advances in Modeling Earth Systems, 11, 2547-2566. http://doi.org/10.1029/2019MS001663

Braithwaite, R.J. (1995), Positive degree-day factors for ablation on the Greenland ice sheet studied by energy-balance modelling. *Journal of Glaciology, 41*(137), 153–160.

Bruckner, M.Z. (2019). A primer on stable isotopes and some common uses in hydrology. Microbial Life Educational Resources. Retrieved from https://serc.carleton.edu/microbelife/research_methods/environ_sampling/stableisotopes.html

Centre for Ice and Climate. (2019b). Fractionation and temperature; Why do reflect temperature. Retrieved from http://www.iceandclimate.nbi.ku.dk/research/past_atmos/past_temperature_moisture/fractionation_and_temperature/

Centre for Ice and Climate. (2019a). The central Greenland ice cores. Retrieved from http://www.iceandclimate.nbi.ku.dk/research/drill_analysing/history_drilling/central_ice_cores/

CESM Land Ice CESM2.0 documentation. (2018). CESM land ice documentation and user guide. Retrieved from https://escomp.github.io/cism-docs/cism-in-cesm/release-cesm2.0/html/index.html

Church, J.A., Clark, P.U., Cazenave, A., Gregory, J.M., Jevrejeva, S., Levermann, A. … Unnikrishnan, A.S. (2013). *Sea level change. In: Climate Change 2013: the physical science basis. contribution of working group I to the fifth assessment report of the intergovernmental panel on climate change*. Stocker, T.F., D. Qin, G.-K. Plattner, M. Tignor, S.K. Allen, J. Boschung, A. Nauels, Y. Xia, V. Bex & Midgley, P. M. (Eds.). Cambridge University Press, Cambridge, United Kingdom and New York, NY, USA.

Clarke, G.K.C., Lhomme, N., & Marshall, S.J. (2005). Tracer transport in the Greenland ice sheet: Three-dimensional isotopic stratigraphy. *Quaternary Science Reviews, 24*, 155–171.

Clarke, G., & Marshall, S. (2002). Isotopic balance of the Greenland Ice Sheet: Modelled concentrations of water isotopes from 30,000 BP to present. *Quaternary Science Reviews, 21,* 419-430.

Compute Canada. (2016). About. Retrieved from https://www.computecanada.ca/about/

Cuffey, K.M., & Clow, G.D. (1997). Temperature, accumulation, and ice sheet elevation in central Greenland through the last deglacial transition. *Journal of Geophysical Research, 102*(C12)*,* 26383-26396.

Cuffey, K.M. & Clow, G.D. (1999). GISP2 accumulation rate history. *Pangaea.* doi.org/10.1594/PANGAEA.56075

Cuffey, K.M. & Marshall, S.J. (2000). Substantial contributions to sea-level rise during the last interglacial from the Greenland ice sheet. *Nature, 404*, 591–594.

Dansgaard, W. (1964). Stable isotopes in precipitation, *Tellus*, *16*, 436–468.

Dansgaard, W. (2005). *Frozen annal Greenland ice cap research.* Retrieved from http://www.iceandclimate.nbi.ku.dk/publications/FrozenAnnals.pdf

Dutton, A., Carlson, A. E., Long, A. J., Milne, G. A., Clark, P. U., DeConto, R., Horton, B. P., Rahmstorf, S., & Raymo, M. E. (2015). Sea-level rise due to polar ice-sheet mass loss during past warm periods. *Science, 349*, aaa4019. doi: 10.1126/science.aaa4019

Fyke, J.G., Weaver, A.J., Pollard, D., Eby, M., Carter, L., & Mackintosh, A. (2011). A new coupled ice sheet/climate model: Description and sensitivity to model physics under eemian, last glacial maximum, late holocene and modern climate conditions. *Geoscientific Model Development, 4,* 117-136.

Gat, J. R. (1996). Oxygen and hydrogen isotopes in the hydrologic cycle. *Annual Review of Earth and Planetary Science, 24*, 225–62.

Gat, J. R., Mook, W. G., & Meijer, H. A. J. (Ed.). (2001). *Environmental isotopes in the hydrological cycle.* Volume II. Atmospheric water. Paris, France: UNESCO.

Gregory, J.M., & Huybrechts, P. (2006). Ice-sheet contributions to future sea level change. *Philosophical Transactions of Royal Society A, 364*, 1709–1731. doi: 10.1098/rsta.2006.1796

Gonfiantini R, Togliatti V, & Tongiorgi E. (1963). Snow stratigraphy and oxygen isotope variations in the glaciological pit of king Baudouin Station, Queen Maud Land, Antarctica. *Journal of Geographical Research 68*, 3791-3798.

Goto-Azuma, K., Koerner,R.M., & Fisher, D.A. (2002). An ice-core record over the last two

centuries from Penny Ice Cap, Baffin Island, Canada. *Annals of Glaciology, 35*(1), 29–35.

Hanna, E., Navarro, F. J., Pattyn, F., Domingues, C.M., Fettweis, X., Ivins, E.R., … & Zwally, H.J. (2013). Ice-sheet mass balance and climate change. *Nature, 498*, 51-59.

Hoffmann, G. & Jouzel, J. (2001). Deuterium excess record from central Greenland over the last millennium' hints of a North Atlantic signal during the little ice age. *Journal of Geophysical Research, 106*, 14,265-14,274.

Huybrechts, P. (1986). A three-dimensional time-dependent numerical model for polar ice sheets: Some basic testing with a stable and efficient finite-difference scheme. Vrije Universiteit Brussel Geog Inst Report 86/1.

Huybrechts, P., Letreguilly, A., & N. Reeh. (1991). The Greenland ice sheet and greenhouse warming. *Paleogeographical Paleoclimate Paleoecology, 89*, 399–412.

Huybrechts, P., & de Wolde, J.H. (1999). The dynamic response of the Greenland and Antarctic ice sheets to multiple-century climatic warming. *Journal of Climate, 12,* 2169-2188.

IPCC. (2013). *Summary for policymakers. In: Climate change 2013: The physical science basis. Contribution of working group I to the Fifth Assessment Report of the Intergovernmental Panel on climate change.* Stocker TF, Qin D, Plattner GK, Tignor MMB, Allen SK, Boschung J, Nauels A, Xia Y, Bex V, Midgley PM (Eds.). Cambridge University Press. Retrieved from https://www.ipcc.ch/site/assets/uploads/2018/03/WG1AR5_SummaryVolume_FINAL.pdf

IPCC. (2019). *Summary for policymakers. In: IPCC special report on the ocean and cryosphere in a changing climate.* Portner H.O., Roberts D.C., Masson-Delmotte V., Zhai P., Tignor M., Poloczanska E., Mintenbeck K., Nicolai M., Okem A., Petzold J., Rama B., Weyer (Eds.). In press.

Jenssen, D. (1977). A three-dimensional polar ice-sheet model. *Journal of Glaciology, 18*(80), 373-389. Retrieved from https://www.igsoc.org/journal/18/80/igs_journal_vol18_issue080_pg373-389.pdf

Johnsen, S.J., Dahl-Jensen, D., Gundestrup, N., Steffensen, J.P., Clausen, H.B., Miller, H., Masson-Delmotte, V., … White, J. (2001). Oxygen isotope and palaeotemperature records from six Greenland ice-core stations: Camp Century, Dye-3, GRIP, GISP2, Renland and NorthGRIP. *Journal of Quaternary Science, 16*(4), pp. 299–307.

Jouzel, J., Alley, R.B., Cuffey, K M., Dansgaard, W., Grootes, P., Hoffmann, G., … White, J. (1997). Validity of the temperature reconstruction from water isotopes in ice cores. *Journal of Geophysical Research, 102*(C12), 26471-26487.

Jouzel, J., Delaygue, G., Landais, A., Masson-Delmotte, V., Risi, C., & Vimeux, F. (2013). Water isotopes as tools to document oceanic sources of precipitation. *Water Resources Research, 49*(11), 7469–7486. doi:10.1002/2013WR013508.

Jouzel, J., Koster, R.D., Suozzo, R.J. & Russell, G.L. (1994). Stable water isotope behavior during the last glacial maximum: A general circulation model analysis. *Journal of Geographical Research, 99*(D12)*,* 25791-25801.

Jouzel, J., & Merlivat, L. (1984). Deuterium and oxygen-18 in precipitation: Modelling of the isotopic effects during snow formation. *Journal of Geophysical Research. 89*(D7), 11749–11757.

Jouzel, J., Merlivat, L., Petit, J R., & Lorius, C. (1983). Climatic information over the last century deduced from a detailed isotopic record in the South Pole snow. *Journal of Geophysical Research, 88*(C4), 2693-2703.

Kopp, R.E., Simons, F.J., Mitrovica, J.X., Maloof, A.C., & Oppenheimer, M. (2009). Probabilistic assessment of sea level during the last interglacial stage. *Nature, 462,* 863–867.

Letreguilly, A., Huybrechts, P. & Reeh, N. (1991). Steady-state characteristics of the Greenland ice sheet under different climates. *Journal of Glaciology, 37*(125), 149-157.

Lhomme, N., Clarke, G.K.C., & Marshall, S.J. (2005). Tracer transport in the Greenland ice sheet: Constraints on ice cores and glacial history. *Quaternary Science Reviews, 24*, 173-194.

Lipscomb, W. (2010). *The CESM land ice model: Documentation and user's guide. Los Alamos National Laboratory.* Retrieved from http://www.cesm.ucar.edu/models/cesm1.0/cism/docs/CESM_ice_sheets_documentation.pdf

Lunt, D. J., Abe-Ouchi, A., Bakker, P., Berger, A., Braconnot, P., ... Zhang, Z.S. (2013), A multi-model assessment of last interglacial temperatures. *Climate of the Past, 9*(2), 699–717. doi:10.5194/cp-9-699-2013

Marshall, S.J. (2012). *The cryosphere.* New Jersey, United States of America: Princeton University Press.

Marshall, S., & Clarke, G. (1997). A continuum mixture model of ice stream thermomechanics in the Laurentide ice sheet 1. Theory. *Journal of Geophysical Research, 102*(B9)*,* 20599–20613.

Marshall, S., & Cuffey, K.M. (2000). Peregrinations of the Greenland ice sheet divide in the last glacial cycle: implications for central Greenland ice cores. *EPSL, 179*, 73-90.

Martos, Y.M., Jordan, T.A., Catalan, M., Jordan, T.M., Bamber, J.L., & Vaughan, D.G. (2018). Geothermal heat flux reveals the Iceland hotspot track underneath Greenland. *Geophysical research letters, 45*(16), 8214-8222.

Masson-Delmotte, V., Kageyama, M., Braconnot, P., Charbit, S., Krinner, G., Ritz, C., ... YU, Y. (2006). Past and future polar amplification of climate change: Climate model intercomparisons and ice-core constraints. *Climate Dynamics, 26,* 513-529. doi: 10.1007/s00382-005-0081-9

McKay, N.P., Overpeck, J. T., & Otto-Bliesner, B. L. (2011). The role of ocean thermal expansion in last interglacial sea level rise. *Geophysical Research Letters, 38,* L14605. doi:10.1029/2011GL048280

Moran, T., & Marshall, S. (2009). The effects of meltwater percolation on the seasonal isotopic signals in an Arctic snowpack. *Journal of Glaciology, 55*(194)*,* 1012-1024.

Moran, T., Marshall, S.J., & Sharp, M.J. (2011). Isotope thermometry in melt-affected ice cores. *Journal of Geophysical Research, 116,* F02010. doi:101029/2010JF001738

National Snow and Ice Data Center. (2018). Quick facts on ice sheets. Retrieved from https://nsidc.org/cryosphere/quickfacts/icesheets.html

Nature. (2013). Greenland defied ancient warming. Retrieved from https://www.nature.com/news/greenland-defied-ancient-warming-1.12265

NEEM community members. (2013). Eemian interglacial reconstructed from a Greenland folded ice core. *Nature, 493*, 489-494. doi:10.1038/nature11789

NOAA Research News. (2014). NOAA launches research on next generation of high performance weather, climate models. Retrieved from https://research.noaa.gov/article/ArtMID/587/ArticleID/1209/NOAA-launches-research-on-next-generation-of-high-performance-weather-climate-models

Nolin, A. W. & Payne, M. C. (2007). Classification of glacier zones in western Greenland using albedo and surface roughness from the multi-angle imaging spectro radiometer (MISR). *Remote Sensing of Environment, 107,* 264–275. doi.org/10.1016/j.rse.2006.11.004

Otto-Bliesner, B.L., Marshall, S., Overpeck, J., Miller, G., Hu, A., & CAPE Last Interglacial Project Members. (2006). Simulating Arctic climate warmth and icefield retreat in the last interglaciation. *Science, 311,* 1751-1753.

Otto-Bliesner, B.L., Rosenbloom, N., Stone, E.J., McKay, N.P., Lunt, D.J., Brady, E.C., & Overpeck, J.T. (2013). How warm was the last interglacial? New model–data comparisons. *Philosophical Transactions of the Royal Society A, 371*, 20130097, 1-20. http://dx.doi.org/10.1098/rsta.2013.0097

Pohjola, V.A., Moore, J.C., Isaksson, E., Jauhiainen, T., van de Wal, R.S.W., Martma, T., Meijer, H.A.J., & Vaikmäe, R. (2002). Effect of periodic melting on geochemical and isotopic signals in an ice core on Lomonosovfonna, Svalbard. *Journal of Geophysics Research, 107*(D4), 4036. doi:10.1029/2000JD000149

Quiquet, A., Ritz,C, Punge, H.J. & Salas y Mélia, D. (2013). Greenland ice sheet contribution to sea level rise during the last interglacial period: A modelling study driven and constrained by ice core data. *Climate of the Past, 9*, 353-366. doi:10.5194/cp-9-353-2013

Raynaud, D., Chappellaz, J.A., Ritz, C., & Matinerie, P.J. (1997). Air content along the Greenland ice core project: A record of surface climatic parameters and elevation in central Greenland. *Journal of Geophysics Research, 102*(C12)*,* 26607-26613.

Reeh, N. (1991). Parameterization of melt rate and surface temperature on the Greenland ice sheet. *Polarforschung, 59*(3)*,* 113-128.

Ridley, J., Gregory, J.M., Huybrechts, P., & Lowe, J. (2010). Thresholds for irreversible decline of the Greenland ice sheet. *Climate Dynamics, 35*, 1065–1073. doi: 10.1007/s00382-009-0646-0

Robinson, A., Calov, R., & Ganopolski, A. (2011). Greenland ice sheet model parameters

constrained using simulations of the eemian interglacial. *Climate of the Past, 7,* 381-396. doi:10.5194/cp-7-381-2011

Schlosser, E., Oerter, H., Masson-Delmotte, V., & Reijmer, C. (2008). Atmospheric influence on the deuterium excess signal in polar firn: Implications for ice-core interpretation. *Journal of Glaciology, 54*(184), 117-124.

Sinclair, K.E., & Marshall, S.J. (2008). Post-depositional modification of stable water isotopes in winter snowpacks in the Canadian Rocky Mountains. *Annals of Glaciology, 49*, 96-106.

Sinclair, K.E., & Marshall, S.J. (2009). Temperature and vapour-trajectory controls on the stable isotope signal in Canadian Rocky Mountain snowpacks. *Journal of Glaciology, 55*(191)*,* 485–498.

Sokratov, S.A., & Golubev, V.N. (2009). Snow isotopic content change by sublimation. *Journal of Glaciology, 55*(193)*,* 823-828. doi: 10.3189/002214309790152456

Stone, E.J., Lunt, D.J., Annan, J.D., & Hargreaves, J.C. (2013). Quantification of the Greenland ice sheet contribution to last interglacial sea level rise. *Climate of the Past, 9*(2), 621–639. doi:10.5194/cp-9-621-2013

Turney, C.S.M., & Jones, R T. (2010). Does the Agulhas current amplify global temperatures during super-interglacials?. *Journal of Quaternary Science, 25*(6)*,* 839–843.

University of Copenhagen. (2013). Greenland ice cores reveal warm climate of the past. Retrieved from https://www.nbi.ku.dk/english/news/news13/greenland-ice-cores-reveal-warm-climate-of-the-past/

University of Copenhagen. (2019). History of ice core drilling in Greenland. Retrieved http://www.iceandclimate.nbi.ku.dk/research/drill_analysing/history_drilling/

van den Broeke, M., Bamber, J., Ettema, J., Rignot, E., Schrama, E., van der Berg, W.J., ... Wouters, B. (2009). Partitioning recent Greenland mass loss. *Science, 326*(5955)*,* 984-986. doi: 10.1126/science.1178176

Vizcaíno, M., Mikolajewicz, U., Groger, M., Maier-Reimer, E., Schurgers, G., & Winguth, A.M.E. (2008). Long-term ice sheet-climate interactions under anthropogenic greenhouse forcing simulated with a complex Earth System Model. *Climate Dynamics, 31,* 665–690.

Wake, L.M., & Marshall, S.J. (2015). Assessment of current methods of positive degree-day calculation using in situ observations from glaciated regions. *Journal of Glaciology, 61*(226), 329-344. doi: 10.3189/2015JoG14J116

WestGrid. (2016). What we do. Retrieved from https://www.westgrid.ca/about_westgrid/what_we_do

Yau, A.M., Bender, M.L., Robinson, A. & Brooke. E.J. (2016). Reconstructing the last interglacial at Summit, Greenland: Insights from GISP2. PNAS early edition, 1-6. Retrieved from http://www.pnas.org/cgi/doi/10.1073/pnas.1524766113.

SPRINGER NATURE LICENSE
TERMS AND CONDITIONS

Jan 14, 2020

This Agreement between University of Calgary -- Zahra Rahimian ("You") and Springer Nature ("Springer Nature") consists of your license details and the terms and conditions provided by Springer Nature and Copyright Clearance Center.

License Number	4747191136410
License date	Jan 13, 2020
Licensed Content Publisher	Springer Nature
Licensed Content Publication	Nature News
Licensed Content Title	Greenland defied ancient warming
Licensed Content Author	Quirin Schiermeier
Licensed Content Date	Jan 23, 2013
Type of Use	Thesis/Dissertation
Requestor type	academic/university or research institute
Format	electronic
Portion	figures/tables/illustrations
Number of figures/tables/illustrations	1

High-res required	no
Will you be translating?	no
Circulation/distribution	1 - 29
Author of this Springer Nature content	no
Title	Modelling long term ice sheet changes to understand the stability of the Greenland Ice Sheet in a warmer world
Institution name	University of Calgary
Expected presentation date	Jan 2020
Portions	The warm spell figure of NEEM
Requestor Location	University of Calgary 219 31 Ave NW Calgary, AB T2M2P3 Canada Attn: University of Calgary
Total	0.00 CAD

Terms and Conditions

Springer Nature Customer Service Centre GmbH
Terms and Conditions

This agreement sets out the terms and conditions of the licence (the **Licence**) between you and **Springer Nature Customer Service Centre GmbH** (the **Licensor**). By clicking 'accept' and completing the transaction for the material (**Licensed Material**), you also confirm your acceptance of these terms and conditions.

1. Grant of License

1. 1. The Licensor grants you a personal, non-exclusive, non-transferable, world-wide licence to reproduce the Licensed Material for the purpose specified in your order

only. Licences are granted for the specific use requested in the order and for no other use, subject to the conditions below.

1. 2. The Licensor warrants that it has, to the best of its knowledge, the rights to license reuse of the Licensed Material. However, you should ensure that the material you are requesting is original to the Licensor and does not carry the copyright of another entity (as credited in the published version).

1. 3. If the credit line on any part of the material you have requested indicates that it was reprinted or adapted with permission from another source, then you should also seek permission from that source to reuse the material.

2. Scope of Licence

2. 1. You may only use the Licensed Content in the manner and to the extent permitted by these Ts&Cs and any applicable laws.

2. 2. A separate licence may be required for any additional use of the Licensed Material, e.g. where a licence has been purchased for print only use, separate permission must be obtained for electronic re-use. Similarly, a licence is only valid in the language selected and does not apply for editions in other languages unless additional translation rights have been granted separately in the licence. Any content owned by third parties are expressly excluded from the licence.

2. 3. Similarly, rights for additional components such as custom editions and derivatives require additional permission and may be subject to an additional fee. Please apply to Journalpermissions@springernature.com/bookpermissions@springernature.com for these rights.

2. 4. Where permission has been granted **free of charge** for material in print, permission may also be granted for any electronic version of that work, provided that the material is incidental to your work as a whole and that the electronic version is essentially equivalent to, or substitutes for, the print version.

2. 5. An alternative scope of licence may apply to signatories of the STM Permissions Guidelines, as amended from time to time.

3. Duration of Licence

3. 1. A licence for is valid from the date of purchase ('Licence Date') at the end of the relevant period in the below table:

Scope of Licence	Duration of Licence
Post on a website	12 months
Presentations	12 months
Books and journals	Lifetime of the edition in the language purchased

4. Acknowledgement

4. 1. The Licensor's permission must be acknowledged next to the Licenced Material in print. In electronic form, this acknowledgement must be visible at the same time as the figures/tables/illustrations or abstract, and must be hyperlinked to the journal/book's homepage. Our required acknowledgement format is in the Appendix below.

5. Restrictions on use

5. 1. Use of the Licensed Material may be permitted for incidental promotional use and minor editing privileges e.g. minor adaptations of single figures, changes of format, colour and/or style where the adaptation is credited as set out in Appendix 1 below. Any other changes including but not limited to, cropping, adapting, omitting material that affect the meaning, intention or moral rights of the author are strictly prohibited.

5. 2. You must not use any Licensed Material as part of any design or trademark.

5. 3. Licensed Material may be used in Open Access Publications (OAP) before publication by Springer Nature, but any Licensed Material must be removed from OAP sites prior to final publication.

6. Ownership of Rights

6. 1. Licensed Material remains the property of either Licensor or the relevant third party and any rights not explicitly granted herein are expressly reserved.

7. Warranty

IN NO EVENT SHALL LICENSOR BE LIABLE TO YOU OR ANY OTHER PARTY OR ANY OTHER PERSON OR FOR ANY SPECIAL, CONSEQUENTIAL, INCIDENTAL OR INDIRECT DAMAGES, HOWEVER CAUSED, ARISING OUT OF OR IN CONNECTION WITH THE DOWNLOADING, VIEWING OR USE OF THE MATERIALS REGARDLESS OF THE FORM OF ACTION, WHETHER FOR BREACH OF CONTRACT, BREACH OF WARRANTY, TORT, NEGLIGENCE, INFRINGEMENT OR OTHERWISE (INCLUDING, WITHOUT LIMITATION, DAMAGES BASED ON LOSS OF PROFITS, DATA, FILES, USE, BUSINESS OPPORTUNITY OR CLAIMS OF THIRD PARTIES), AND
WHETHER OR NOT THE PARTY HAS BEEN ADVISED OF THE POSSIBILITY OF SUCH DAMAGES. THIS LIMITATION SHALL APPLY NOTWITHSTANDING ANY FAILURE OF ESSENTIAL PURPOSE OF ANY LIMITED REMEDY PROVIDED HEREIN.

8. Limitations

8. 1. ***BOOKS ONLY:***Where **'reuse in a dissertation/thesis'** has been selected the following terms apply: Print rights of the final author's accepted manuscript (for clarity, NOT the published version) for up to 100 copies, electronic rights for use only on a personal website or institutional repository as defined by the Sherpa guideline

(www.sherpa.ac.uk/romeo/).

9. Termination and Cancellation

9. 1. Licences will expire after the period shown in Clause 3 (above).

9. 2. Licensee reserves the right to terminate the Licence in the event that payment is not received in full or if there has been a breach of this agreement by you.

Appendix 1 — Acknowledgements:

For Journal Content:
Reprinted by permission from [**the Licensor**]: [**Journal Publisher** (e.g. Nature/Springer/Palgrave)] [**JOURNAL NAME**] [**REFERENCE CITATION** (Article name, Author(s) Name), [**COPYRIGHT**] (year of publication)

For **Advance Online Publication papers:**
Reprinted by permission from [**the Licensor**]: [**Journal Publisher** (e.g. Nature/Springer/Palgrave)] [**JOURNAL NAME**] [**REFERENCE CITATION** (Article name, Author(s) Name), [**COPYRIGHT**] (year of publication), advance online publication, day month year (doi: 10.1038/sj.[JOURNAL ACRONYM].)

For Adaptations/Translations:
Adapted/Translated by permission from [**the Licensor**]: [**Journal Publisher** (e.g. Nature/Springer/Palgrave)] [**JOURNAL NAME**] [**REFERENCE CITATION** (Article name, Author(s) Name), [**COPYRIGHT**] (year of publication)

Note: For any republication from the British Journal of Cancer, the following credit line style applies:

Reprinted/adapted/translated by permission from [**the Licensor**]: on behalf of Cancer Research UK: : [**Journal Publisher** (e.g. Nature/Springer/Palgrave)] [**JOURNAL NAME**] [**REFERENCE CITATION** (Article name, Author(s) Name), [**COPYRIGHT]** (year of publication)

For **Advance Online Publication** papers:
Reprinted by permission from The [**the Licensor**]: on behalf of Cancer Research UK: [**Journal Publisher** (e.g. Nature/Springer/Palgrave)] [**JOURNAL NAME**] [**REFERENCE CITATION** (Article name, Author(s) Name), [**COPYRIGHT**] (year of publication), advance online publication, day month year (doi: 10.1038/sj.[JOURNAL ACRONYM])

For Book content:
Reprinted/adapted by permission from [**the Licensor**]: [**Book Publisher** (e.g. Palgrave Macmillan, Springer etc) [**Book Title**] by [**Book author**(s)] [**COPYRIGHT**] (year of publication)

Other Conditions:

Version 1.2

Questions? customercare@copyright.com or +1-855-239-3415 (toll free in the US) or +1-978-646-2777.